A FEM STUDY ON THE MECHANICAL BEHAVIOR OF CORRUGATED-CORE STEEL SANDWICH WELDED PANELS IN BRIDGE DECK APPLICATIONS

by

Mehdi Tehrani

A THESIS SUBMITTED IN PARTIAL FULFILLMENT OF

THE REQUIREMENTS FOR THE DEGREE OF

MASTER OF APPLIED SCIENCE

in

THE COLLEGE OF GRADUATE STUDIES

(Civil Engineering)

THE UNIVERSITY OF BRITISH COLUMBIA

(Okanagan)

January 2015

Abstract

A critical challenge in bridge design and construction process is to reduce the weight of bridge deck. Designers and manufactures tend to put a lot of effort to come up with different solutions for innovative bridge decks. Specifically, in small aged bridges, light modules provide an easy and fast bridge deck renewal. Sandwich panels were introduced as such light weight bridge decks a few decades ago. Steel sandwich panel is composed of three layers of plates; two face sheets and a corrugated core. Low density and high specific strength of the panels provide remarkable advantages for a wide variety of industrial applications.

The main objective of this study is to investigate the effect of geometric parameters on the mechanical behavior of the corrugated-core steel sandwich panel. In order to mathematically simulate the panel two mechanical responses of maximum panel deflection and maximum shear force at core and face sheets interface are investigated. A regression model is introduced for each response which obtained from the contributions of the geometric parameters and their interactions. The effect plots revealed that core and face sheet thicknesses highly affect the panel deflection response and weld spacing highly affects the maximum shear force response. Predicted response values obtained from regression model are reasonably close to FEM results. The research also focuses on potential failure scenarios which may occur at the core and face sheets bonding connected via spot weld in the case of over loading. The failure analysis showed that the spot weld detachment in all welding paths starts from the panel edges near the girder supports and propagates toward the center of panel. In addition, as the applied load increases up to 300% of service load, the number of failed welds increases exponentially.

Table of Contents

Abstract .... **i**

Table of Content .... **ii**

List of Tables .... **iv**

List of Figures .... **v**

Acknowledgement .... **viii**

Dedication .... **ix**

Chapter 1: Introduction and thesis organization **1**

1.1. General 1

1.2. Literature review 3

1.3. Objective of the study 10

1.4. Research significance and contribution 11

1.5. Thesis limitation 12

1.6. Thesis outline 12

Chapter 2: FEM Analysis **13**

2.1. General 13

2.2. Finite Element Analysis 13

2.2.1 Geometry modeling 14

2.2.2 Meshing 18

2.2.3 Boundary conditions 21

2.2.4 Weld modeling 22

2.2.5 Loading 25

Chapter 3: Results **28**

3.1. General 28

3.2. Finite element model verification 28

3.3. Parametric study 32

3.3.1 Maximum deflection analysis 34

3.3.2 Maximum shear force analysis 47

3.3.3 Sensitivity analysis for panel height and sheet thickness parameters 58

3.4. Failure Analysis 66
3.4.1 Spot weld failure analysis algorithm 66
3.4.2 Spot weld failure analysis in sandwich panel under applied overloading 70
3.4.3 Spot weld failure propagation analysis 73
Chapter 4: Summary and Conclusion 82
4.1. Summary 82
4.2. Conclusion 82
4.3. Future study recommendation 84
References 85

List of Tables

Table 2-1 Assumed mechanical properties for steel material applied to face and core sheets and spot weld 20

Table 3-1 Input factors used in the parametric study with low and high level values 34

Table 3-2 Full factorial design with first-order interactions along with panel maximum deflection results 35

Table 3-3 Parameters effect values for the panel maximum deflection response 36

Table 3-4 list of coefficient values for the regression equation for the factors and first order interactions 41

Table 3-5 ANOVA test results for the sandwich panel maximum deflection response 43

Table 3-6 Regression model results comparison with ANSYS 44

Table 3-7 Random models geometrical parameters 46

Table 3-8 Panel maximum deflection response for two random models as per ANSYS and regression equation result 47

Table 3-9 Full factorial design with first-order interactions along with maximum shear force values at spot welds 48

Table 3-10 Effect values for the maximum shear response 49

Table 3-11 ANOVA test results for the maximum shear force at spot welds response 54

Table 3-12 Regression equation coefficients for the maximum shear force value 55

Table 3-13 Comparison between the regression equation and ANSYS results for the maximum shear force response 56

List of Figures

Figure 1-1 Sandwich panel installation as bridge deck (Adapted from Kennedy and Murray, 2004)....................7

Figure 1-2 Schematic illustration of resistant welding mechanism....................8

Figure 1-3 Laser welding mechanism illustration (Adapted from Abbott et al., 2008)....................9

Figure 1-4 Single-Sided spot welding machine (Adapted from prospot.com)....................10

Figure 2-1 Corrugated steel sandwich panel configurations (Adapted from Kujala and Klanac, 2002)....................14

Figure 2-2 Sandwich panel geometry overview....................15

Figure 2-3 Sandwich panel corrugated core cross-section....................15

Figure 2-4 Corrugated core unit cell geometrical properties....................16

Figure 2-5 Applied symmetry lines in longitudinal and transverse directions....................17

Figure 2-6 Quarter panel with two unit cells....................17

Figure 2-7 Element geometrical shape for Shell 181 element (left picture) and Beam 188 element (right picture). (ANSYS Release 14.0, 2012)....................19

Figure 2-8 Element convergence study for two responses of panel maximum deflection and maximum shear force at spot welds....................20

Figure 2-9 Quarter panel with meshed elements....................21

Figure 2-10 Applied boundary conditions on steel sandwich panel....................21

Figure 2-11 Applied welding lines through the corrugated core at top and bottom face sheets....................24

Figure 2-12 Applied welding lines showed only on top face sheet.....................24

Figure 2-13 Traffic pattern assumption for vehicles on bridge deck....................26

Figure 2-14 Simulated quarter sandwich panel in ANSYS with added tire load on top face sheet....................26

Figure 3-1 Obtained results by Tan et al. (1989) for two models with different boundary conditions in a closed form, experimental, and FEM methods....................29

Figure 3-2 Displacement contours in Y-direction for the quarter panel simulation....................30

Figure 3-3 Simulated FEM model verification with Tan et al. (1989) experimental work.........32

Figure 3-4 Geometric factors main effect plot for sandwich panel maximum deflection response 37

Figure 3-5 Geometric factors interaction effect plots for the panel maximum deflection response; a) [SR], b) [ST_c], c) [ST_f], d) [SP], e) [RT_c], f) [RT_f], g) [RP], h) [T_cT_f], i) [T_cP], j) [T_fP]...40

Figure 3-6 Predicted versus Actual results for the sandwich panel maximum deflection response 42

Figure 3-7 ANOVA test assumption validity proof for the panel maximum deflection response; (a) Normal plot, (b) Residual versus Predicted plot, (c) Residual versus Run number plot...45

Figure 3-8 Geometric factors main effect plot for maximum shear force response at spot welds...50

Figure 3-9 Interaction effect plots for the maximum shear force at spot welds response; a) [SR], b) [ST_c], c) [ST_f], d) [SP], e) [RT_c], f) [RT_f], g) [RP], h) [T_cT_f], i) [T_cP], j) [T_fP]...53

Figure 3-10 Predicted versus Actual results for the panel maximum deflection response..........57

Figure 3-11 ANOVA test assumption validity proof for the maximum shear force at spot welds response; (a) Normal plot, (b) Residual versus Predicted plot, (c) Residual versus Run number plot..58

Figure 3-12 Sandwich panel cross-section with three different heights; a) h = 107.5 mm, b) h= 139 mm, c) h = 170.5 mm...60

Figure 3-13 Panel height effect on maximum deflection response 60

Figure 3-14 Spot welding path numbers...61

Figure 3-15 Panel height effect on shear force responses at spot welds. a) welding path #1, b) welding path #2, c) welding path #3, d) welding path #4, e) welding path #5, f) welding path #6, g) welding path #7, h) welding path #8. 63

Figure 3-16 Core and face sheet thickness effect on panel maximum deflection 64

Figure 3-17 Core and face sheet thicknesses effect on panel maximum deflection....................65

Figure 3-18 Spot weld failure analysis algorithm 68

Figure 3-19 shear force values at spot welds along all welding paths over the entire top and bottom face sheets 69

Figure 3-20 Shear force values at spot welds at loading 100%, 200%, and 300% of service load along a) welding path #1, b) welding path #2, c) welding path #3, d) welding path #4, e) welding path #5, f) welding path #6, g) welding path #7, h) welding path #8 72

Figure 3-21 Location of failed spot welds on top face sheet for the panel with sheet thickness of 3.17 mm....74

Figure 3-22 Location of failed spot welds on bottom face sheet for the panel with sheet thickness of 3.17 mm....74

Figure 3-23 Location of failed spot welds on top face sheet for the panel with sheet thickness of 2.38 mm....75

Figure 3-24 Location of failed spot welds on bottom face sheet for the panel with sheet thickness of 2.38 mm....75

Figure 3-25 Location of failed spot welds on top face sheet for the panel with sheet thickness of 3.96 mm....76

Figure 3-26 Location of failed spot welds on bottom face sheet for the panel with sheet thickness of 3.96 mm....76

Figure 3-27 Shear force values at spot welds at loading 300% of service load for sandwich panels with three sheet thickness values of 2.38 mm, 3.17 mm, and 3.96 mm along a) welding path #1, b) welding path #2, c) welding path #3, d) welding path #4, e) welding path #5, f) welding path #6, g) welding path #7, h) welding path #8 79

Figure 3-28 Number of failed spot welds at each load step for three sandwich panels with core and face sheet thickness values of 2.38 mm, 3.17 mm, and 3.96 mm....80

Figure 3-29 load capacity curves for the sandwich panels with three sheet thickness values of 2.38 mm, 3.17 mm, and 3.96 mm 81

Acknowledgements

I would like to thank my supervisor, Dr. Shahria Alam, for the opportunity to perform the research under his supervision. I would have not been able to complete the research work without his guidance, teaching, and support.

DEDICATED TO MY WIFE

Chapter 1: Introduction and thesis organization

1.1. General

Demand for lighter and modular structures is increasing in recent years due to some driving factors in construction projects such as tight scheduling, labour, management and overall cost. For instance, in any construction project, reducing the required man hours on site is highly favourable for construction companies. Furthermore, the use of prefabricated modular structures leads to lesser construction workers on site and, instead, longer fabrication time in shop which is translated to less cost. Moreover, specifically in bridge construction projects, regarding the renewal of aged and deteriorated bridges, the installation of modular superstructure components definitely helps minimize the disruption to public traffic.

Beside the modular concept that contributes to an easy and faster construction, the weight of the bridge superstructure also plays an important role in the design and construction of bridge substructure such as girders and piers. Specifically, one of the critical challenges in the design process of a bridge construction is the weight of bridge deck in which any design innovation toward the weight reduction is vital. Therefore, design of a deck structure with minimum possible weight would be an important achievement in bridge construction. In order to address this need, corrugated-core steel sandwich panels offer a significant high stiffness to weight ratio. Low density and high specific strength characteristics of the panel provide remarkable advantages for a wide variety of industrial applications compared to conventional structures. The other significant advantage of the sandwich panel is its high energy absorption capacity during an impact loading. For example, commercial and military ship industry is interested to find an adequate solution for submerged rock impact and collision with other vessels to minimize the hit damage. The sandwich panel possesses a high potential to be a reasonable structure to address the need without adding additional weight to the ship structure. Over the past decade researches have been carried out regarding the application of sandwich panels in ship industry (Paik, 2003). Generally, in structural applications, sandwich panel refers to a thick panel assembly with two main components; an inner core, and top and bottom outer layers. The core usually corresponds to a section between outer layers filled with a light weight material or hollow sections formed by corrugated sheets. Moreover, based on the application of the panel, the core can also be fully filled with compressed foam or polymer. The outer layers usually correspond to flat metal sheets which are attached to the core by means of an adhesive agent or welding. In this study, the focus is on the corrugated-core steel sandwich panel composed of two face sheets and a corrugated core. The main reason that the panel provides an effective response in bending is due to positioning two metal face sheets far from the neutral axis which offers a high stiff cross-section. Regarding the shear load flow through the panel, it is noted that the upper face sheet transfers the applied loads to the corrugated core and bottom face sheet via the spot welds at the interface of the core and face sheets. Therefore, the main duty of the core is to tightly join the both face sheets together to enable the panel to be remained stiff. There is no doubt that the amount of transferred load should be within the shear capacity of spot welds.

It is critical to design a panel with desired mechanical properties and at the same time with the minimum weight. Since the fabrication cost depends on the number of spot welds, decreasing the number of required welding points is cost- effective. Therefore, the mechanical behavior of sandwich panels with different geometries should be studied in order to present the most efficient design. In order to investigate the panel's mechanical behavior, in the presented study, two responses have been selected to be monitored: *Panel global maximum deflection* and *shear force distribution* at the interface between corrugated core and face sheets. In order to predict panel's geometric properties in terms of these two responses, a mathematical regression model is introduced based on the calculated contributions from a set of geometrical parameters.

Generally, in steel structures, the critical hot spots where failure may take place are located near joints and fasteners that transfer the applied loads in different parts. The stress concentration and insufficient strength at such joints may cause unpredicted failure. Therefore, a failure analysis could reveal the potential weaknesses of the structure at these spots in order to apply a strengthening method to prevent such failures. Based on this fact, the presented research also focuses on potential failure scenarios which may occur at spot welds in the case of applied excessive loading. According to the available spot weld manual

(CMW, 2014), if the shear force value in welds exceeds a certain limit, these spot welds will fail. Consequently, the detached welds cannot transfer the shear load from face sheets to the core. Accordingly, if the number of failed welds increases, it may result in sandwich panel failure. It is expected that as long as the panel is designed as per code requirements where the loads are within the service load limit, the failure should not occur. However, due to increased traffic volume and loads, it is important to understand the potential failures in the case of over loading. This approach would help designers predict the panel's response to overloading and also the location of possible spot weld detachments. Therefore, at the next step, by reinforcing those regions the potential failure may be avoided.

1.2. Literature review

According to the available literatures, the first investigation in sandwich panels was proposed by Libove and Batdorf in 1948. They suggested a simplified deflection theory for a sandwich panel which is based on presenting an equivalent elastic modulus for the sandwich panel. Three years later, in 1951, Libove and Hubka presented a method to obtain an equivalent elastic modulus for a corrugated-core sandwich panel. Plantema (1966) and Allen (1969) described the mechanical behavior of the sandwich panels. They explained that sandwich concept plays an important role in the efficient engineering system development due to their significant advantages. The most remarkable features include high stiffness to weight ratio, high thermal insulation properties, and high impact and vibration absorption rate (Zenkert, 1995).

Lloyd (2000) found out that the sandwich plate system had a number of advantages over a stiffened steel plate in maritime applications. He determined that a composite sandwich plate has distributed stress over a larger area compared to a conventional steel plate for a double-hull oil tanker design. Crack formation is less likely to occur due to the elimination of stiffeners. Also, the simplified structural system was easier to coat and maintain; other advantages of a sandwich plate are the integrated acoustic and thermal insulation and increased impact resistance. The sandwich panel also presents other advantages. Lok and Cheng (2000) summarized several advantages including simplification of traditional connection processes (since stiffeners or joist members can be eliminated), accurate and rapid construction method, more rigid surface, reasonable uniform pressure distribution over the panel surface, capability to design curve structures, and easier transportation.

Kennedy et al. (2002) discussed the need for a lightweight, cost efficient bridge deck for portable bridge decks. In this research, they pointed out that traditional steel plate bridge decks are expensive due to the amount of required welding in manufacturing process. They compared a traditional steel box girder with a stiffened sandwich plate box girder and a composite core sandwich plate box girder. In their study, only the effects of traffic loads were examined on the different deck configurations. Both sandwich plate alternatives were more cost efficient and performed satisfactorily at ultimate, fatigue, and serviceability limit states. They concluded that the system is an attractive alternative to traditional bridge decks due to reduced welding parts and ease of erection.

Vaughn et al. (2005) and Xue and Hutchinson (2004) provided an easy and cost-effective manufacturing technology for steel sandwich panels. Regarding the application of sandwich panels, the structural behavior of panels needs to be characterized by means of analytical methods which should be validated by experimental results. Such investigations have been carried out for panels with truss and honeycomb core configuration (Rathbun et al., 2004; Zok et al., 2005).

Besides the corrugated-core sandwich panels, truss-core sandwich panels are also investigated by researchers. As a first step to analyze the mechanical response of these types of sandwich panels, Chiras et al. (2002) and Rathbun et al. (2004) conducted quasi-static experiments and numerical analysis for the compressive and shear response of truss core panels. These studies showed that trusses under compression load collapse due to buckling while trusses under tension load fail due to fracture. Rathbun et al. (2004) measured the behavior of tetrahedral truss sandwich panels in shear and bending. Deshpande et al. (2001) measured the collapse responses of truss core sandwich beams in bending for 3-point applied loading and obtained upper bound expressions for the loading limits. Wallach and Gibson (2001) analyzed the equivalent elastic moduli and the uniaxial and shear strengths of a three-dimensional truss geometry. They also investigated the ways in which the corrugated-core structural defects could result failure in sandwich panels (Wallach and Gibson, 2001). These studies were then applied to obtain optimal design and develop continuum constitutive models (Wicks and Hutchinson, 2001; Rathbun et al., 2005).

In a composite sandwich panel, two thin metal face sheets are separated by a lightweight core material. The core guaranties that both face sheets are tightly involved together in order to resist against the applied load on top of the sandwich panel. It also contributes in stiffening the face sheets to postpone local buckling. On the other hand, the face sheets significantly help protect the core material in the case of any physical damage or degradation. Therefore, the composite sandwich panel is a reasonable example of combination of two different types of materials application in one structure. Steel sandwich panels have been also investigated due to their multifunctional advantages such as light weight structure and at the same time high resistance in applied blast loading (Evans et al., 2001; Qiu et al., 2003; Xue and Hutchinson, 2003; Deshpande et al., 2001). In these investigations steel sandwich panels with different core geometries have been studied such as truss configuration, square honeycomb, and corrugated cores. Sandwich panel manufacturing methods in which different techniques are introduced to fabricate panels with various core geometries are described by Sypeck and Wadley (2001), Wadley et al. (2003) and others. The investigation of the pyramidal truss core steel sandwich panel describes the failure modes of the panel under applied loading. It also reveals the patterns in which the failure modes change as the applied load increases (Sypeck and Wadley, 2001). Sypeck and Wally also tried to limit core sheet thickness in order to restrict the sandwich panel design with thin plates. The method was also applied to different core geometries such as square honeycomb and corrugated core sheet. Analytical models were introduced to investigate the mechanical behavior of the hollow structure sandwich panels. They evaluated the effect of geometric parameters and demonstrated the influence of different core topologies in mechanical properties of the sandwich panel. The same methodology was developed for sandwich panels with honeycomb core structure (Bezazi et al., 2005; Chung and Waas, 2000; Gibson and Ashby, 1999; Goswami, 2006). All of these studies introduced equivalent core mechanical properties in order to simplify the complex analysis of the core geometry. The technique also allows FEM analysis to replace the complex core geometry with a single layer homogeneous material which possesses effective material properties.

Tsakopoulos and Fisher (2003) investigated the Williamsburg Bridge in New York City, New York where they discovered fatigue cracks in weld connections of sandwich panel deck to girders during rehabilitation of the bridge. They proposed two connections at the interface of sandwich panels and girders. The first connection entirely consists of fillet welds, and the second connection was a combination of a partial joint penetration weld and fillet welds. After conducting fatigue tests on the weld options, they concluded that the connection with only fillet welds had inconsistent performance. Cracks were developed in both the tension and compression regions well below the stress range specified by AASHTO LRFD Bridge Design Specifications (2005).

Intelligent Engineering (2002) carried out a research for the Austrian military where a 5-40-5 Sandwich Plate System (SPS) bridge deck panel was used to replace a traditional stiffened bridge deck panel. The 5-40-5 numbering denotes the thickness of the steel plate, elastomer core and the other steel plate, respectively, in millimeters. Three static load tests were performed on the 5-40-5 sandwich plate system in Ludwigshafen, Germany. The obtained results showed that the sandwich panel carried 1.29 times the design load applied at the maximum eccentricity. A fatigue test was also conducted up to 5 million cycles without showing any sign of cracks. In order to simulate the sandwich panel, a finite element analysis was performed using ANSYS where the difference between the predicted and experimental deflection results was only 7%. The experimental strains were in reasonable agreement with the analytical model, and there was no sign of creep during any of the experimental testing.

Steel sandwich panels with web-core configuration in which face sheets are attached to the core by the application of laser welding are significantly effective in bending loading in comparison with stiffened plate structure applied in ship manufacturing industry (Klanac and Kujala, 2004). The main reason of the high stiff structure is due to the positioning of web-core material far from neutral axis. By the application of the hollow structure sandwich panel as a component in a larger structure, such as a bridge deck, the obtained benefits can be considerably noticeable. The sandwich panels with periodic core geometry have been developed by the use of fabrication techniques such as casting and forming. On the other hand, sandwich panels with compressed polymer core are also applicable as bridge deck. In this type of sandwich panel two face sheets are attached to the polymer core with applying an adhesive agent. Generally, the sandwich panel introduces less stiffness in comparison with the steel corrugated core sandwich panel. Therefore, the application of polymer core sandwich panel is limited up to a certain load capacity. It should be noted that the delamination at the interface of polymer and face sheets is one of the common failures that may occur in polymer core sandwich panel. Figure 1-1 demonstrates the installation of polymer core sandwich panel modules on top of girders in Shenley Bridge in Quebec (Kennedy and Murray, 2004). As it is mentioned, the main advantage of the sandwich panel application as bridge deck over regular concrete deck is the fast onsite installation for small bridges. Since panels are prefabricated at shop and should be just assembled onsite, the bridge construction phase is simplified remarkably.

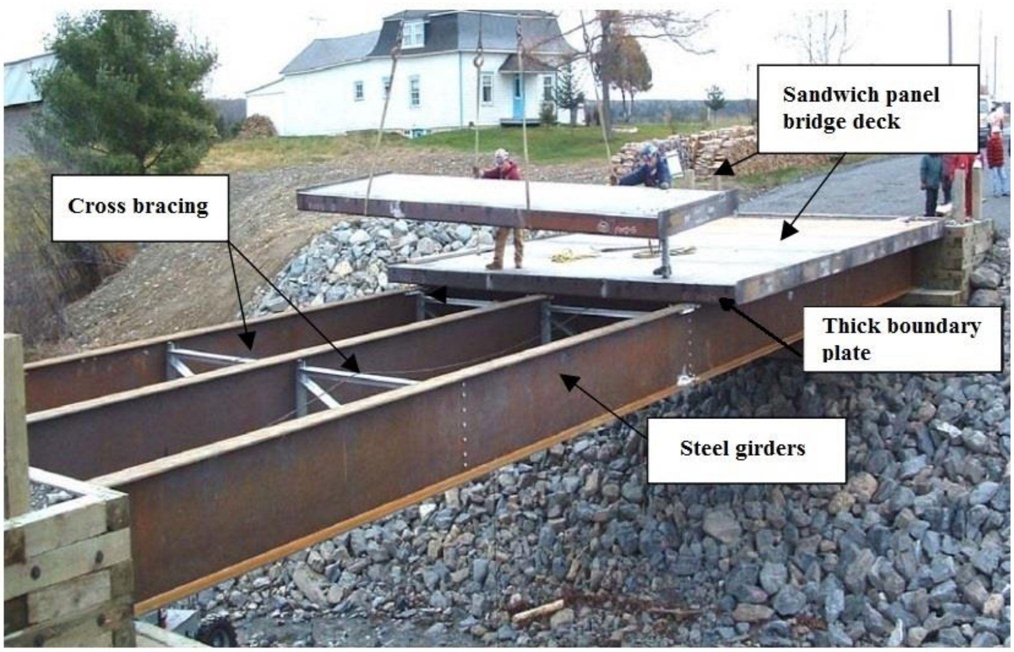

Figure 1-1 Sandwich panel installation as bridge deck (Adapted from Kennedy and Murray, 2004)

The fabrication process of sandwich panels has been improved over the last decade leading to faster and easier manufacturing techniques. Although the achieved improvements help fabricate higher quality panels, few challenges still exist and need investigation. Cost and manufacturing time are the most important challenges which should be taken into account to maximize the efficiency of the product. The challenge in the fabrication (related to cost and time optimization) is to provide adequate bonding at the interface of face sheets and corrugated core. The bonding is a key factor in the long-term performance and durability of the sandwich panels. The most common connection in steel sandwich panels is welding; however, in the past riveting, self-tap screwing, and applying adhesive were also common to provide the bonding (Fung et al., 1996). There are two types of welding which can be performed in sandwich panel fabrication; resistance welding and laser welding. Figures 1-2 and 1-3 show the schematic process of resistance and laser welding, respectively.

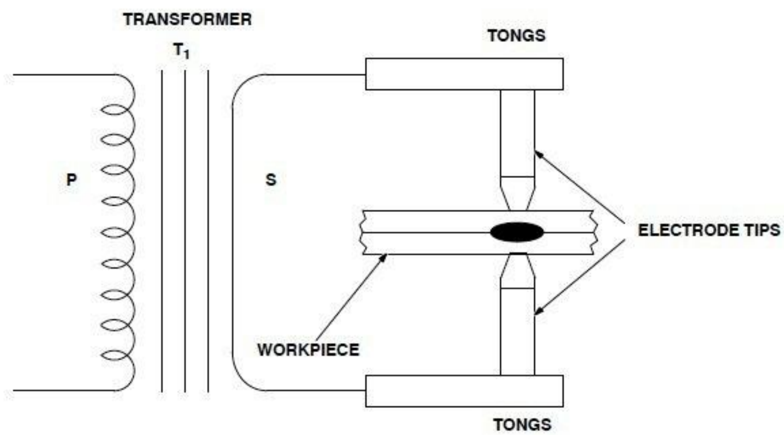

Figure 1-2 Schematic illustration of resistant welding mechanism

These welding techniques offer valuable advantages and also disadvantages. Regarding the speed of the process, the laser welding is faster and can be performed on a component which is only accessible from one side (Abbott et al., 2008). However, the resistance welding is not as fast as laser one and it may be difficult to apply on close cross-sections. Although laser welding outweighs resistance welding in terms of manufacturing speed, it needs much higher energy and its initial capital cost is remarkably higher. Therefore, manufacturers are still interested in resistance welding known as spot welding which has much less initial capital cost as well as lower energy and maintenance cost.

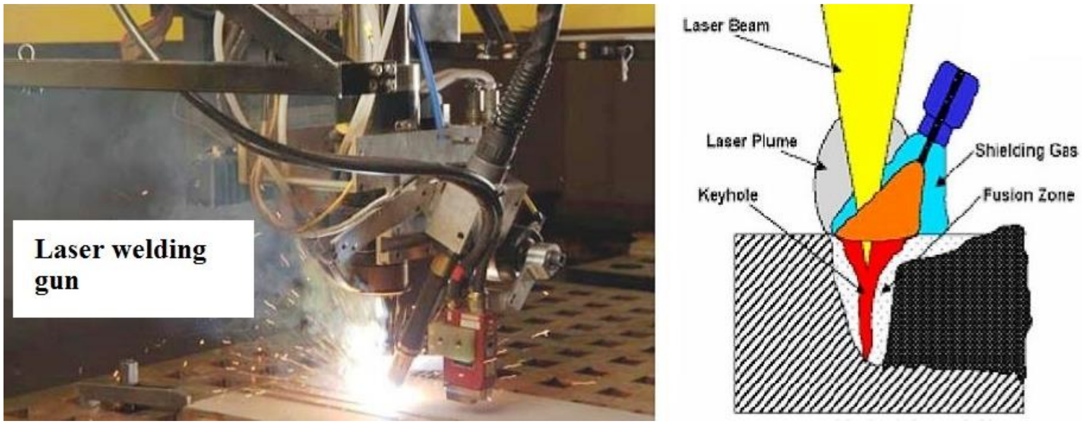

Figure 1-3 Laser welding mechanism illustration (Adapted from Abbott et al., 2008)

As demonstrated in Figure 1-2, the spot welding device includes two electrode heads which should be placed on both sides of two attaching plates. As electric current transfers from one head to the other through both plates, the metal temperature at the vicinity of electrodes significantly increases leading to melting of plates and merging them together after they become cold. The welding of first face sheet to the corrugated core is easier than the second one. As the first face sheet is attached, the corrugated section will be closed and it will be difficult to put the inner electrode inside the corrugated core to weld the next face sheet. However, by applying a special electrode which has smaller holding arm than the height of the sandwich panel, the second sheet can be connected to the core. It should be noted that a new method of spot welding called Single-Sided spot welding performs the welding by using only one electrode head at one side. As shown in Figure 1-4, the whole copper-coated surface on working table underneath the panel plays the role as the second electrode head. Therefore, the combination of these two spot welding techniques is the most optimal and convenient fabrication process for corrugated steel sandwich panels.

Figure 1-4 Single-Sided spot welding machine (Adapted from prospot.com)

1.3. Objective of the study

One of the main features of the corrugated-core sandwich panel is its low weight to stiffness ratio. In order to reduce the weight of the panel within the allowable range of panel deflection and shear stress at spot welds, a comprehensive understanding of the effect of geometric parameters on the panel’s mechanical behavior is essential. The main objectives of the study are as follows.

- Investigating the effect of geometric parameters on the mechanical behavior of the steel sandwich panel.
- Introducing regression models for the both mechanical responses; panel maximum deflection and maximum shear force at spot welds.
- Investigating potential failure scenarios which may occur at spot welds in the case of applied overloading.

The main goal of the thesis is to provide fabricators with a qualitative analysis tool to be able to assess the corrugated-core sandwich panel mechanical behavior for different loading profiles and geometric parameters.

1.4. Research significance and contribution

The main focus in this study is to present the effect of geometric parameters on the mechanical behavior of corrugated core steel sandwich welded panels. In this research, it is demonstrated that by changing the input geometric factors, how the panel maximum deflection and the shear force flow at the interface between face sheets and the corrugated core get affected. The qualitative results are employed to investigate the failure scenarios in spot welds due to passing their shear strength capacity.

The significance and contribution of the presented research work is summarized as follows.

- It provides a comprehensive qualitative approach for fabricators to understand the effects of various sandwich panel design parameters (e.g. thickness of the core and face sheet, panel height, spot weld distance, spot weld radius) on the mechanical response (deflection, shear force distribution) of the panel.

- Spot weld failure analysis method introduced in this study will further help predict the weld failure pattern in the case of over loading, which has important implication in the design phase.

The contribution of the thesis is mostly applicable for manufacturers by providing qualitative recommendation regarding the geometry of the sandwich panel to satisfy the design requirements. A substantial contribution of this study is the proposed analysis tool which will help design engineers validate their sandwich panel design and make sure that the panel deflection and shear forces are within the limiting range.

1.5. Thesis limitation

The presented results and discussions in the research work are limited to the considered assumptions in following items.

- The steel material with specific mechanical properties
- Homogenous and bilinear material model
- Sandwich panel geometry
- Similar boundary conditions for all edges
- Single lane each way traffic load
- Static assumption for tire load
- Two axle vehicle traffic
- 30 kN maximum axle load
- Spot weld failure due to shear force only

1.6. Thesis outline

This research work is presented in four chapters. The outline of these chapters is as follows.

Chapter -1 provides a general introduction on sandwich panels, literature review, and the objectives and the scope of the study.

Chapter-2 covers FEM simulation of sandwich panel including geometry modeling, meshing, boundary condition, and loading.

Chpater-3 presents FEM model verification, parametric study results, and failure analysis.

Chapter -4 describes the conclusions derived from this study and provides recommendations for future research directions.

Chapter 2: FEM Analysis

2.1. General

Finite Element Method (FEM) is a powerful numerical technique in the field of structural analysis to obtain accurate results from a simulation in which an analytical solution is complex enough to be achieved. Moreover, it is usually more practical to run a FEM analysis on a simulated geometry of the structure before implementing the experimental test on a real specimen. In this case, interpreting the FEM results could help significantly reduce the number of tests and as a result, certainly decrease the cost of experiment. Furthermore, usually by verifying the obtained result of a simulated model with an experimental data, FEM demonstrates a satisfactory agreement. However, it should be added that in the verification process, boundary conditions and applied loading assumptions should be manipulated properly. Furthermore, usually the number of elements affects the results significantly. Therefore, in order to present reliable results, a comprehensive understanding of the required assumptions is necessary.

2.2. Finite Element Analysis

This chapter of the study demonstrates the FEM structural analysis of the proposed corrugated steel sandwich panel by means of finite element software ANSYS (ANSYS Release 14.0, 2012). Generally, the FEM analysis consists of three stages; modeling, solving, and post-processing. Modeling phase includes geometrical modeling of the structure, material definition, meshing, and applying boundary conditions and mechanical forces. Solving phase consists of applying load steps under the specific load sequence and solver numerical setting which controls the mathematical method for properly solving nodal displacement equations. Post-processing stage introduces the interpretation and analysis of FEM results in order to find the structural response of the model under the applied loadings.

2.2.1 Geometry modeling

The flexural properties of the corrugated sandwich panel highly depend on the panel cross-section geometry where several parameters influence its behavior. It should be noted that except the face sheet thickness, other contributing geometric parameters are related to the core shape. Therefore, the core configuration plays an important role in the modeling phase. For example, as the number of corrugation changes, panel's stiffness varies. Generally, the corrugations are classified into two categories; continuous and discontinuous. A continuous core is fabricated by folding one steel sheet repeatedly; however, a discontinuous one is fabricated from several steel-sheet cuts. Based on the application of the sandwich panels, core geometries for the panels can be designed in a variety of forms and shapes. The most common core configurations applied in steel sandwich panel fabrication (Kujala and Klanac, 2002) are shown in Figure 2-1.

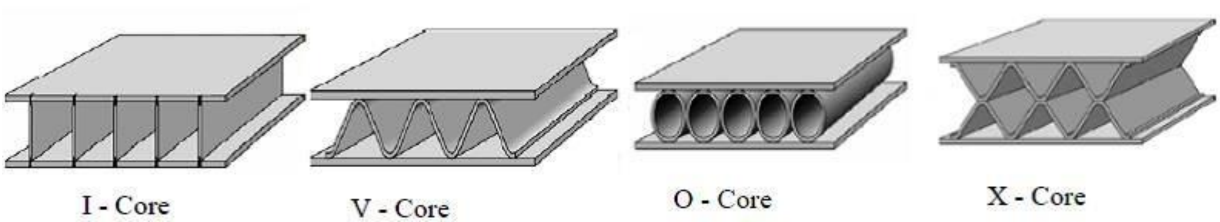

Figure 2-1 Corrugated steel sandwich panel configurations (Adapted from Kujala and Klanac, 2002)

As observed in Figure 2-1, the I- and O- cores are classified as discontinuous cores while the V- and X-cores are called continuous. The selected geometry for the sandwich panel presented in this study is obtained from the experimental work accomplished by Tan et al. (1989). Figure 2-2 illustrates the sandwich panel geometry. It includes upper and lower face sheets and a continuous corrugated core which is a modified V-Core configuration.

The assumed panel's width, length and height are 2.12 m, 5.996 m, and 0.1075 m, respectively. In order to increase the rigidity and strength of the entire panel, two thick surrounding boundary plates are also added to two longitudinal sides of the panel. The longitudinal sides are welded together while assembling several panels to form the entire bridge deck. Thus, the thicker plates installed on the longitudinal sides provide more rigid connection at the interface of two panels.

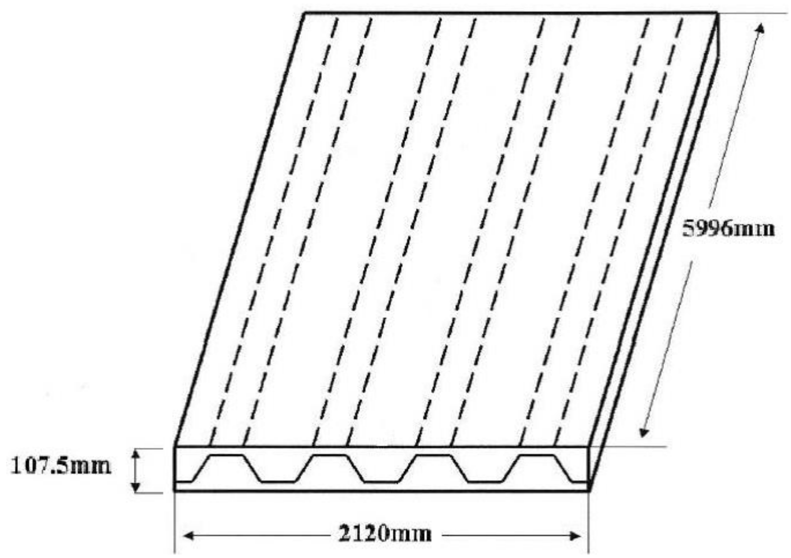

Figure 2-2 Sandwich panel geometry overview

Generally, the core's corrugations are mostly a repeated form of a unique *unit cell* along the panel's cross-section. Figure 2-3 illustrates the detail of the panel's core unit cell that is considered in this study. In the presented simulation, the core includes four similar unit cells. At each unit cell, core sheet is attached to face sheets by four paths of spot welding through the depth; two paths of spot welds attach the core to the top sheet and two other paths attach it to the bottom sheet. Each path consists of equal number of spot welds through the depth of panel. The distance between the two spot welds in a same path is called *weld spacing* which is considered as a design parameter in the study.

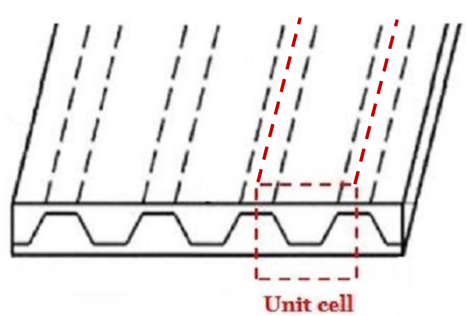

Figure 2-3 Sandwich panel corrugated core cross-section

The thickness of face and core sheets are assumed to be the same i.e. to 2.5 mm. However, in order to investigate the effect of thickness on the structural behaviour of panel, the thickness varies in the range of 2.5 mm to 6 mm. Figure 2-4 shows the assumed unit cell dimensions.

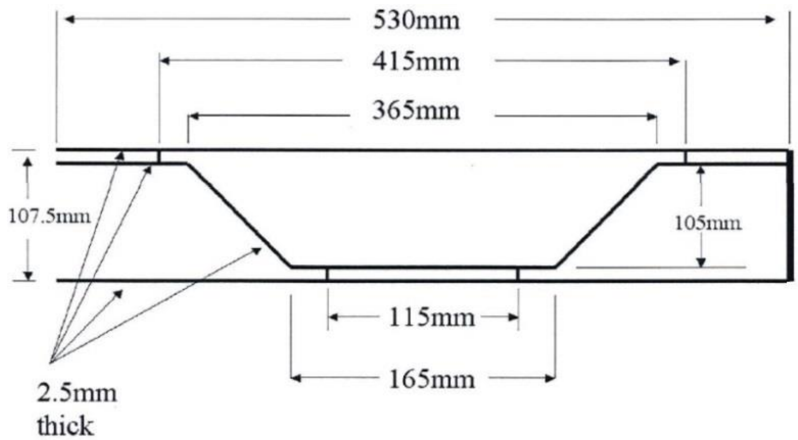

Figure 2-4 Corrugated core unit cell geometrical properties

The thickness of the sandwich panel, or in other words, the height of the unit cell is assumed to be 107.5 mm which is also considered as a design parameter. Since the spot weld elements are applied at the interface of the core and face sheets in meshing phase, a 1.25 mm gap is considered between the two sheets. The unit cell includes one corrugation as the core segment which is connected to bottom and top face sheets with two weld paths at the distance of 115 mm and 415 mm, respectively.

In order to reduce the complexity of geometry in FEM simulations, one of the common modeling techniques is the application of symmetry planes. This method helps present a modified geometrical model with a fewer number of elements which leads to less numerical computation by FEM software and also quicker run time. Therefore, two planes of symmetry at the length and width centerlines are applied to the presented sandwich panel that divide the model into four equal sections. Figure 2-5 indicates the symmetry lines in longitudinal and transverse directions. The shaded section shows the quarter model which will be analyzed in the next chapter.

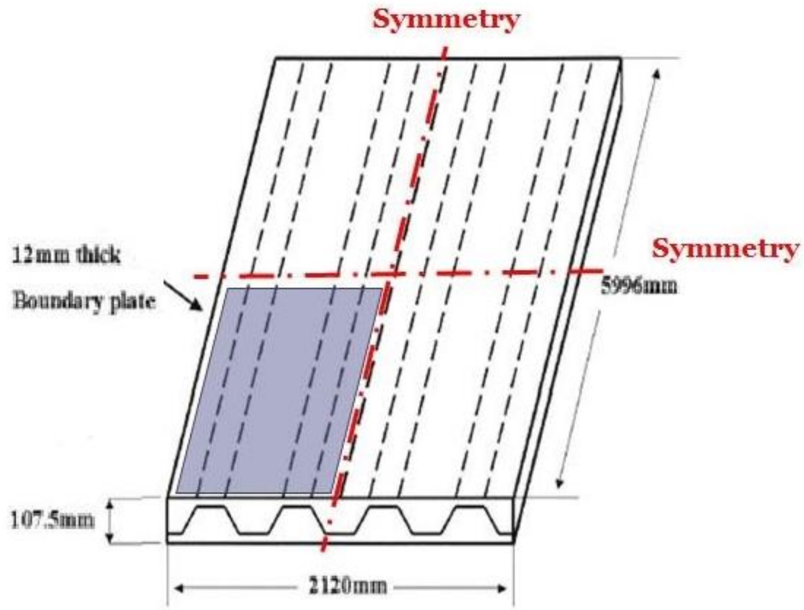

Figure 2-5 Applied symmetry lines in longitudinal and transverse directions

The cross-section shown in Figure 2-6 presents the one-quarter of panel face and core sheets configuration under the symmetric boundary conditions. The one-quarter panel includes two unit cells and its length and width decreases to 2998 mm and 1060 mm, respectively, which are half length in comparison with the original panel.

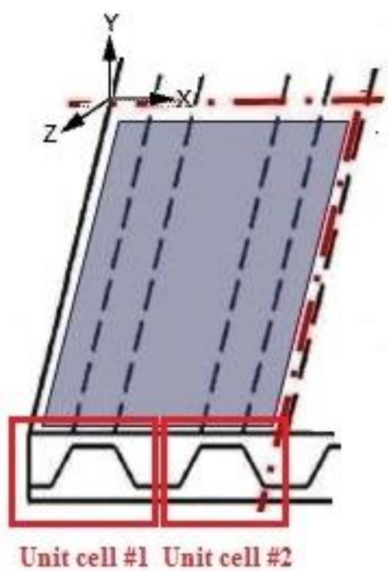

Figure 2-6 Quarter panel with two unit cells

2.2.2 Meshing

One of the steps in FEM modeling which plays a significant role in obtaining a converged solution is to introduce proper meshing for the simulated geometry. Generally, there are two key factors which should be taken into account in the meshing process: meshing size and element types. In order to perform an efficient run, it is recommended that the number of elements should not exceed convergence limit. The convergence limit refers to the number of elements in a meshed model in which increasing the number of elements above the limit does not change the model response significantly. It is noted that as the number of elements increases more than the convergence limit, the run time gets longer remarkably. It is true that a finer mesh leads to more accurate results. However, a model with a higher number of elements requires a higher amount of computer memory and time to be consumed. Since there is no significant difference in terms of accuracy of the output results of the model with a certain number of elements more than the convergence limit, the minimum number of elements is needed to experience a converged solution.

In the current study, the core and face sheets are meshed with SHELL181 element obtained from ANSYS element library (ANSYS Release 14.0, 2012). SHELL181 element is a reasonable choice to analyze thin to moderately-thick shell structures. The element offers a 4 noded rectangular shape with six degrees of freedom at each node: translations in the x, y, and z directions, and rotations about the x, y, and z-axes. According to ANSYS element library, the SHELL 181 is a well-suited element for large strain nonlinear applications. Although SHELL 181 is a two dimensional element, the sheet thickness can be added to the element properties through real constant adjustment. Furthermore, BEAM188 element is also selected to mesh spot welds at the interface of core and face sheets. The spot weld simulation will be discussed in detail later. Figure 2-7 shows the nodes, coordinate system, and general shape of these elements.

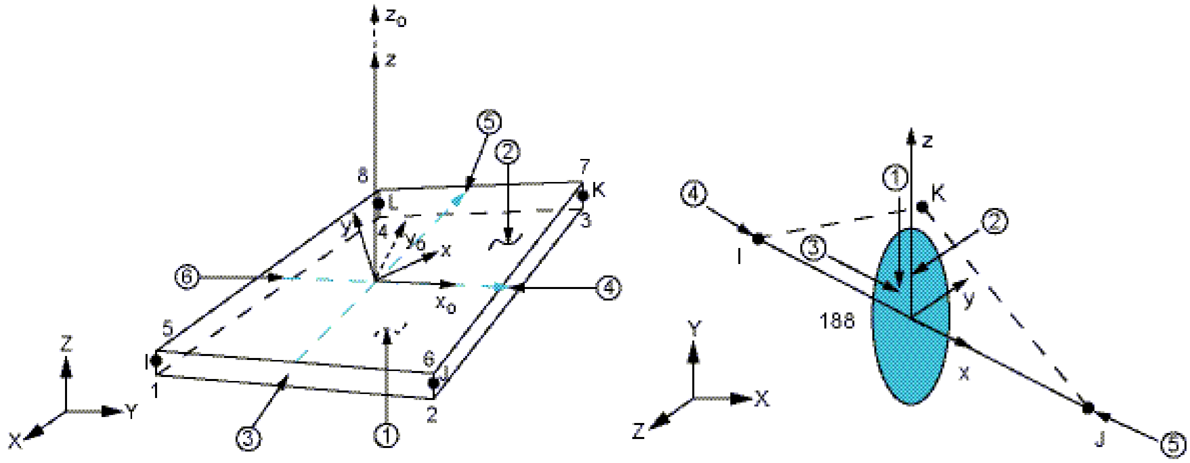

Figure 2-7 Element geometrical shape for Shell 181 element (left picture) and Beam 188 element (right picture). (ANSYS Release 14.0, 2012)

As mentioned earlier, a convergence study is performed to obtain the required number of shell elements. In this study, two main mechanical responses of the panel are considered to assess the numerical convergence of the model. Maximum global deflection of the panel and maximum shear force at spot welds are the two responses which are considered as converging variables to justify the required number of elements. Figure 2-8 presents convergence of the variables in terms of the number of elements. As it is seen, the rate of change of the obtained result decreases as the number of elements increases. Based on the panel maximum deflection graph, the deflection increases from 8.01 mm to 8.11 mm for the FEM models with 48,000 and 65,000 elements, respectively, which denotes 1.2% increase in deflection. Regarding the maximum shear force, the same increase in the number of elements changes the shear force by 0.18%. Therefore, the FEM model with approximately 65,000 elements is opted to be used in FEM analyses in this study.

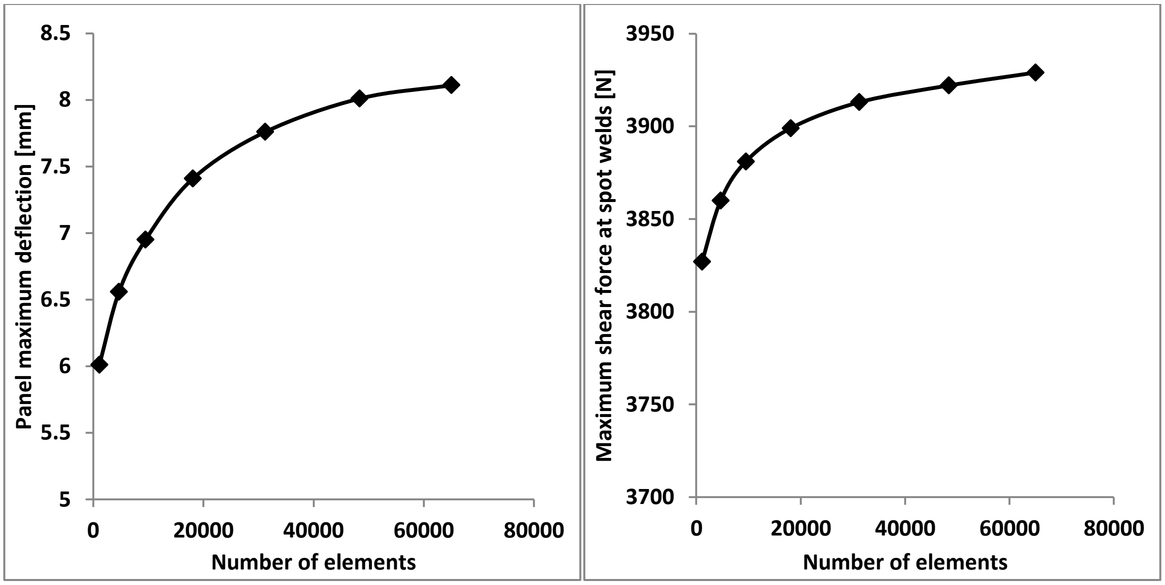

Figure 2-8 Element convergence study for two responses of panel maximum deflection (left side figure) and maximum shear force (right side figure) at spot welds

Before finishing the meshing step, the material properties should be also attributed to the element's properties. As mentioned earlier, the selected material for both face and core sheets is stainless steel which is characterized as a bilinear material. Table 2-1 shows the considered assumptions for the mechanical properties of steel.

Table 2-1 Assumed mechanical properties for steel material applied to face and core sheets and spot weld

Steel mechanical properties	
Modulus of Elasticity (GPa)	209
Poisson's Ratio	0.3
Density (kg/m^3)	7800
Yield Stress (MPa)	310
Post Elastic Stiffness (GPa)	1.23

Since there is no filler material in the spot welding process, the simulated welds have the same material properties as of the entire panel. Figure 2-9 shows the quarter panel with meshing.

Figure 2-9 Quarter panel with meshed elements

2.2.3 Boundary conditions

Regarding the boundary conditions, based on the test setup used by Tan et al. (1989), the sandwich panel is assumed simply supported on all sides. As shown in Figure 2-10, the nodes located on the left and front sides of one-quarter model have zero displacement in Y direction. The displacement of all nodes located on the symmetry planes is restricted to in-plane movement and there is no translation perpendicular to the plane of symmetry. It should be added that due to thick surrounding boundary plates around the panel, the side plates are assumed to be rigid in comparison with core and face sheets, thus, all the nodes placed on the side plates are assumed to have negligible Y-direction displacement.

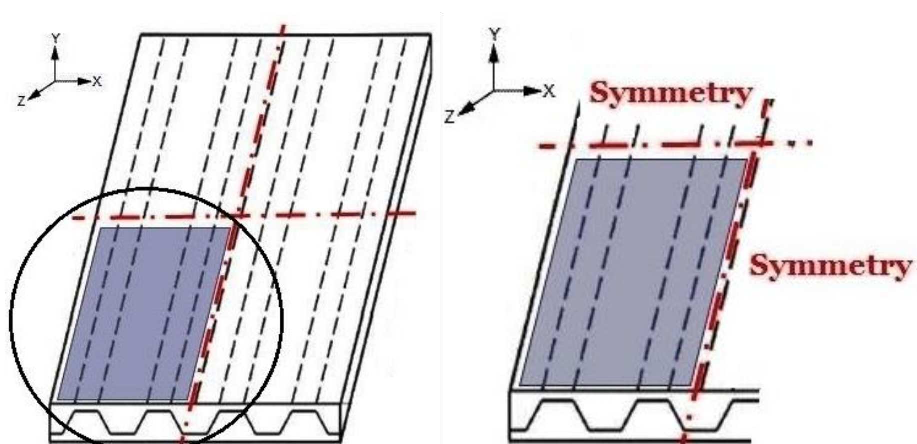

Figure 2-10 Applied boundary conditions on steel sandwich panel

2.2.4 Weld modeling

The welding technique investigated in this study is resistance welding known as spot welding. The welding process is a thermo-electric process that generates heat at the interface of two metal sheets by conducting electrical current through the electrode heads to the metal parts. Spot welding is also one of the available fabrication techniques to attach the core and face sheets together at their interfaces. The welding process includes heating up two electrodes by means of resistance to the electric current. This method is a quick and easy process in which there is no need to apply fluxes or filler metal to create a joint and it can be performed without any special skill. The process can be also carried out by automated machines to speed up production. Spot welding can be applied to many different metals, and can join plates with different thicknesses to each other. Sheets as thin as 0.25 inch can be spot welded and multiple sheets may be joined together at the same time as well. As described earlier, Figures 1-2 and 1- 4 demonstrate two types of spot welding machines; two-sided and single-sided spot weld. Two-sided machine which is the most common one has two same electrodes. However, in the single-sided spot welder the second electrode is replaced with a table. The main purpose of using the new machine is the spot welding of closed area sections in which the second electrode cannot be placed on the other side of attaching plates. In other words, in order to attach the bottom face sheet to the core, the common spot welder with two electrodes can be applied. In the next step, in order to connect the top face sheet to the core due to closed area between the bottom sheet and core, the second electrode cannot move through the depth of sandwich panel. Therefore, by the application of single-sided welder, the whole panel sits on the welding table and one electrode is placed above the top sheet. So, the panel can be moved easily on the table to implement the welding process along the panel's length using the electrode on the top sheet.

Regarding the FEM simulation of the spot weld, ANSYS is utilized with the spot weld feature which connects two adjacent nodes on attaching plates by introducing a beam element in the considered tiny gap between the two sheets. The feature also adds a contact interface between the two sheets at weld locations to prevent the possible sheets penetration into each other in the case of large deformation. Furthermore, the feature is also capable of considering electrode's diameter effect by applying constraint equations to the nodes on both sheets at the vicinity of beam elements. Based on the selected electrode diameter, the ANSYS spot welding feature constraints all of the nodes located inside the weld circle on both sheets in a way that they all have same displacement. Therefore, the electrode head diameter feature guarantees the perfect simulation of fused zone in spot welding process.

According to the spot weld wizard in ANSYS, the beam element is assigned as a rigid connection by default. However, there is no doubt that the weld, itself, may experience deflection or even detaching failure. Moreover, the rigid connection makes the entire simulated panel stiffer than the real fabricated one. Therefore, the rigid assumption is not valid. In order to set the beam element's attributions, the weld modeling process should be implemented by manual option instead of automatic wizard. Thus, by assigning the same mechanical properties of the steel material (Table 2-1) to the BEAM188 element the weld behavior is simulated with the same stiffness as face and core sheets.

In order to perform the weld simulation, BEAM elements are placed at the interface of two SHELL elements along straight paths through the depth of panel with an assigned weld spacing. One of the parameters which plays a significant role in the panel's stiffness is the distance between spot welds; the distance between two welds on the same weld path through the depth of sandwich panel. If the distance decreases, the number of welds will increase and as a result, the panel will be much stiffer. However, due to the fact that the panel design should be optimized in terms of the number of required welds, the weld spacing should be limited to a maximum value. In this chapter, the effect of the weld spacing is investigated on the panel deflection and the shear force distribution. Figure 2-11 shows the spot welding location in the quarter panel cross-section. As observed, four paths are located on top and four paths are located on the bottom face sheet.

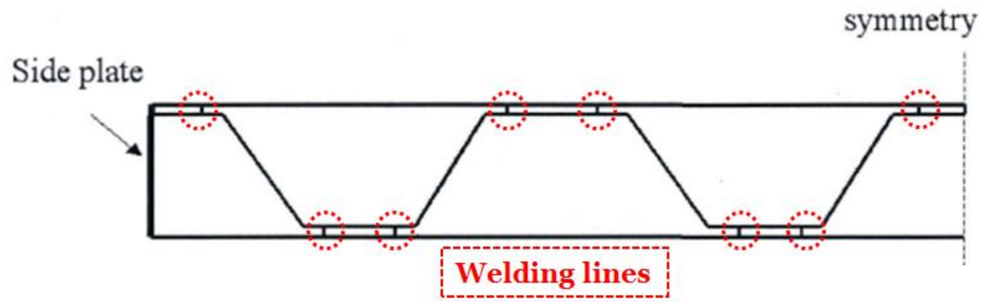

Figure 2-11 Applied welding lines through the corrugated core at top and bottom face sheets

Once the spot welding process is completed, the diameter of the final fused zone at weld spots becomes smaller than the electrode's diameter. The fused zone diameter depends on electrode head diameter, holding time, and weld force. Therefore, the fused zone diameter is considered in the weld simulation in ANSYS assuming a 5 mm radius (CMW, 2014). It should be added that ANSYS applies the radius to the beam element with a circular cross-sectional area. As a result, the displacement of the nodes on either top or bottom sheet located within the radius distance of a spot weld are the same. Figure 2-12 illustrates the position of eight welding paths on the upper face sheet of the complete panel by dashed lines.

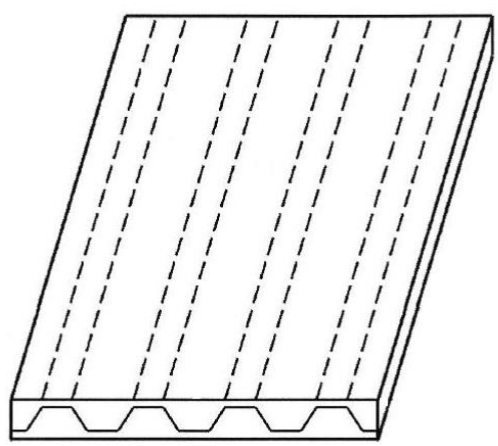

Figure 2-12 Applied welding lines showed only on top face sheet.

2.2.5 Loading

One of the design requirements for the sandwich panel is working load limit. Regarding the application of the panel as a small bridge deck, the load limit is considered based on the light-weight vehicles passing over the bridge with the restriction of maximum total weight of 5000 kg. The bridge deck traffic pattern is assumed single lane at each direction with the total width of 6 m. Due to the fact that panel installation layout may affect the load distribution over the deck, the assembly of panels configuration should be taken into account. As it was shown in Figure 1-1, each panel is installed along the width of the bridge deck on top of the girders. The connection of two adjacent panels at their interface is provided by arc welding along the length of panels on both top and bottom edges. Furthermore, in order to attach panels to girders, they can be bolted or welded together along the width of panels at the edge of girder flange.

According to the bridge traffic pattern assumption and panels' assembly arrangement, the deck may experience different loading scenarios by overpassing vehicles. Based on the maximum applied moment, the worst case scenario is passing of two 5000 kg two-axle cars side by side driving on opposite directions. Regarding the maximum tire load distribution, the worst case scenario occurs when the wheel base, the distance between the centers of the front and rear wheels, for vehicle is less than 2120 mm and, therefore, the total weight of the vehicle transfers to a single panel. However, it is noted that in this case the tire position on panel will be close to panel's longitudinal underneath supports. Since in terms of experiencing maximum deflection, the tire load should be applied at the longitudinal centerline of panel the described loading scenario is not of interest. The next loading scenario is passing of two vehicles following each other on each lane. Therefore, the rear wheels of the front car and the front wheels of the rear car can be located on a single panel. Figure 2-13 illustrates the described traffic pattern on three adjacent sandwich panels. As it is shown, four axles from four vehicles are located on middle panel.

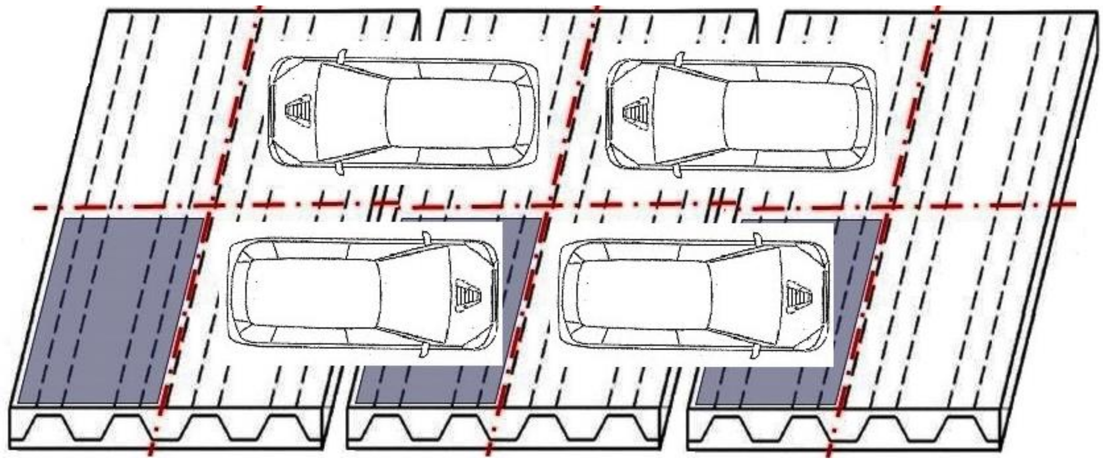

Figure 2-13 Traffic pattern assumption for vehicles on bridge deck

According to the applied longitudinal and transverse symmetry lines in panel FEM simulation, all axle loads are assumed equal. Although the front and rear axle loads are usually 40% and 60% (Canadian Highway Bride Design Code, 2005), respectively, in order to simulate the tire load symmetrically, the assumed axle load for all vehicles is 3000 kg. The transferred load from each axle acts as a uniform distributed load over two equal areas with the foot print of 10 cm by 40 cm on the panel. Due to considering the maximum applied moment scenario, the vehicle position is considered closer to the longitudinal centerline of the bridge deck. Figure 2-14 shows the location of the applied load on the panel.

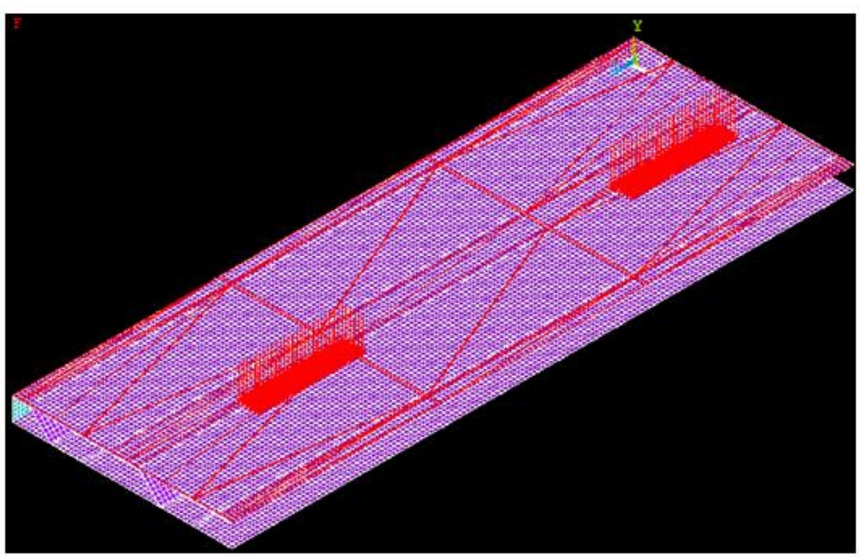

Figure 2-14 Simulated quarter sandwich panel in ANSYS with added tire load on top face sheet

Apart from the vehicle loading, the applied dead load due to the weight of the road pavement should be also considered on top of the panels. Therefore, a uniform distributed load of 10 kN/m^2 is applied over the entire panel. It should be mentioned that in this study, the axle loading is considered as a static load, and effects of snow and dynamic loading are ignored. Figure 2-14 presents uniform distributed load over entire top surface as well as the two tire loads which are uniformly distributed over the tire foot prints.

Chapter 3: Results

3.1. General

This chapter presents the results obtained from FEM analysis on the simulated sandwich panel. First, the mechanical response of the model is validated with the Tan et al. (1989) experimental results. Then, a parametric study is established to demonstrate the effect of geometric parameters on the mechanical behavior of the panel. Therefore, the contribution of each parameter on the panel maximum deflection and the maximum shear force at spot welds are investigated and, thereafter, regression equations for the two responses are presented. Finally, the spot weld failure scenarios of the steel sandwich panel under excessive applied loading are studied.

3.2. Finite element model verification

It is necessary to proof the accuracy of the presented sandwich panel's FEM simulation before analyzing the effect of geometric parameters. Therefore, first, obtained result from the FEM model should be validated by the experimental test conducted on the same model. Considering the experiment performed by Tan et al. (1989), numerical and experimental results can be compared. However, it should be noted that the only difference is in applied mechanical loading since Tan et al. (1989) only considered uniformly distributed load on the top face sheet rather than the tire load. Therefore, in order to validate the presented model, the loading condition in the FEM model is increased up to 14 kN/m^2 as noted by Tan et al. (1989). Figure 3-1 presents the test results obtained by Tan et al. (1989). As it is seen, the plotted reference response indicates the panel maximum deflection variation versus the applied load. The test has been performed for two boundary conditions (BCs); simply supported in all edges of panel and simply supported only at two ends. The obtained test results were also compared with a FEM simulation and analytical solution results. In order to carry out the comparison, Tan et al. (1989) increased the distributed load up to 14 kN/m^2 and the mid span deflection values were recorded at 10 loading points.

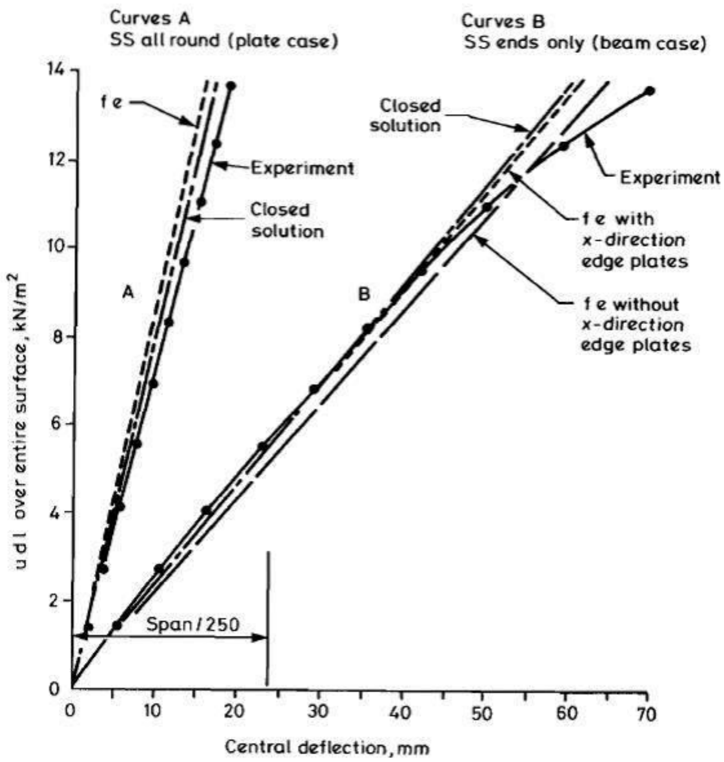

Figure 3-1 Obtained results by Tan et al. (1989) for two models with different boundary conditions in a closed form, experimental, and FEM methods (Tan et al., 1989)

The illustrated graph indicates three considerable notes. First, as the applied load increases, in both cases, the difference between experiment and FEM or closed solution results increases. However, all of the three results are in an acceptable range of correlation. Second, the model with simply supported boundary condition in all edges shows a more linear behavior in comparison with the simply supported boundary condition in only two ends, specifically, for a higher amount of loadings. Third, all edges with a simply supported boundary condition show remarkably lower deflection with the same amount of loading in comparison with the two edges with simply supported boundary condition. According to the desired panels' assembly as bridge deck and also based on the attachment between panels and the girder supports underneath, the all-around simply supported model is in the scope of the presented study. Therefore, the FEM model validation is performed based on the comparison of the results of ANSYS simulation with the Tan et al. (1989) experimental result shown as curve A in Figure 3-1. Regarding the ANSYS output results, Figure 3-2 shows the vertical deflection distribution in Y axis direction for the simulated panel at the last load step of the applied loading of 14 kN/m^2.

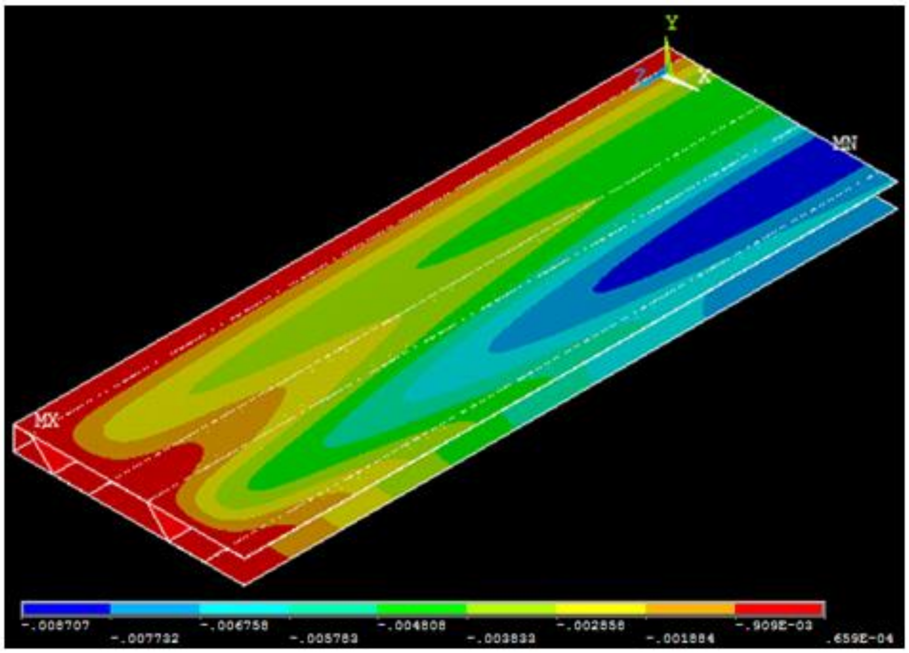

Figure 3-2 Displacement contours in Y-direction for the quarter panel simulation

The red shaded region refers to zero deflection while the dark blue region denotes the maximum vertical deflection in panel. As it is expected, based on the applied simply supported boundary conditions, both left and bottom edges experience zero deflection and the maximum deflection occurs at the top right corner of the model indicating the center point of full-size panel. However, it is noted that due to the shape of the corrugated core, the node with maximum deflection is located at the center of the unit cell rather than the center point of the whole panel. The main reason of such a behavior at the top face sheet is due to the less stiffened face at the center of the unit cell than the center point of the panel stiffened by attaching core and face plates.

Figure 3-3 illustrates the comparison of ANSYS FEM results with Tan et al. (1989) experimental work. The graph depicts a close correlation between the two results. As can be seen, at loading value of 14 kN/m^2, the deflection magnitude difference between these two results is around 5%, which is very close to the difference of FEM and experimental results presented by Tan et al. (1989) in curve A in Figure 3-3. There are several reasons that may contribute to the difference as follows.

- Human error can be involved in setting up the experiment, whereas in FEM simulation this type of error does not contribute.

- Material properties assumption in FEM simulation may not exactly matched with the properties of steel material used in test sample fabrication.

- Material homogeneity in FEM simulation is an ideal assumption, whereas the actual material may not be fully homogeneous.

- The boundary conditions applied in FEM model may not be exactly applied symmetrical in test setup.

- Load sensors and deflection measurement instruments may cause some errors in obtained results.

- The shell element which is employed to mesh the steel sheets does not reflect the stress variation through the thickness.

After validation of the FEM simulation, the parametric analysis can be accomplished based on the model mechanical responses.

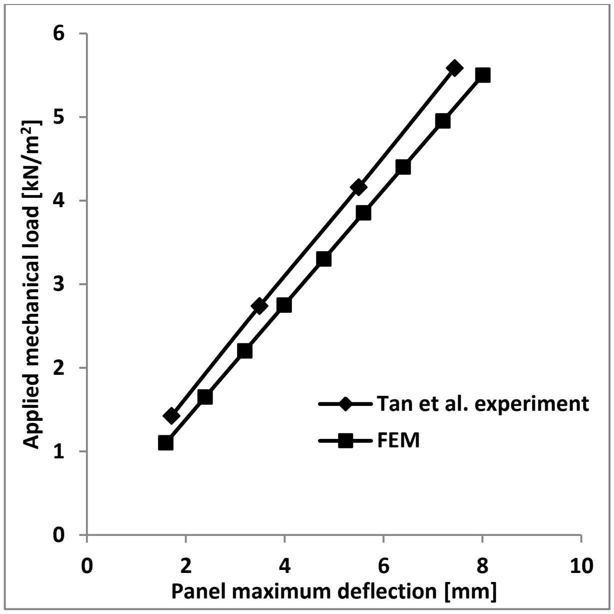

Figure 3-3 Simulated FEM model verification with Tan et al. (1989) experimental work

3.3. Parametric study

One of the most significant criterion which should be taken into account in steel bridge design process is the dead load due to the weight of structures, specifically, the weight of bridge deck. With a fixed substructure sizing, a higher amount of dead load remarkably decreases the live load capacity of the bridge deck. In addition, with the same live load capacity, a lighter deck leads to a smaller size of girders and piers by which the cost of construction may significantly reduce. Furthermore, it could help design a bridge with a fewer number of piers or longer spans. Thus, due to decreasing the construction cost, fewer number of column and girder are more desirable in designing the substructure of a bridge. Therefore, in order to meet this essential objective, bridge superstructure should be designed based on the minimum possible weight.

Regarding satisfying the critical objective, in this proposed research, a concrete deck is suggested to be replaced with steel sandwich panels in order to reduce the superstructure's weight in small bridge deck applications. Based on the average density of reinforced concrete in the range of 2500 to 2600 kg/m^3, the applied dead load due to a concrete slab with 30 cm thickness would be approximately 750 kg/m^2. On the other hand, the dead load of the proposed sandwich panel with an adequate live load capacity for a small bridge would be approximately 250 kg/m^2. Therefore, by using the sandwich panel the dead load can be reduced up to 65%. However, it should be noted that the sandwich panel application is limited to small bridges in which there is a load limit and restriction for passing vehicles.

The sizing of sandwich panel plays an important role in improving the mechanical performance of the assembled deck. Therefore, optimizing the panel's geometry to obtain maximum flexural properties and at the same time minimum weight is of great interest. The presented parametric study investigates the effect of geometric parameters on the mechanical response of the sandwich panel. The two most important responses which should be taken into account are the face sheets deflection and the shear stress distribution on spot welds. Due to the fact that the finished surface of the deck on top of the panel is pavement, the panel's deflection should be controlled to prevent cracking in the pavement. Furthermore, since the limited shear capacity of spot welds play an important role in the structural integrity of the panel, the shear force magnitude in spot welds should be minimized.

At the first stage, five geometric parameters are chosen as input factors including: core and face sheet thicknesses (T_c and T_f, respectively), distance between two adjacent welding paths in the unit cell in transverse direction (P), spot weld spacing in the longitudinal direction (S), and spot weld radius (R). Variation of each factor has its own pros and cons on the considered responses. For instance, increasing core and face sheet thicknesses leads to a stiffer structure; however, it increases the weight of panel remarkably. By increasing the weld spacing the number of spot welds decreases and as a result, the manufacturing time and fabrication cost drop, however, the panel deflection and the shear force on welds increase significantly. So, the advantages and disadvantages of the variations should be balanced to reach the desired mechanical properties. In addition, not only a single factor, but also the combination of factors, known as *Interaction*, may have significant effect. Factors' interaction is the effect of combination of two or more input factors on output response. If only two input factors are considered, the interaction is called first-order interaction and the interaction obtained from three or more factors is called second or higher-order interaction. In the presented study, only the effect of first-order interaction is analyzed. The interactions include [SR], [ST_c], [ST_f], [SP], [RT_c], [RT_f], [RP], [T_cT_f], [T_cP], and [T_fP].

Regarding the effect analysis, two levels are assigned for each factor; low level and high level which are shown as [-1] and [+1], respectively. The levels correspond to two values for each parameter by which the FEM models are simulated. In order to obtain the effect of the five input factors on the two mentioned mechanical responses, a full factorial analysis is established including 2^5 runs. These 32 runs which are 32 simulated sandwich panels cover the effect analysis of 5 input factors and 10 first-order interactions. Table 3-1 illustrates the considered input factors along with their values. It should be noted that the listed values for the input factors are selected based on the obtained pre analysis results from the FEM model.

Table 3-1 Input factors used in the parametric study with low and high level values

Parameter	Symbol	Level (mm)	
		Low (-1)	High (+1)
Weld Spacing	S	80	160
Weld Radius	R	5	20
Core sheet thickness	T_c	4	6
Face sheet thickness	T_f	4	6
Weld paths distance	P	65	115

3.3.1 Maximum deflection analysis

As it is mentioned, 32 different FEM models are constructed based on the presented geometry parameters in Table 3-1. Table 3-2 indicates the results obtained from ANSYS for the panel maximum deflection response. Each row represents a FEM model introduced with a set of assigned values for the five input factors. The first-order interaction values are calculated by multiplying the assigned values for the two contributing parameters. For example, the assigned value for [SP] at run number 3 is calculated by multiplying corresponding values of [S] and [P] which means [-1] × [-1] = [1]. It is noted that [-1] and [+1] refer to low and high values of each parameter, respectively.

Table 3-2 Full factorial design with first-order interactions along with panel maximum deflection results

Run No.	**S**	**R**	**T_c**	**T_f**	**P**	**SR**	**ST_c**	**ST_f**	**SP**	**RT_c**	**RT_f**	**RP**	**T_cT_f**	**T_cP**	**T_fP**	**Max Deflection (m)**
1	-1	-1	-1	-1	-1	1	1	1	1	1	1	1	1	1	1	0.0256
2	1	-1	-1	-1	-1	-1	-1	-1	-1	1	1	1	1	1	1	0.0264
3	-1	1	-1	-1	-1	-1	1	1	1	-1	-1	-1	1	1	1	0.0245
4	1	1	-1	-1	-1	1	-1	-1	-1	-1	-1	-1	1	1	1	0.0255
5	-1	-1	1	-1	-1	1	-1	1	1	-1	1	1	-1	-1	1	0.0158
6	1	-1	1	-1	-1	-1	1	-1	-1	-1	1	1	-1	-1	1	0.0162
7	-1	1	1	-1	-1	-1	-1	1	1	1	-1	-1	-1	-1	1	0.0156
8	1	1	1	-1	-1	1	1	-1	-1	1	-1	-1	-1	-1	1	0.0159
9	-1	-1	-1	1	-1	1	1	-1	1	1	-1	1	-1	1	-1	0.0146
10	1	-1	-1	1	-1	-1	-1	1	-1	1	-1	1	-1	1	-1	0.0157
11	-1	1	-1	1	-1	-1	1	-1	1	-1	1	-1	-1	1	-1	0.0141
12	1	1	-1	1	-1	1	-1	1	-1	-1	1	-1	-1	1	-1	0.0149
13	-1	-1	1	1	-1	1	-1	-1	1	-1	-1	1	1	-1	-1	0.0097
14	1	-1	1	1	-1	-1	1	1	-1	-1	-1	1	1	-1	-1	0.0098
15	-1	1	1	1	-1	-1	-1	-1	1	1	1	-1	1	-1	-1	0.0097
16	1	1	1	1	-1	1	1	1	-1	1	1	-1	1	-1	-1	0.0097
17	-1	-1	-1	-1	1	1	1	1	-1	1	1	-1	1	-1	-1	0.0228
18	1	-1	-1	-1	1	-1	-1	-1	1	1	1	-1	1	-1	-1	0.0262
19	-1	1	-1	-1	1	-1	1	1	-1	-1	-1	1	1	-1	-1	0.0224
20	1	1	-1	-1	1	1	-1	-1	1	-1	-1	1	1	-1	-1	0.0233
21	-1	-1	1	-1	1	1	-1	1	-1	-1	1	-1	-1	1	-1	0.0123
22	1	-1	1	-1	1	-1	1	-1	1	-1	1	-1	-1	1	-1	0.0151
23	-1	1	1	-1	1	-1	-1	1	-1	1	-1	1	-1	1	-1	0.0117
24	1	1	1	-1	1	1	1	-1	1	1	-1	1	-1	1	-1	0.0132
25	-1	-1	-1	1	1	1	1	-1	-1	1	-1	-1	-1	-1	1	0.0139
26	1	-1	-1	1	1	-1	-1	1	1	1	-1	-1	-1	-1	1	0.0149
27	-1	1	-1	1	1	-1	1	-1	-1	-1	1	1	-1	-1	1	0.0136
28	1	1	-1	1	1	1	-1	1	1	-1	1	1	-1	-1	1	0.0141
29	-1	-1	1	1	1	1	-1	-1	-1	-1	-1	-1	1	1	1	0.0084
30	1	-1	1	1	1	-1	1	1	1	-1	-1	-1	1	1	1	0.0087
31	-1	1	1	1	1	-1	-1	-1	-1	1	1	1	1	1	1	0.0083
32	1	1	1	1	1	1	1	1	1	1	1	1	1	1	1	0.0085

As observed in Table 3-2, in addition to the five input factors only first-order interactions are considered while higher-order ones are neglected. Based on the obtained ANSYS results, the effect of each parameter is calculated by subtracting low average value from high average value. Low and high averages of a parameter denote the means of sixteen responses in which the factor corresponding value is (-1) and (+1), respectively. The obtained effect values show the contribution of each parameter on changing the output response. It is noted that the positive effect value means that increasing the input factor increases the output response while the negative effect value indicates that increasing the input decreases the output. Since the input factors are coded to (-1) and (+1), and as a result, the coded factors have the same order where the magnitude is a representative of the sensitivity of the factor to the response. As the magnitude of a factor increases the response becomes more sensitive to that input factor.

Table 3-3 illustrates the high and low averages, the obtained effect values for the five input factors, and first-order interactions based on the obtained deflection values. In order to visualize the contribution of each parameter on the output variation, the normalized effect of each factor and interaction is calculated based on absolute values of effects. The percentage of the normalized effect shows the contribution of factors in the maximum deflection of the panel. As it is seen, [T_c] and [T_f] are the factors with the highest contributions with the same effect value of 41%.

Table 3-3 Parameters effect values for the panel maximum deflection response

	[S]		**[R]**		**[T_c]**		**[T_f]**		**[P]**	
	High	Low	High	Low	High	Low	High	Low	High	Low
Average	0.0161	0.0152	0.0153	0.0160	0.0118	0.0195	0.0118	0.0195	0.0148	0.0165
Effect	0.0009		-0.0007		-0.0078		-0.0077		-0.0017	
Normalized Effect	0.050		0.038		0.413		0.412		0.088	

Furthermore, in order to qualitatively compare the factors contributions in panel's maximum deflection response, the effect plot in Figure 3-4 is presented. As can be seen, the horizontal axis shows two levels of [-1] and [+1], while the vertical axis indicates the associated deflection response value. The effect plot denotes key points, i.e., the qualitative comparison of effect magnitudes for all input factors. The slope of the lines indicates the variation of the response value when input factors increase. Therefore, the line with a higher slope shows that the deflection response is more sensitive to the associated input factor. It is noted that positive slope indicates that by increasing the input value the response value increases, while negative slope denotes that by increasing the input value the response value decreases. As Figure 3-4 shows, core and face sheet thicknesses, [T_c] and [T_f], show the highest effect among all factors which is also confirmed on Table 3-3. [T_c] and [T_f] effect plot curves have negative slope which means that as the sheet thickness increases the maximum deflection decreases. [R], [P], and [S] show marginally effect on panel maximum deflection.

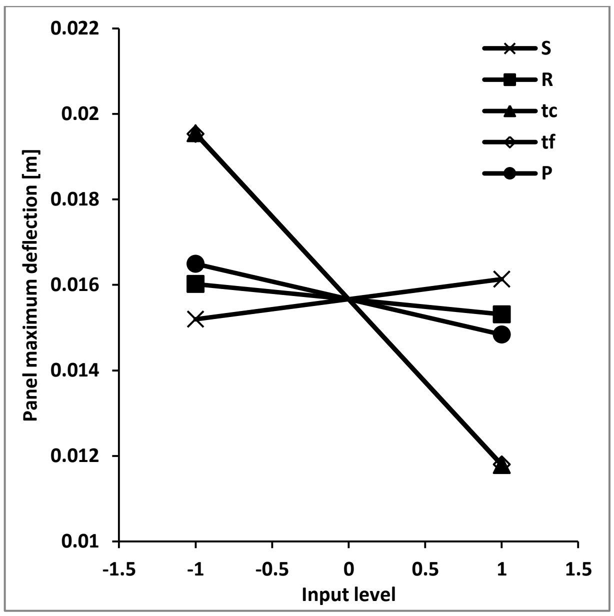

Figure 3-4 Geometric factors main effect plot for sandwich panel maximum deflection response

As mentioned earlier, there are 10 first-order interactions for the five input factors considered in this study. Figures 3-5 (a) to 3-5 (j) demonstrate the interaction effect plots for all first-order interactions. Regarding the effect of interactions, the graphs qualitatively demonstrate the effect value of the associated interaction. The intersection of lines is the main indicator to check if there is any significant interaction. If there is an intersection between the two curves in the range of [-1] to [+1] or it is expected to be an intersection beyond the two points, the interaction of the two associated factors is considerable. The wider angle between the two lines shows that their interaction is more significant. On the other hand, a sharper angle or even the case of parallel lines refers to less significant interaction. The comparison of the all plotted interactions reveals that only [T_cT_f] interaction is relatively significant rather than the other ones.

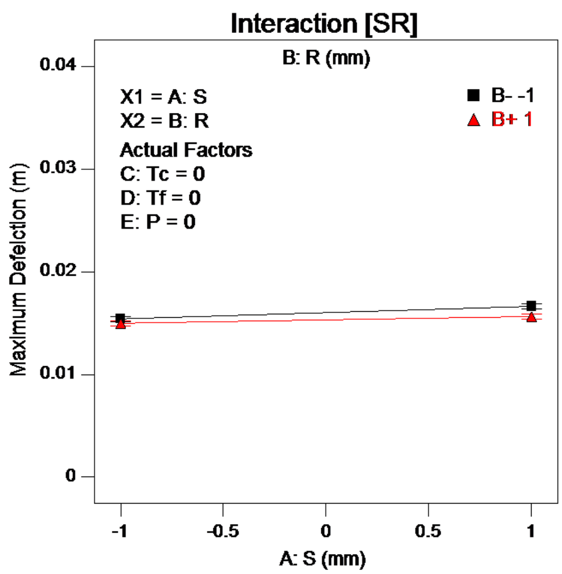

(a)

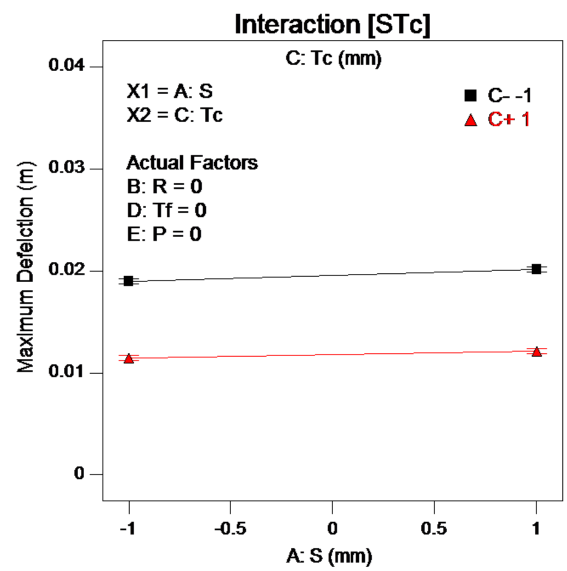

(b)

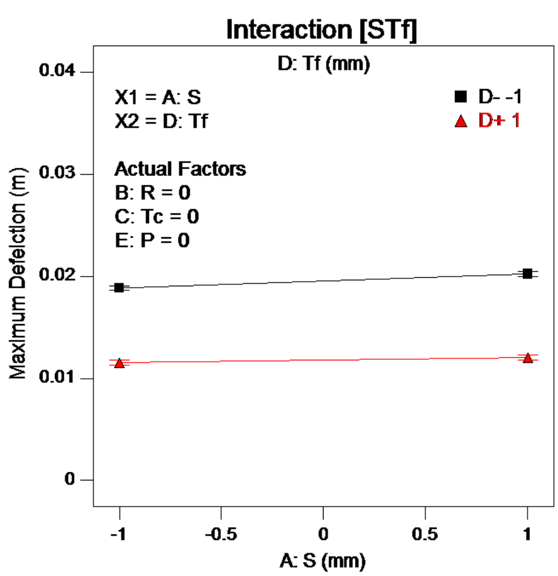

(c)

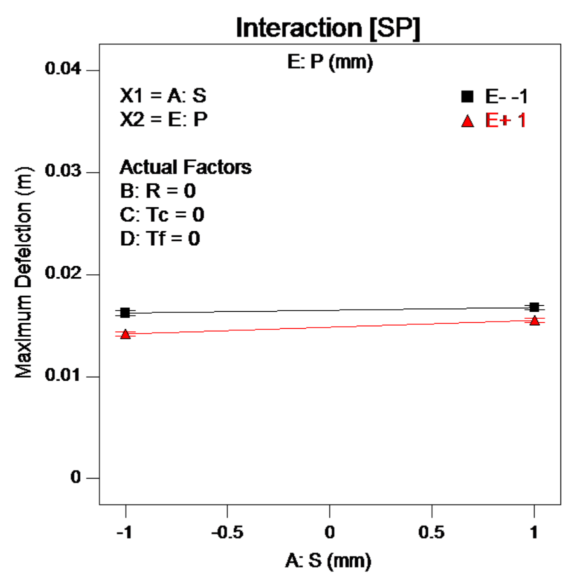

(d)

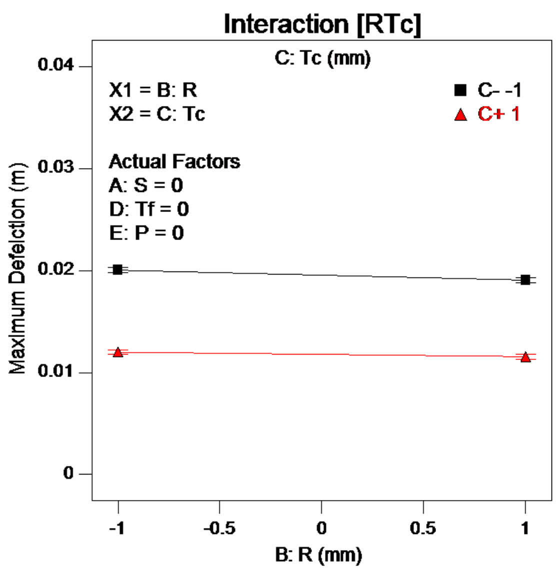
Interaction [RTc]
C: Tc (mm)
X1 = B: R
X2 = C: Tc
C- -1
C+ 1
Actual Factors
A: S = 0
D: Tf = 0
E: P = 0
Maximum Defelction (m)
0.04
0.03
0.02
0.01
0
-1
-0.5
0
0.5
1
B: R (mm)

(e)

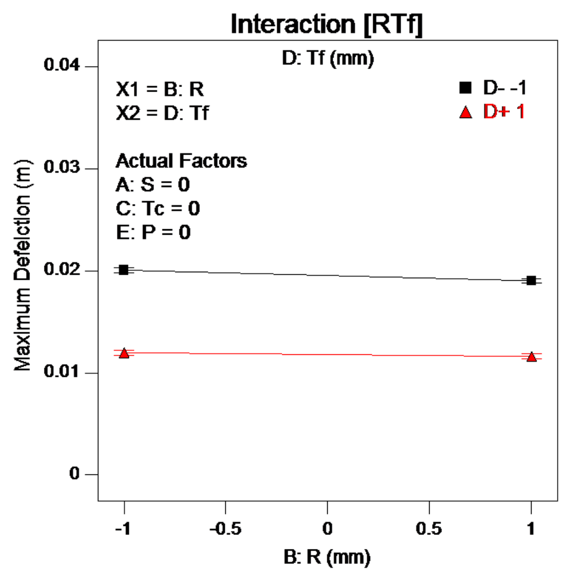
Interaction [RTf]
D: Tf (mm)
X1 = B: R
X2 = D: Tf
D- -1
D+ 1
Actual Factors
A: S = 0
C: Tc = 0
E: P = 0
Maximum Defelction (m)
0.04
0.03
0.02
0.01
0
-1
-0.5
0
0.5
1
B: R (mm)

(f)

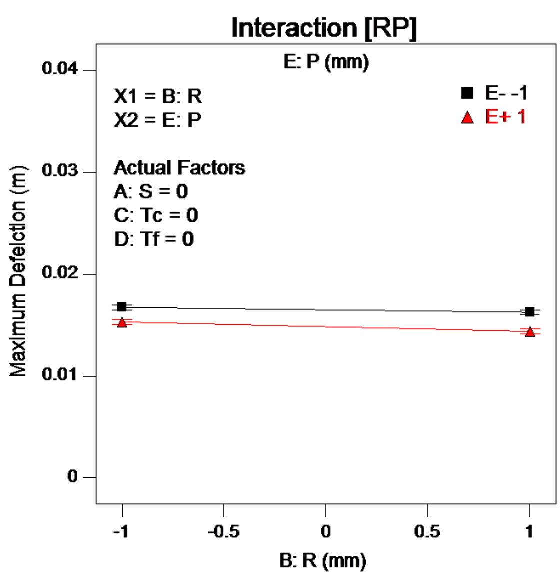
Interaction [RP]
E: P (mm)
X1 = B: R
X2 = E: P
E- -1
E+ 1
Actual Factors
A: S = 0
C: Tc = 0
D: Tf = 0
Maximum Defelction (m)
0.04
0.03
0.02
0.01
0
-1
-0.5
0
0.5
1
B: R (mm)

(g)

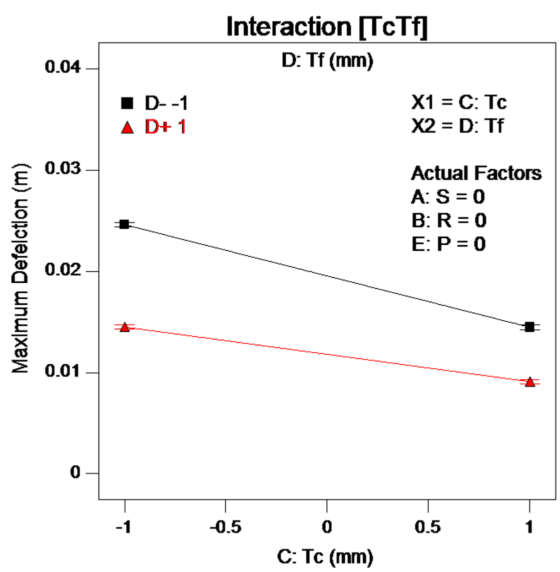
Interaction [TcTf]
D: Tf (mm)
D- -1
D+ 1
X1 = C: Tc
X2 = D: Tf
Actual Factors
A: S = 0
B: R = 0
E: P = 0
Maximum Defelction (m)
0.04
0.03
0.02
0.01
0
-1
-0.5
0
0.5
1
C: Tc (mm)

(h)

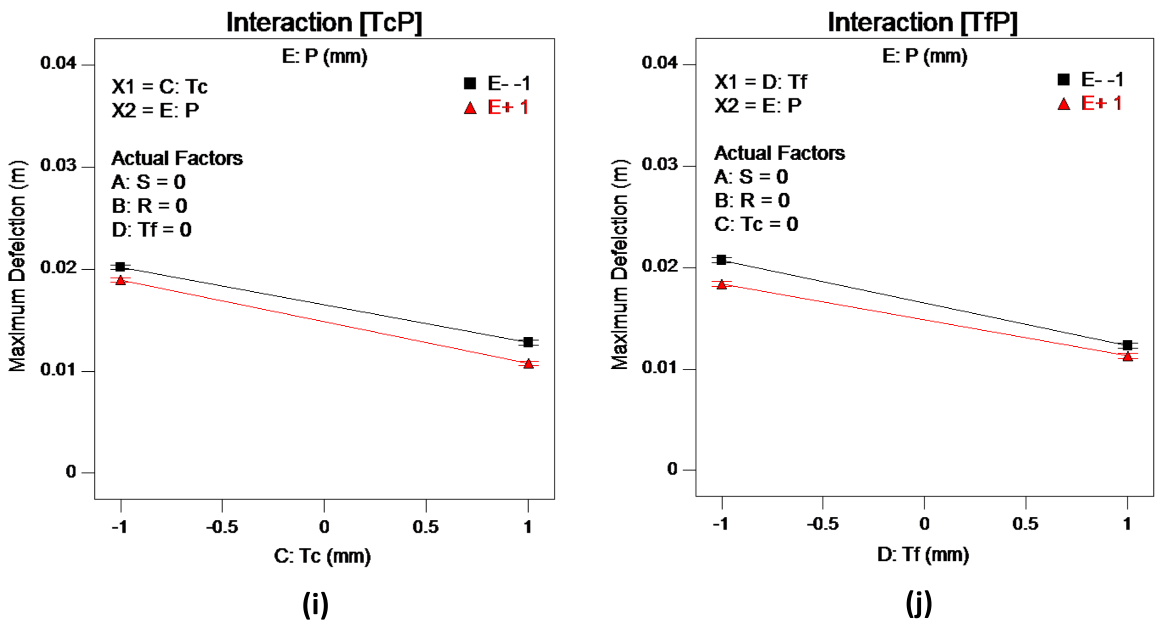

Figure 3-5 Geometric factors interaction effect plots for the panel maximum deflection response; a) [SR], b) [ST$_c$], c) [ST$_f$], d) [SP], e) [RT$_c$], f) [RT$_f$], g) [RP], h) [T$_c$T$_f$], i) [T$_c$P], j) [T$_f$P]

The main advantage of designing the test schedule with 32 runs is to provide a regression model which can mathematically predict the mechanical behaviour of the sandwich panel for further investigation. The mathematical regression simulation links the panel's desired response to the factors and their interactions by introducing a mathematic formula. Based on the order of considered interactions, the accuracy of simulation may change. In this regard, including higher order interactions may lead to more accurate results. The regression equation introduces a polynomial formula which can be presented as a linear or nonlinear relationship in the form of Equation 3.1.

$$y\,(x_1, x_2, \ldots, x_n) = \bar{y} + a_1\boldsymbol{x_1} + a_2\boldsymbol{x_2} + \cdots + a_n\boldsymbol{x_n} + a_{12}\boldsymbol{x_1}\boldsymbol{x_2} + a_{13}\boldsymbol{x_1}\boldsymbol{x_3} + \cdots + a_{nm}\boldsymbol{x_n}\boldsymbol{x_m} \quad (3.1)$$

In this study the applied regression equation components include an intercept term which is the average of responses over entire 32 runs, ($\bar{y}$), main input factor terms, ($a_n x_n$), and first order interaction effects ($a_{nm}x_n x_m$). It should be added that these coefficients can be obtained whether by dividing the calculated effect values in Table 3-3 by two or directly by means of *Data Analysis* toolbox in Excel software. Note that since the effect values are calculated based on the input factors varying in the range of [-1] to [+1], the coefficients in the regression equation are the effects divided by the number of levels which is two. Table 3-4 depicts the coefficients associated with factors and their main and first-order interaction effects.

Table 3-4 list of coefficient values for the regression equation for the factors and first order interactions

Factors	*Coefficients*
Intercept	0.01567
[S]	0.00047
[R]	-0.00035
[T_c]	-0.00388
[T_f]	-0.00387
[P]	-0.00083
[SR]	-0.00014
[ST_c]	-0.00012
[ST_f]	-0.00023
[SP]	0.00020
[RT_c]	0.00013
[RT_f]	0.00017
[RP]	-0.00011
[T_cT_f]	0.00118
[T_cP]	-0.00020
[T_fP]	0.00033

Investigating the coefficients obtained from MS Excel shows that there is a good agreement between the results and the effect plot presented in Figure 3-4. [T_c] and [T_f] have the largest coefficients (-0.0038) and their interaction, [T_cT_f], has the next larger contribution (0.00118). The effect magnitudes of nine other interactions are not significant in comparison with the main factors effects. However, the most noticeable interaction after [T_cT_f] would be [T_fP] with a contribution of 0.00033. Equation 3.1 presents the general form of a second order polynomial equation in the regression study. In order to obtain the governing mathematical equation, the coefficients shown in Table 3-4 are inserted into Equation 3.1 by substituting

(a_n) and (a_{nm}) values. The obtained mathematical equation presenting the panel maximum deflection is shown in Equation 3.2.

$$y\,(x_1, x_2, \ldots, x_n) = 0.01567 + 0.00047\,\boldsymbol{S} - 0.00035\,\boldsymbol{R} - 0.00388\,\boldsymbol{T_c} - 0.00387\,\boldsymbol{T_f} - 0.00083\,\boldsymbol{P} - 0.00014\,\boldsymbol{SR} - 0.00012\,\boldsymbol{ST_c} - 0.00023\,\boldsymbol{ST_f} + 0.00020\,\boldsymbol{SP} + 0.00013\,\boldsymbol{RT_c} + 0.00017\,\boldsymbol{RT_f} - 0.00011\,\boldsymbol{RP} + 0.00118\,\boldsymbol{t_cT_f} - 0.00020\,\boldsymbol{T_cP} + 0.00033\,\boldsymbol{T_fP} \tag{3.2}$$

There is no doubt that neglecting the second and higher-order interactions may affect the accuracy of simulation. However, the provided plot depicted in Figure 3-6 indicates that assuming just the first-order interaction effects can be accurate enough to present the sandwich panel maximum deflection response. Figure 3-6 compares the predicted panel deflection results obtained from Equation 3.2 versus the actual ones obtained from ANSYS. The graph shows the predicted values on vertical axis and the actual values on horizontal axis. The distance of each point from the plotted line demonstrates the difference between the predicted and actual values. The distribution of plotted points reveals that the regression equation properly presents the panel maximum deflection results.

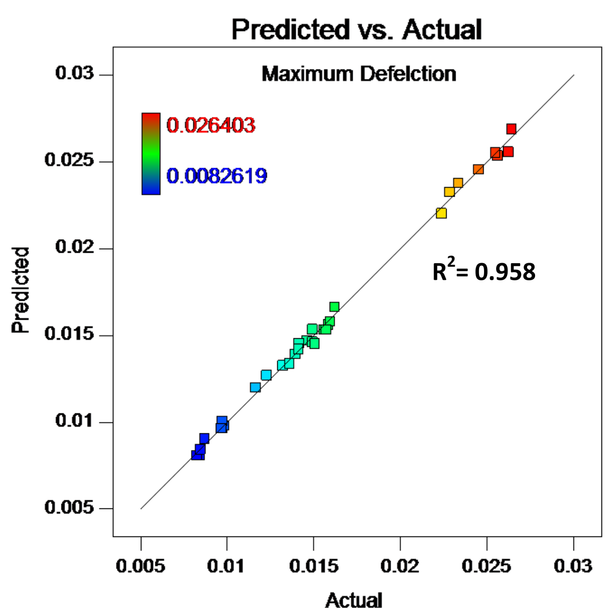

Figure 3-6 Predicted versus Actual results for the sandwich panel maximum deflection response

Table 3-5 shows the ANOVA analysis results for the panel maximum deflection response obtained from Design Expert software. Table 3-5 presents the P-value for all factors and interactions. Since in the ANOVA analysis the **α** value is equal to 0.05, P-values less than 0.05 indicate a significant contribution for the associated term. Therefore, according to Table 3-5, [S], [R], [T_c], [T_f], [P], [ST_f], [SP], [T_cT_f], [T_cP], and [T_fP] contributions are considerable which are highlighted in the P-value column. It is noted that among all contribution factors the [T_cT_f] and [T_fP] have the minimum P-values which are also confirmed from interaction plots.

Table 3-5 ANOVA test results for the sandwich panel maximum deflection response

Source	Sum of Squares	df	Mean Square	p-value
Model	1.049E-003	15	6.994E-005	< 0.0001
A-S	7.058E-006	1	7.058E-006	< 0.0001
B-R	3.993E-006	1	3.993E-006	0.0004
C-Tc	4.817E-004	1	4.817E-004	< 0.0001
D-Tf	4.789E-004	1	4.789E-004	< 0.0001
E-P	2.192E-005	1	2.192E-005	< 0.0001
AB	6.393E-007	1	6.393E-007	0.0921
AC	4.854E-007	1	4.854E-007	0.1380
AD	1.631E-006	1	1.631E-006	0.0113
AE	1.263E-006	1	1.263E-006	0.0228
BC	5.688E-007	1	5.688E-007	0.1104
BD	8.866E-007	1	8.866E-007	0.0509
BE	3.633E-007	1	3.633E-007	0.1955
CD	4.479E-005	1	4.479E-005	< 0.0001
CE	1.290E-006	1	1.290E-006	0.0216
DE	3.570E-006	1	3.570E-006	0.0006

Table 3-6 shows the comparison between ANSYS and regression equation results for the panel maximum deflection response. The difference between ANSYS and regression values is called residual. In order to substitute the real geometrical values as input factors in the regression model, they should be scaled to the range of [-1] to [+1]. For example, for the weld spacing factor, 80 and 160 mm refer to [-1] and [+1], respectively, and any values between 80 and 160 mm should be linearly interpolated to be scaled down to the range of

[-1] and [+1]. Table 3-6 summarizes the calculated regression values for the 32 models and compares them with ANSYS results for the maximum deflection response.

Table 3-6 Regression model results comparison with ANSYS

Panel Maximum Deflection (m)					
Run No.	ANSYS	Regression	Run No.	ANSYS	Regression
1	0.0256	0.0253	17	0.0228	0.0232
2	0.0264	0.0269	18	0.0262	0.0256
3	0.0245	0.0245	19	0.0224	0.0220
4	0.0255	0.0255	20	0.0233	0.0238
5	0.0158	0.0156	21	0.0123	0.0127
6	0.0162	0.0166	22	0.0151	0.0145
7	0.0156	0.0153	23	0.0117	0.0120
8	0.0159	0.0158	24	0.0132	0.0132
9	0.0146	0.0147	25	0.0139	0.0139
10	0.0157	0.0153	26	0.0149	0.0153
11	0.0141	0.0145	27	0.0136	0.0134
12	0.0149	0.0146	28	0.0141	0.0142
13	0.0097	0.0097	29	0.0084	0.0081
14	0.0098	0.0098	30	0.0087	0.0090
15	0.0097	0.0101	31	0.0083	0.0081
16	0.0097	0.0096	32	0.0085	0.0084

In order to verify that the ANOVA analysis is valid, three graphs are provided; Normal plot of residuals, residuals versus predicted plot, and residuals versus run number plot which are illustrated in Figures 3-7 (a) to 3-7 (c). As shown in Figure 3-7 (a), the distribution of residual is reasonably even relative to the interpolated line. Figures 3-7 (b) and 3-7 (c) also show a satisfactory distribution of residuals above and under the horizontal axis.

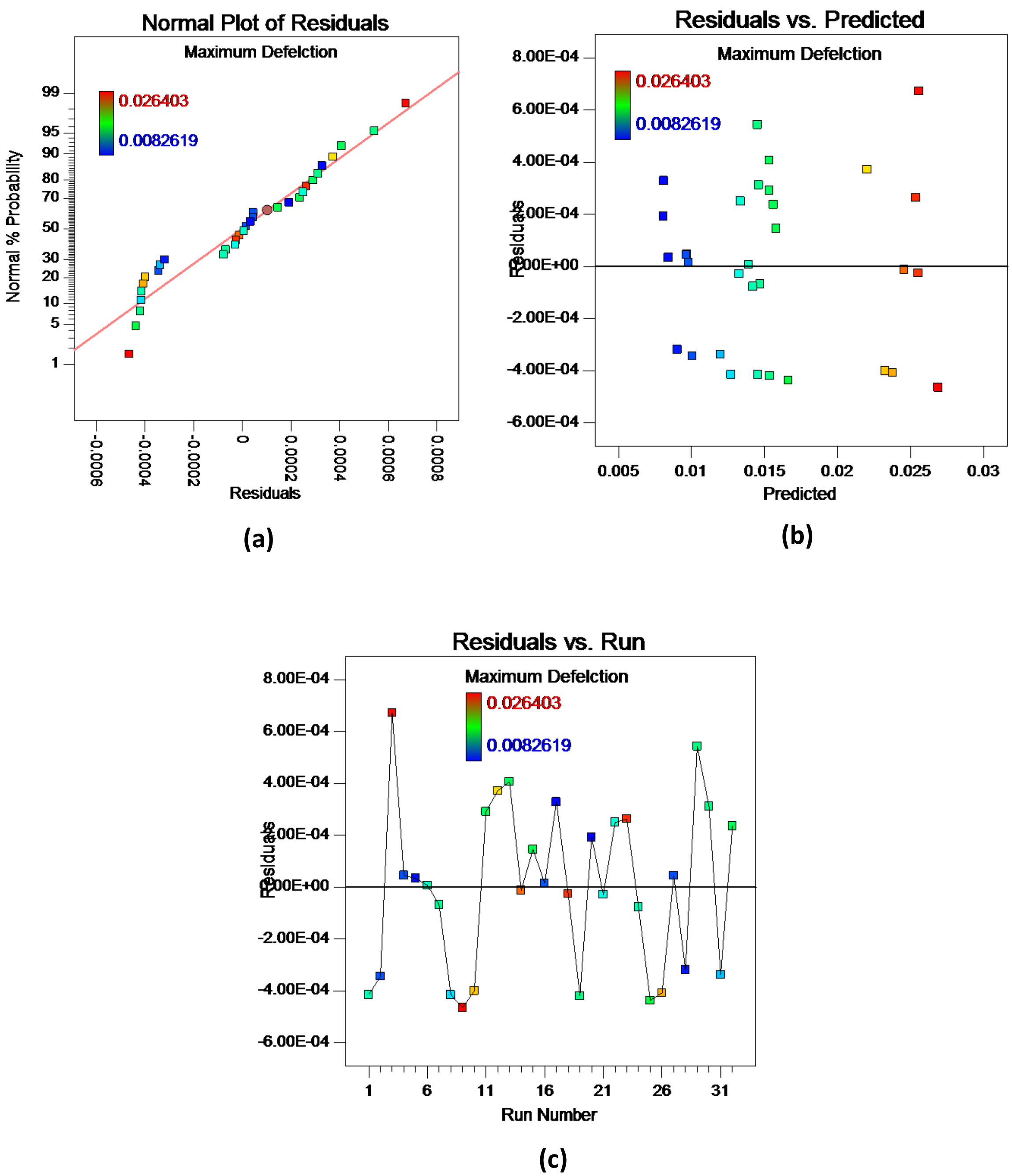

Figure 3-7 ANOVA test assumption validity proof for the panel maximum deflection response; (a) Normal plot, (b) Residual versus Predicted plot, (c) Residual versus Run number plot

According to the residual analysis, the regression model shows a satisfactory agreement with ANSYS results. However, from the prediction point of view, for any random geometry the regression equation should represent the maximum deflection response of the sandwich panel with an acceptable amount of error in comparison with ANSYS result. It means that the maximum deflection value obtained by the mathematical regression equation should correlate with the result of simulated panel in ANSYS for any random values of the five geometrical parameters in the range of [-1] to [+1]. In this regard, two randomly generated models are considered to be applied to the regression equation and also simulated in ANSYS. Table 3-7 summarizes the selected geometries and the maximum deflection responses for both ANSYS and regression equation. It is noted that the actual values selected for the five factors should be in the range of low to high levels and scaled to the range of [-1] to [+1] in order to substitute them into Equation 3.2.

Table 3-7 Random models geometrical parameters

	Random Model I		Random Model II	
Input Factors	Test value (mm)	Scaled value	Test value (mm)	Scaled value
Weld Spacing [S]	100	-0.50	130	0.25
Weld Radius [R]	15	0.33	10	-0.33
Core sheet Thickness [T_c]	4.5	-0.50	5.2	0.20
Face sheet Thickness [T_f]	4.5	-0.50	5.6	0.60
Welding path Distance [P]	80	-0.40	95	0.20

Table 3-8 demonstrates a summary of the panel maximum deflection values obtained from ANSYS and regression mathematical Equation 3.2 for the two selected random models. The comparison between the two deflection values for each model indicates that the regression model can predict the panel maximum deflection response within the range of the ANSYS outputs. The regression values have a difference of 12% lower and 20% higher with ANSYS results for Model I and II, respectively. There are few reasons that may contribute to the difference between the actual ANSYS result and the predicted values by regression equation. The most important reason is that the regression model is a linear simulation whereas the panel mechanical behavior is a nonlinear response. Therefore, the simplified linear regression equation predicts the panel deflection response within a bandwidth of actual FEM result.

Table 3-8 Panel maximum deflection response for two random models as per ANSYS and regression equation result

	Panel Maximum Deflection Response (mm)	
	Random Model I	Random Model II
ANSYS	21.7	11.1
Regression	19.1	13.4

3.3.2 Maximum shear force analysis

The second output response for the steel sandwich panel investigated in this study is the maximum shear force at spot welds. Since the spot welds are the main component to transfer the shear force from the face sheets to the corrugated core, they are considered as hot spot locations for the potential failure. Due to the fact that the spot weld shear force capacity is limited by welding schedule which will be more explained in the failure analysis section, the shear force flow at the interface of face sheets and the core should be less than the spot weld shear force capacity. Therefore, once the ANSYS solution is obtained, a list of shear forces for all spot welds is established and the maximum value is chosen as the second response. It is noted that the applied shear force vectors at each spot weld provided by ANSYS are in x and z directions. Therefore, the total shear force value should be calculated based on the vector sum of shear force components in the x and z directions and need to be checked with the weld shear capacity.

Based on the total shear force values obtained from 32 ANSYS runs shown in Table 3-9, by applying the same method of full factorial applied for the maximum deflection analysis presented in section 3.3.1, the effect values of the five input factors and their first-order interactions are calculated for the maximum shear force response. It is noted that in this section, the higher-order interactions are not considered.

Table 3-9 Full factorial design with first-order interactions along with maximum shear force values at spot welds

Run No.	S	R	T_c	T_f	P	SR	ST_c	ST_f	SP	RT_c	RT_f	RP	T_cT_f	T_cP	T_fP	Max Shear Force (N)
1	-1	-1	-1	-1	-1	1	1	1	1	1	1	1	1	1	1	12863
2	1	-1	-1	-1	-1	-1	-1	-1	-1	1	1	1	1	1	1	21921
3	-1	1	-1	-1	-1	-1	1	1	1	-1	-1	-1	1	1	1	13899
4	1	1	-1	-1	-1	1	-1	-1	-1	-1	-1	-1	1	1	1	26559
5	-1	-1	1	-1	-1	1	-1	1	1	-1	1	1	-1	-1	1	8502
6	1	-1	1	-1	-1	-1	1	-1	-1	-1	1	1	-1	-1	1	16527
7	-1	1	1	-1	-1	-1	-1	1	1	1	-1	-1	-1	-1	1	9264
8	1	1	1	-1	-1	1	1	-1	-1	1	-1	-1	-1	-1	1	19467
9	-1	-1	-1	1	-1	1	1	-1	1	1	-1	1	-1	1	-1	10301
10	1	-1	-1	1	-1	-1	-1	1	-1	1	-1	1	-1	1	-1	19762
11	-1	1	-1	1	-1	-1	1	-1	1	-1	1	-1	-1	1	-1	11859
12	1	1	-1	1	-1	1	-1	1	-1	-1	1	-1	-1	1	-1	20673
13	-1	-1	1	1	-1	1	-1	-1	1	-1	-1	1	1	-1	-1	7735
14	1	-1	1	1	-1	-1	1	1	-1	-1	-1	1	1	-1	-1	15216
15	-1	1	1	1	-1	-1	-1	-1	1	1	1	-1	1	-1	-1	7735
16	1	1	1	1	-1	1	1	1	-1	1	1	-1	1	-1	-1	16829
17	-1	-1	-1	-1	1	1	1	1	-1	1	1	-1	1	-1	-1	13498
18	1	-1	-1	-1	1	-1	-1	-1	1	1	1	-1	1	-1	-1	22766
19	-1	1	-1	-1	1	-1	1	1	-1	-1	-1	1	1	-1	-1	15182
20	1	1	-1	-1	1	1	-1	-1	1	-1	-1	1	1	-1	-1	27700
21	-1	-1	1	-1	1	1	-1	1	-1	-1	1	-1	-1	1	-1	9370
22	1	-1	1	-1	1	-1	1	-1	1	-1	1	-1	-1	1	-1	17934
23	-1	1	1	-1	1	-1	-1	1	-1	1	-1	1	-1	1	-1	9838
24	1	1	1	-1	1	1	1	-1	1	1	-1	1	-1	1	-1	20704
25	-1	-1	-1	1	1	1	1	-1	-1	1	-1	-1	-1	-1	1	10970
26	1	-1	-1	1	1	-1	-1	1	1	1	-1	-1	-1	-1	1	18886
27	-1	1	-1	1	1	-1	1	-1	-1	-1	1	1	-1	-1	1	11818
28	1	1	-1	1	1	1	-1	1	1	-1	1	1	-1	-1	1	22906
29	-1	-1	1	1	1	1	-1	-1	-1	-1	-1	-1	1	1	1	8750
30	1	-1	1	1	1	-1	1	1	1	-1	-1	-1	1	1	1	16662
31	-1	1	1	1	1	-1	-1	-1	-1	1	1	1	1	1	1	9606
32	1	1	1	1	1	1	1	1	1	1	1	1	1	1	1	18839

Table 3-10 summarizes the effect values of input factors for the maximum shear force response. The effect values reveal that as the weld spacing increases, the shear force magnitude at each spot weld also increases. The reason of this behaviour is that as the weld spacing increases, the number of spot welds at each welding line and consequently, the total number of welds decreases. Therefore, the share of each spot weld from the total shear forces increases.

Table 3-10 Effect values for the maximum shear response

	[S]		**[R]**		**[T_c]**		**[T_f]**		**[P]**	
	High	Low	High	Low	High	Low	High	Low	High	Low
Average	20209.4	10699.3	16429.9	14478.9	13311.1	17597.7	14284.2	16624.5	15964.2	14944.5
Effect	9510.1		1951.0		-4286.6		-2340.3		1019.7	
Normalized Effect	0.498		0.102		0.224		0.122		0.053	

Regarding the T_c and T_f factor effects, as it is expected, the calculated effect values are both negative which means as the thickness of steel plate increases the shear strength of the steel plate improves, and consequently the flexural property of the sandwich panel increases. It is noted that comparing T_c and T_f effect values indicates that T_c offers more contribution to reduce the total shear force. As mentioned earlier, in corrugated sandwich panel the total shear force is transferred to the core by face sheets, therefore, the core thickness plays an important role in shear capacity of the panel. In other words, increasing the thickness of the core sheet has more contribution in improving the flexural property than the face sheet thickness. Regarding reducing the weight, increasing the thickness of the core sheet leads to a lighter panel compared to the thickness of face sheet with a same value. For example, as the magnitude of T_c increases from 3.5 mm to 4.5 mm, the panel weight changes from 1020 kg to1140 kg denoting 11.7% increase. However, with the same change for T_f, the panel weight varies from 1104 kg to 1304 kg which refers to an 18% increase. Therefore, in order to provide a higher flexural property, it is highly efficient to increase the thickness of core sheet. Contribution of the weld spacing parameter to the shear force response, with around 5% normalized effect value, is not noticeable among four other factors.

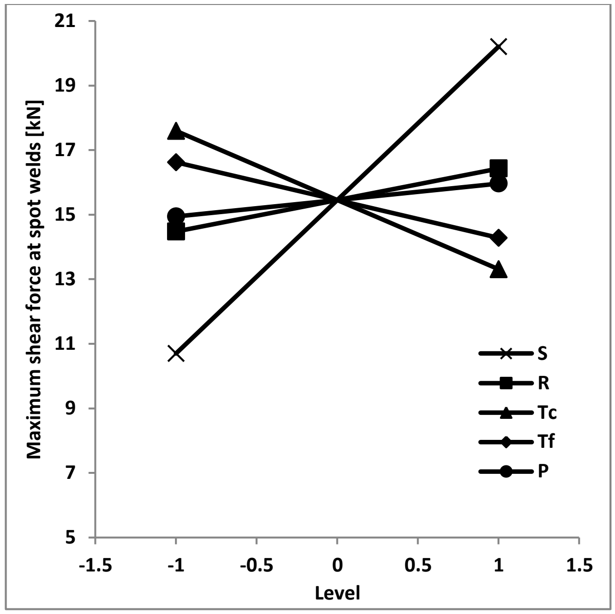

Figure 3-8 Geometric factors main effect plot for maximum shear force response at spot welds

Figure 3-8 demonstrates the main effect plot for the maximum shear force response at spot welds for five geometric parameters. As mentioned earlier, the effect plot provides a qualitative comparison between the input factors in order to understand their contribution in panel shear force response. As also explained in the deflection analysis section, the presented percentages of normalized effect values visualize the contribution of each factor. Thus, the maximum shear force response, [S] shows the highest contribution with 50% and [T_c] is the second most contributing factor with 22%. After that, [T_f] and [R] demonstrate the contributions of 12% and 10%, respectively. Since the spot welds transfer the total shear force from the face sheets to the core, the total number of applied spot welds play an important role in the shear force distribution at the interface of face and core sheets. As the number of spot welds increases, the share of each weld in load transferring decreases, therefore, the maximum shear force reduces.

Regarding the interaction effects, Figures 3-9 (a) to 3-9 (j) illustrate the 10 interaction plots for the maximum shear force at spot welds response.

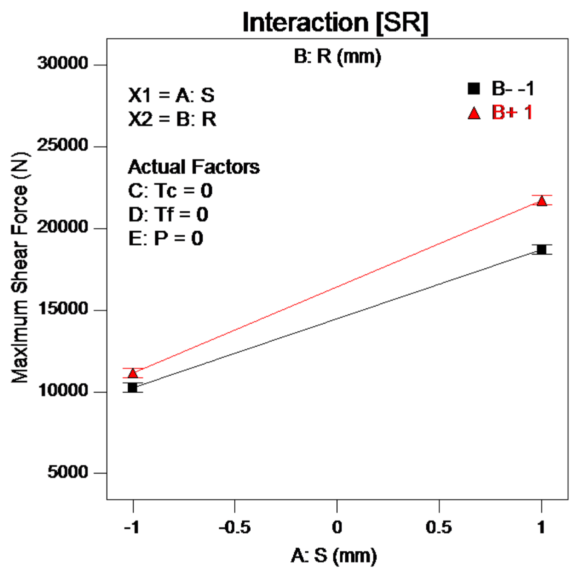
Interaction [SR]
B: R (mm)
X1 = A: S
X2 = B: R
Actual Factors
C: Tc = 0
D: Tf = 0
E: P = 0
B- -1
B+ 1
Maximum Shear Force (N)
30000
25000
20000
15000
10000
5000
-1
-0.5
0
0.5
1
A: S (mm)

(a)

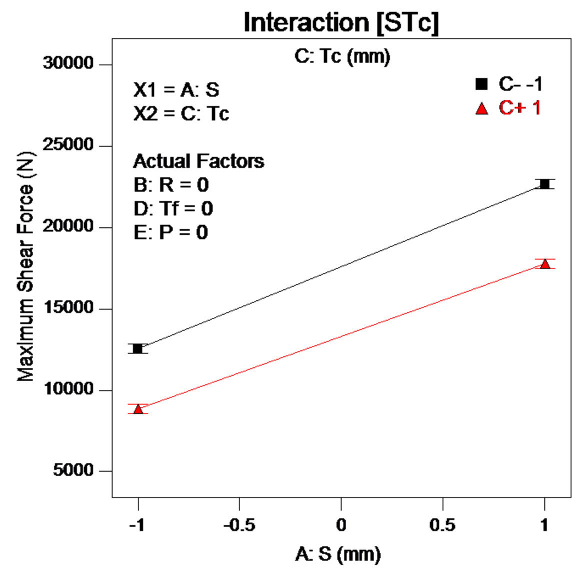
Interaction [STc]
C: Tc (mm)
X1 = A: S
X2 = C: Tc
Actual Factors
B: R = 0
D: Tf = 0
E: P = 0
C- -1
C+ 1
Maximum Shear Force (N)
30000
25000
20000
15000
10000
5000
-1
-0.5
0
0.5
1
A: S (mm)

(b)

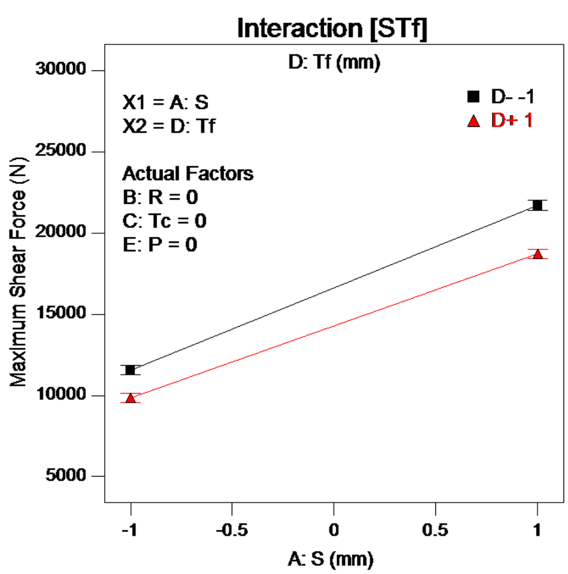
Interaction [STf]
D: Tf (mm)
X1 = A: S
X2 = D: Tf
Actual Factors
B: R = 0
C: Tc = 0
E: P = 0
D- -1
D+ 1
Maximum Shear Force (N)
30000
25000
20000
15000
10000
5000
-1
-0.5
0
0.5
1
A: S (mm)

(c)

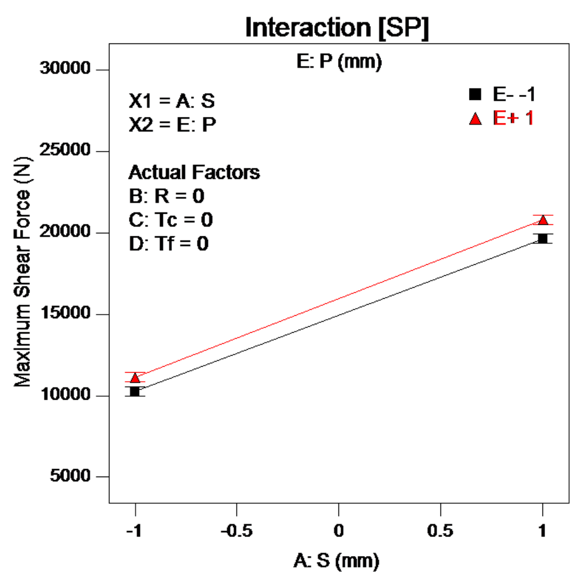
Interaction [SP]
E: P (mm)
X1 = A: S
X2 = E: P
Actual Factors
B: R = 0
C: Tc = 0
D: Tf = 0
E- -1
E+ 1
Maximum Shear Force (N)
30000
25000
20000
15000
10000
5000
-1
-0.5
0
0.5
1
A: S (mm)

(d)

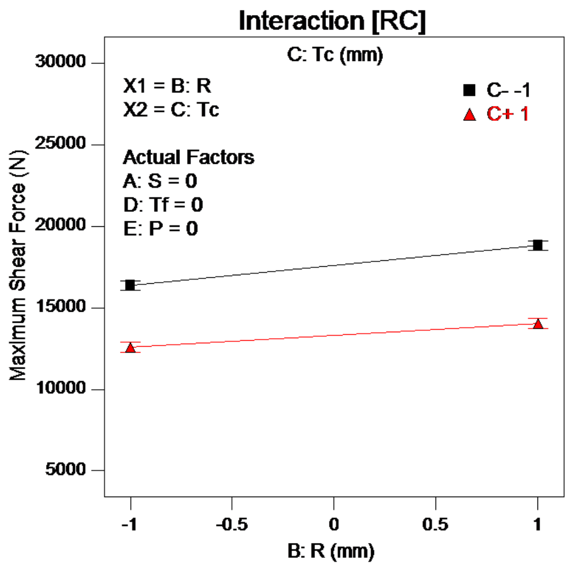
Interaction [RC]
C: Tc (mm)
X1 = B: R
X2 = C: Tc
C- -1
C+ 1
Actual Factors
A: S = 0
D: Tf = 0
E: P = 0
Maximum Shear Force (N)
30000
25000
20000
15000
10000
5000
-1
-0.5
0
0.5
1
B: R (mm)

(e)

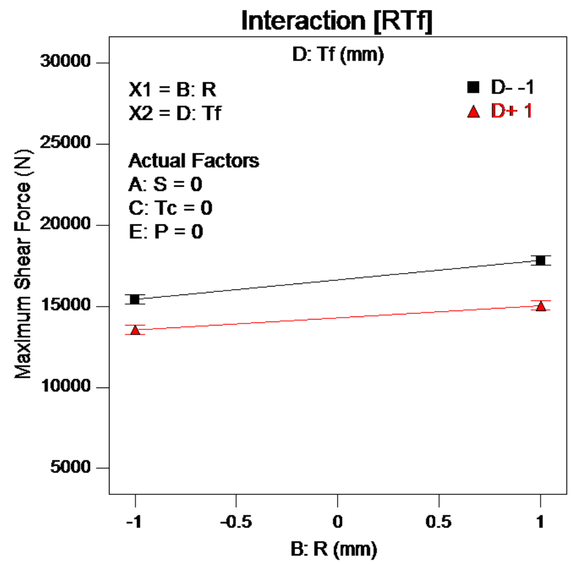
Interaction [RTf]
D: Tf (mm)
X1 = B: R
X2 = D: Tf
D- -1
D+ 1
Actual Factors
A: S = 0
C: Tc = 0
E: P = 0
Maximum Shear Force (N)
30000
25000
20000
15000
10000
5000
-1
-0.5
0
0.5
1
B: R (mm)

(f)

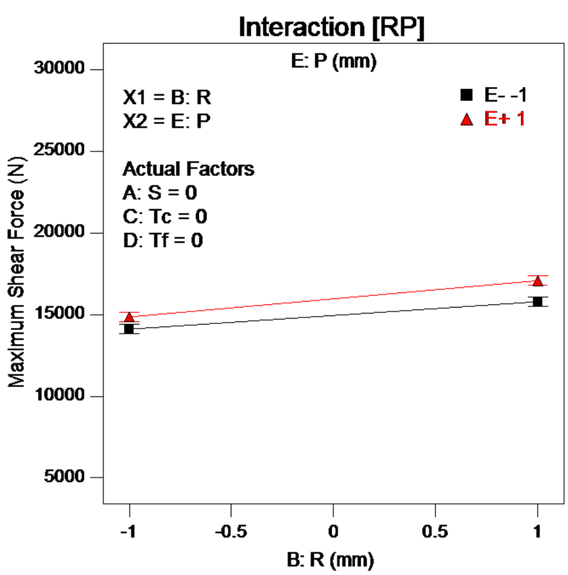
Interaction [RP]
E: P (mm)
X1 = B: R
X2 = E: P
E- -1
E+ 1
Actual Factors
A: S = 0
C: Tc = 0
D: Tf = 0
Maximum Shear Force (N)
30000
25000
20000
15000
10000
5000
-1
-0.5
0
0.5
1
B: R (mm)

(g)

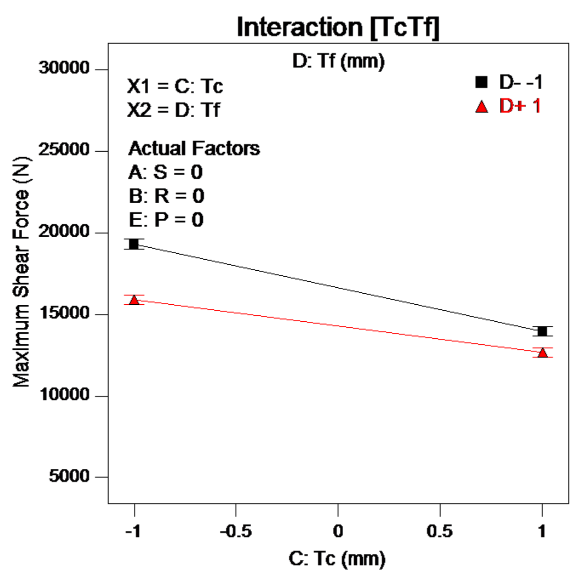
Interaction [TcTf]
D: Tf (mm)
X1 = C: Tc
X2 = D: Tf
D- -1
D+ 1
Actual Factors
A: S = 0
B: R = 0
E: P = 0
Maximum Shear Force (N)
30000
25000
20000
15000
10000
5000
-1
-0.5
0
0.5
1
C: Tc (mm)

(h)

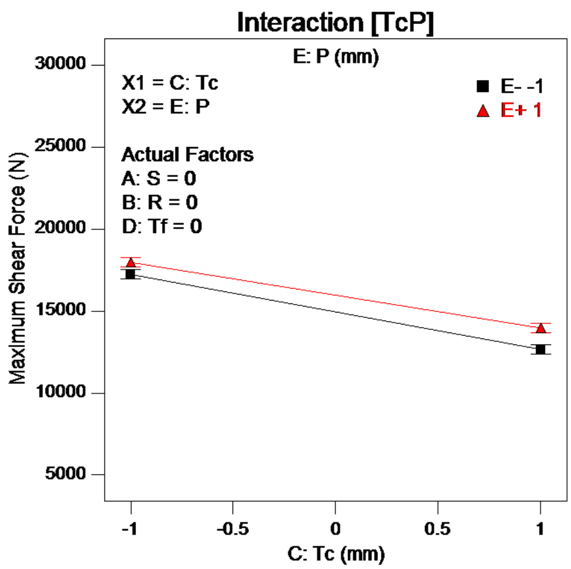

(i)

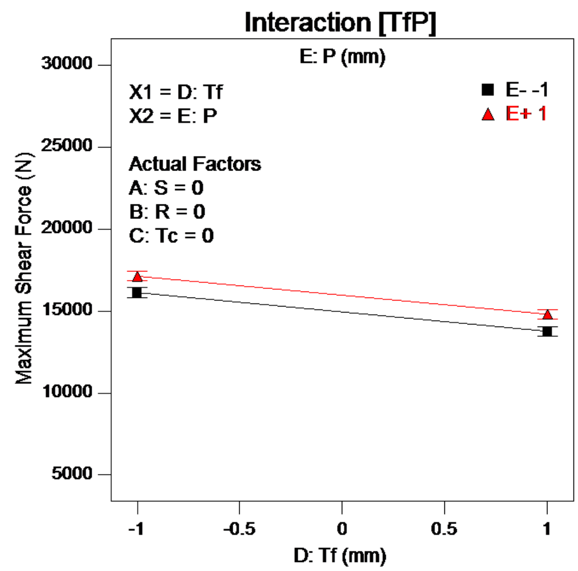

(j)

Figure 3-9 Interaction effect plots for the maximum shear force at spot welds response; a) [SR], b) [ST$_c$], c) [ST$_f$], d) [SP], e) [RT$_c$], f) [RT$_f$], g) [RP], h) [T$_c$T$_f$], i) [T$_c$P], j) [T$_f$P]

As shown in presented graphs, [SR] and [T$_c$T$_f$] indicate the highest effect among other first-order interactions. The ANOVA analysis result presented in Table 3-11 also reveals that the [SR] and [T$_c$T$_f$] interactions contribute significantly in the maximum shear force response. Based on the presented P-values in Table 3-11, all input factors contribute to the response. However, since [SP], [RP], [T$_c$P], and [T$_f$P] P-values are greater than 0.05, their contributions are not considered significant.

Table 3-11 ANOVA test results for the maximum shear force at spot welds response

Source	Sum of Squares	df	Mean Square	p-value
Model	9.820E+008	15	6.547E+007	< 0.0001
A-S	7.235E+008	1	7.235E+008	< 0.0001
B-R	3.045E+007	1	3.045E+007	< 0.0001
C-Tc	1.470E+008	1	1.470E+008	< 0.0001
D-Tf	4.382E+007	1	4.382E+007	< 0.0001
E-P	8.318E+006	1	8.318E+006	< 0.0001
AB	8.810E+006	1	8.810E+006	< 0.0001
AC	2.764E+006	1	2.764E+006	0.0081
AD	3.229E+006	1	3.229E+006	0.0048
AE	2.065E+005	1	2.065E+005	0.4205
BC	2.022E+006	1	2.022E+006	0.0199
BD	1.642E+006	1	1.642E+006	0.0331
BE	5.777E+005	1	5.777E+005	0.1858
CD	9.010E+006	1	9.010E+006	< 0.0001
CE	6.436E+005	1	6.436E+005	0.1638
DE	3554.55	1	3554.55	0.9150

Regarding the regression equation of the maximum shear force response, Table 3-12 presents the regression equation coefficients for all factors and first order interactions. It is noted that the coefficients are the effect values divided by the number of factor levels which is two. It should be noted that the quantitative comparison of the coefficients also confirms that the [SR] and [T_cT_f] interactions contribute significantly in the maximum shear force response.

Table 3-12 Regression equation coefficients for the maximum shear force value

Factors	*Coefficients*
Intercept	15454.4
[S]	4755.1
[R]	975.5
[T_c]	-2143.3
[T_f]	-1170.2
[P]	509.8
[SR]	524.7
[ST_c]	-293.9
[ST_f]	-317.6
[SP]	80.3
[RT_c]	-251.4
[RT_f]	-226.5
[RP]	134.4
[T_cT_f]	530.6
[T_cP]	141.8
[T_fP]	10.5

In order to obtain the regression equation for the maximum shear force response, the obtained coefficients from Excel presented in Table 3-12 are substituted into the general linear regression Equation 3.1. Based on these coefficients, the mathematical regression equation for the maximum shear force at spot welds can be expressed in the form of Equation 3.3.

$$\begin{aligned} y\,(x_1, x_2, \dots, x_n) = \; & 15454.4 + 4755.1\,\boldsymbol{S} - 975.5\,\boldsymbol{R} - 2143.3\,\boldsymbol{T_c} - 1170.2\,\boldsymbol{T_f} \\ & -509.8\,\boldsymbol{P} - 524.7\,\boldsymbol{SR} - 293.9\,\boldsymbol{ST_c} - 317.6\,\boldsymbol{ST_f} + 80.3\,\boldsymbol{SP} - 251.4\,\boldsymbol{RT_c} \\ & -226.5\,\boldsymbol{RT_f} + 134.4\,\boldsymbol{RP} + 530.6\boldsymbol{T_cT_f} + 141.8\,\boldsymbol{T_cP}\;10.5\,\boldsymbol{T_fP} \end{aligned} \tag{3.3}$$

Regarding the residual analysis, Table 3-13 summarizes the calculated regression values for the 32 models and compares them with ANSYS results for the maximum shear force at spot welds. The difference between these two columns denotes the residual value for each run.

Table 3-13 Comparison between the regression equation and ANSYS results for the maximum shear force response

Maximum shear force at spot welds (N)					
Run No.	ANSYS	Regression	Run No.	ANSYS	Regression
1	12863	12860	17	13498	13146
2	21921	22384	18	22766	22990
3	13899	14449	19	15182	15272
4	26559	26071	20	27700	27215
5	8502	8319	21	9370	9172
6	16527	16667	22	17934	17841
7	9264	8903	23	9838	10293
8	19467	19349	24	20704	21061
9	10301	10526	25	10970	10854
10	19762	18779	26	18886	19428
11	11859	11209	27	11818	12074
12	20673	21560	28	22906	22746
13	7735	8108	29	8750	9003
14	15216	15185	30	16662	16401
15	7735	7785	31	9606	9217
16	16829	16960	32	18839	18714

In order to visually demonstrate the residual values, Figure 3-10 shows the predicted and actual maximum shear force response values obtained from the regression equation and ANSYS, respectively. The distance between each point and the 45 degree line denotes the residual value for that run number qualitatively. The distribution of all points around the line shows satisfactory consistent residual values for the regression simulation.

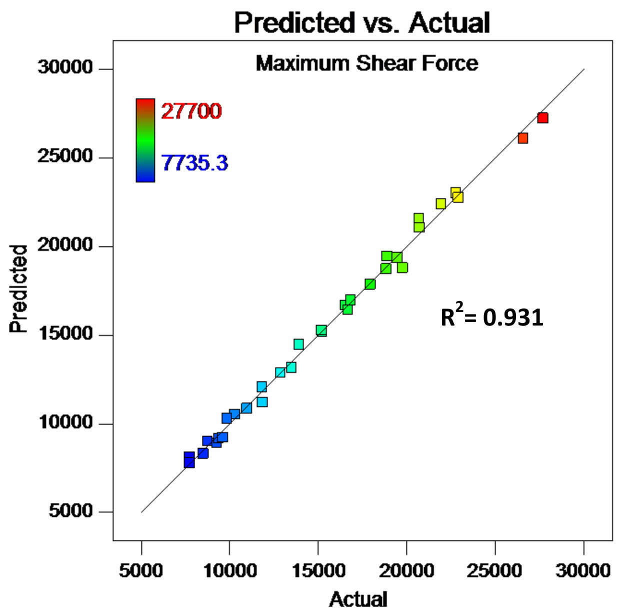

Figure 3-10 Predicted versus Actual results for the panel maximum deflection response

Regarding the assumption verification of the regression simulation, Figures 3-11 (a) to 3-11 (c) present the normal plot of residuals, residuals versus predicted, and residuals versus run numbers, respectively. The even distribution of points around the drafted lines in all graphs indicates the validity of the regression assumption.

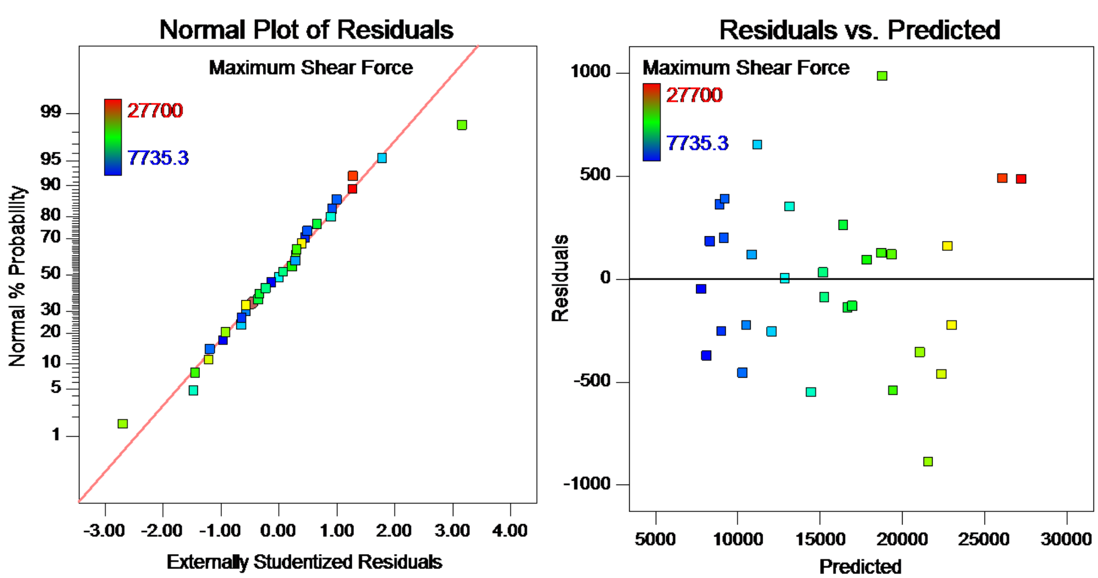

(a) **(b)**

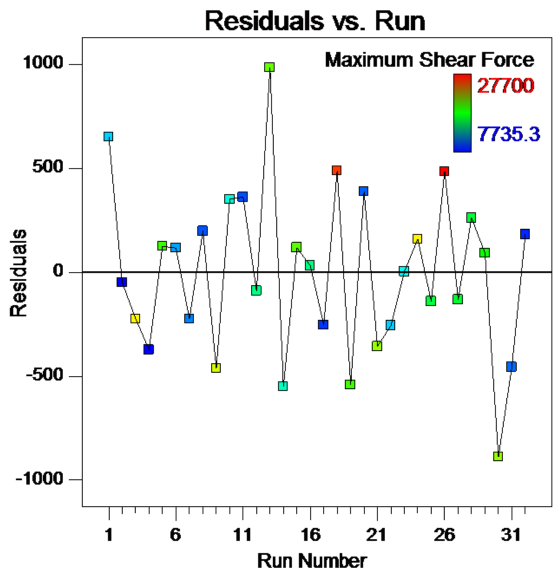

(c)

Figure 3-11 ANOVA test assumption validity proof for the maximum shear force at spot welds response; (a) Normal plot, (b) Residual versus Predicted plot, (c) Residual versus Run number plot

3.3.3 Sensitivity analysis for panel height and sheet thickness parameters

Regarding the fabrication of the corrugated-core steel sandwich panels, there are three geometric parameters that manufacturers may consider as the most important ones. Face sheet thickness, core sheet thickness, and panel height. These three parameters are the driving factors to adjust stiffness to weight ratio as required. Due to the fact that increasing the sheet thicknesses and panel height increases the sandwich panel weight and panel stiffness, a satisfactory balance between the panel weight and stiffness is desirable. Therefore, the main goal of this section is to present the sandwich panel maximum deflection and shear force distribution at spot welds in terms of each of these parameters. Moreover, in order to be able to demonstrate the panel nonlinear mechanical behaviour, the number of considered values for the parameters should be increased. Therefore, in this section, three factors are selected to study their effect on the panel mechanical behaviours in a wider range of variation. The first factor is the panel's height, *h*, which is the distance between the two face sheets. It should be noted that, generally, when the height of the panel increases, moment of inertia of the panel's cross-section, panel’s flexural strength increases. However, by increasing the height, the chance of local buckling at an inclined portion of the corrugated core grows. It is noted that the buckling analysis is not in the scope of this study and it is recommended to be performed as future studies.

Since changing the height of the panel affects the corrugated core geometry, in order to properly simulate the panel with different h values, other involved geometric parameters should be kept constant. Otherwise, the variation of responses may not necessarily refer to the effect of the height factor. According to the panel cross-section, there are two solutions by which h variation can be applied to the presented FEM model with minor changes in other parameters. The height can be increased by either increasing the slope of inclined surface in the core while the base length of the unit cell is fixed, or by keeping the slope unchanged for the inclined surface and decreasing the base length. It is noted that in both alternatives, two unit cells are considered for the panel. Since there are two welding paths on top and bottom of each unit cell, decreasing the length of horizontal section of unit cell is limited by this clear distance due to maintaining the number of two welding paths at each section. Undoubtedly, the main reason of not changing the number of welding points is to be consistent in the shear force distribution pattern in spot welds in order to be able to distinguish the height effect on the shear force response. Thus, the simulation of height variation is chosen to be applied by changing the slope of inclined surface in the core. In the height effect analysis, selected h values are 107.5, 138.5, and 170.5 mm. Figure 3-12 shows the three cross-sections with different heights. As it is seen, when the height increases the slope of inclined sheet in the corrugated core increases.

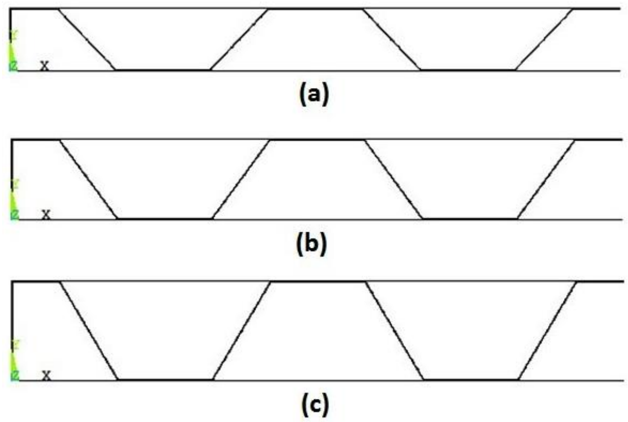

Figure 3-12 Sandwich panel cross-section with three different heights; a) h = 107.5 mm, b) h= 139 mm, c) h = 170.5 mm

Figure 3-13 shows the sandwich panel maximum deflection response versus the applied load for the mentioned three panel heights. As it is expected, the panel maximum deflection decreases by increasing the panel height value. The graph indicates that the slope of load capacity curve increases as *h* increases. In other words, for a same value of applied load, the panel with *h* = 170.5 mm shows the minimum deflection. The decrease in deflection magnitude is desirable; however, as mentioned earlier, increasing the height raises the potential of local buckling at the inclined core surface.

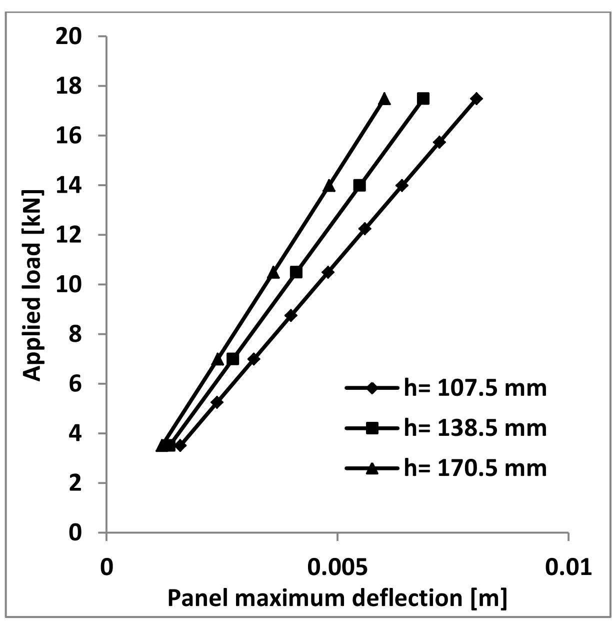

Figure 3-13 Panel height effect on maximum deflection response

The second response which should be also taken in to account is the shear force distribution in spot welds due to the panel height variation. In the first section of the parametric study, the shear force response was only based on a single value of maximum shear force at spot welds; however, in this part the shear force profile along a specific welding path is plotted. The graph is capable of showing the variation of shear force in the span direction in terms of any input factor. Figure 3-14 indicates the welding path numbers shown on panel cross-section. As it is shown, welding path numbers 1, 4, 5, and 8 are located on top face sheet and welding path numbers 2, 3, 6, and 7 are located on bottom face sheet.

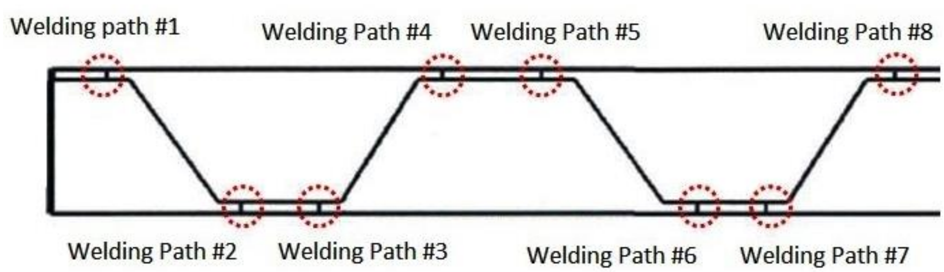

Figure 3-14 Spot welding path numbers

Figures 3-15 (a) to 3-15 (h) indicate the shear force value at each spot weld along eight welding paths in the sandwich panel. Each graph shows the shear force distribution for three panel height, *h*, values; 107.5 mm, 139 mm, and 170.5 mm. The horizontal axis represents the z coordinate of each spot weld and the vertical axis shows the corresponding shear force value at the spot weld. It is noted that z = 0 on the horizontal axis refers to the quarter panel end side with the plane of symmetry which denotes the middle of the complete panel and z = 2.98 m refers to the other end side with simply supported boundary condition.

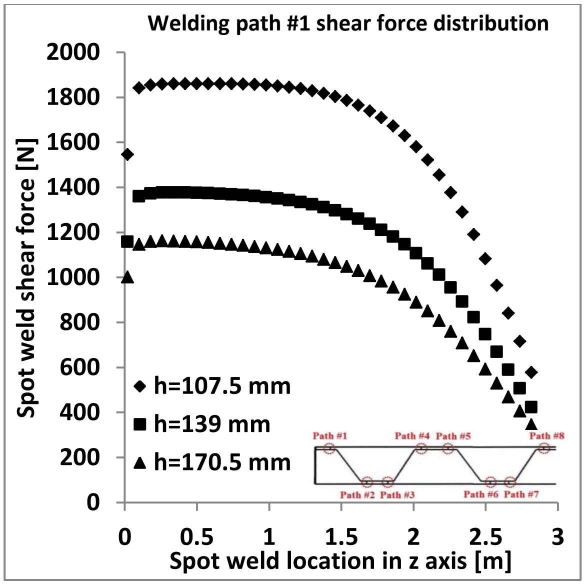
Welding path #1 shear force distribution
Spot weld shear force [N]
2000
1800
1600
1400
1200
1000
800
600
400
200
0
0
0.5
1
1.5
2
2.5
3
Spot weld location in z axis [m]
h=107.5 mm
h=139 mm
h=170.5 mm
Path #1
Path #4
Path #5
Path #8
Path #2
Path #3
Path #6
Path #7

(a)

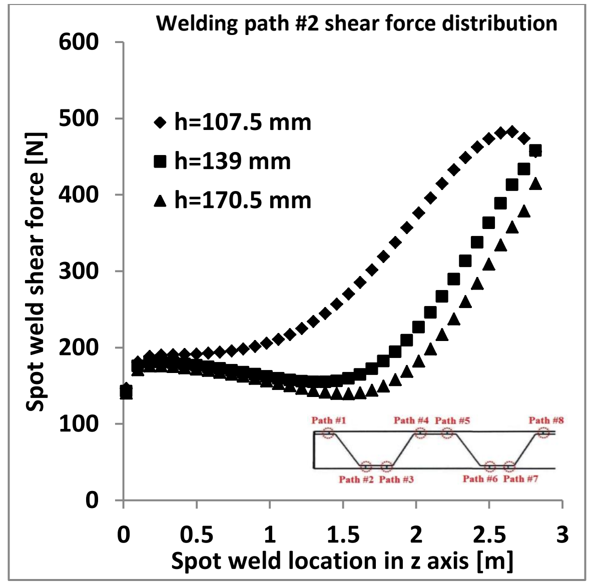
Welding path #2 shear force distribution
Spot weld shear force [N]
600
500
400
300
200
100
0
0
0.5
1
1.5
2
2.5
3
Spot weld location in z axis [m]
h=107.5 mm
h=139 mm
h=170.5 mm
Path #1
Path #4
Path #5
Path #8
Path #2
Path #3
Path #6
Path #7

(b)

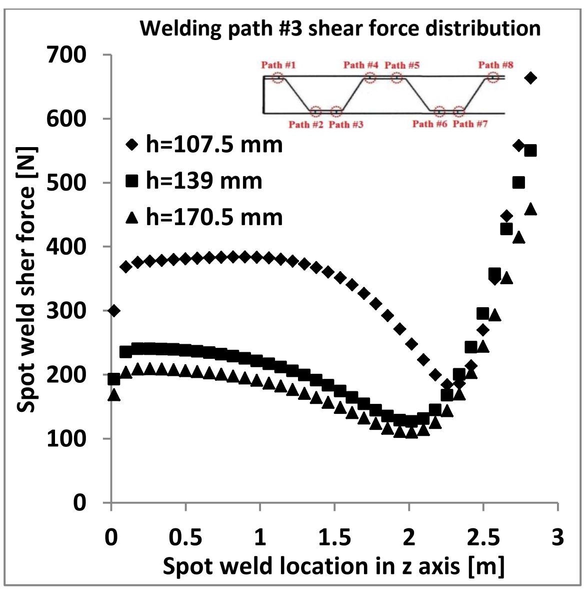
Welding path #3 shear force distribution
Spot weld sher force [N]
700
600
500
400
300
200
100
0
0
0.5
1
1.5
2
2.5
3
Spot weld location in z axis [m]
h=107.5 mm
h=139 mm
h=170.5 mm
Path #1
Path #4
Path #5
Path #8
Path #2
Path #3
Path #6
Path #7

(c)

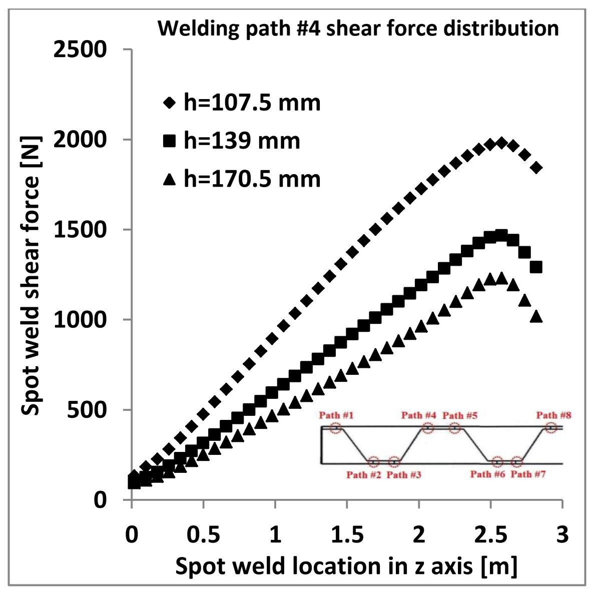
Welding path #4 shear force distribution
Spot weld shear force [N]
2500
2000
1500
1000
500
0
0
0.5
1
1.5
2
2.5
3
Spot weld location in z axis [m]
h=107.5 mm
h=139 mm
h=170.5 mm
Path #1
Path #4
Path #5
Path #8
Path #2
Path #3
Path #6
Path #7

(d)

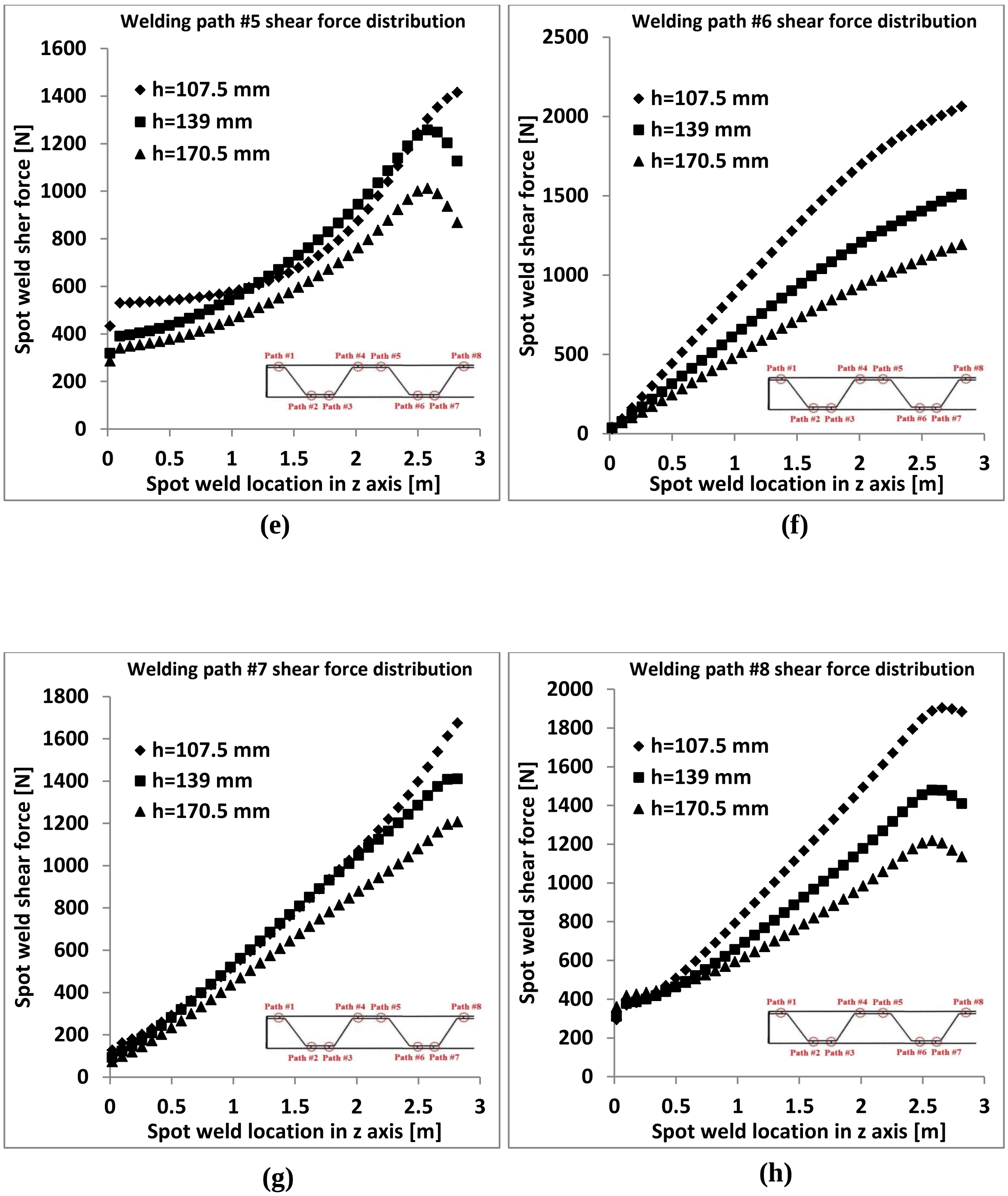

Figure 3-15 Panel height effect on shear force responses at spot welds. a) welding path #1, b) welding path #2, c) welding path #3, d) welding path #4, e) welding path #5, f) welding path #6, g) welding path #7, h) welding path #8.

The graph indicates three significant observations. First, except for the welding path #1, the shear force value increases from z = 0 to z = 2.98 m meaning that as the weld location moves from the center of the complete panel to the both ends, the shear force increases. In other words, the spot welds placed around the center of the panel experience the lowest amount of shear force while the ones located near the panel's supports transfer a higher amount of shear to the core. Second, the shear force decreases by increasing the panel height. In all graphs, the shear force profiles for h = 170.5 mm and h = 139 mm, bottom and middle curves, respectively, are located below the shear profiles for h = 107.5 mm. Third, in order to obtain the shear profile in the complete panel in the range of z = -2.98 m to z = +2.98 m the plotted curves should be mirrored along the vertical axis. It is noted that the graphed shear force values are the vector summation of shear force components in Z and X directions. The two other parameters which are investigated for this nonlinear analysis are thicknesses of the core and the face sheets, T_c and T_f, respectively. In order to investigate the deflection and shear force distribution nonlinear responses, T_c and T_f vary from 1.5 mm to 7.5 mm. It is noted that the *h* value is 107.5 mm and also while T_c changes, T_f value remains 2.5 mm and vice versa.

Figure 3-16 shows the panel maximum deflection variation as T_c and T_f values change from 1.5 mm to 7.5 mm. As it was shown earlier, the panel deflection is expected to be decreased as T_c and T_f increase. The provided curves indicate the nonlinear change in deflection values which couldn't be noticed in the effect analysis section.

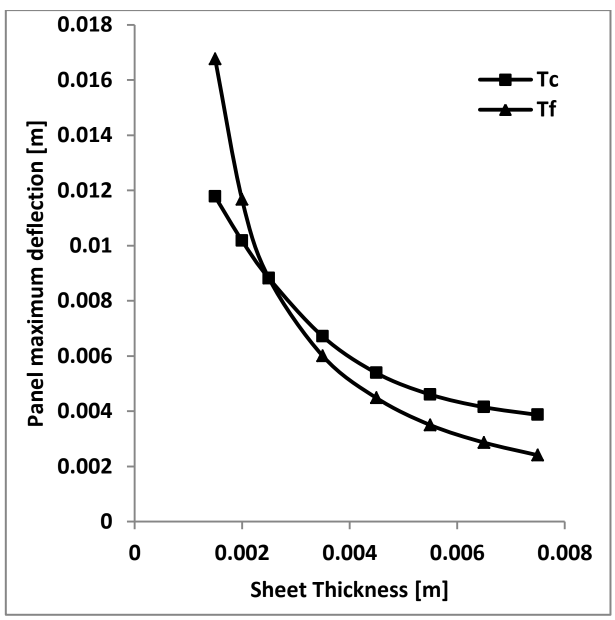

Figure 3-16 Core and face sheet thickness effect on panel maximum deflection

It is observed that the most noticeable deflection decrease occurs when the T_c and T_f increase from 1.5 mm to 4 mm, whereas above 4 mm, the deflection shows a gradual decrease. It is also noted that T_f shows significant role in the deflection reduction in comparison with T_c. For example, as T_c increases from 1.5 mm to 2 mm, the maximum deflection decreases by 13.5%, whereas, when T_f increases from 1.5 mm to 2 mm, the decrease is about 30%.

Figure 3-17 shows the load capacity curves for three T_c and T_f values of 2.5, 3.5, and 4.5 mm. As both graphs indicate, the mechanical load is gradually applied up to the maximum value of 17.5 kN. The panel maximum deflection variation shows almost a linear behaviour for both T_c and T_f variations. The immediate qualitative comparison of line slopes indicates that the load carrying capacity of the panel increases as T_c and T_f increase. Comparing the graphs shown in Figure 3-17 reveals that increasing T_c value from 2.5 mm to 3.5 mm does not increase the load capacity of the panel as much as increasing T_f from 2.5 mm to 3.5 mm. This observation can be also confirmed by the maximum deflection response to T_c and T_f variation presented in Figure 3-16. Therefore, both Figures 3-16 and 3-17 recommend that for sandwich panels with sheet thickness between 1.5 mm to 3.5 mm increased T_f offers more gain than T_c in terms of panel deflection and load carrying capacity.

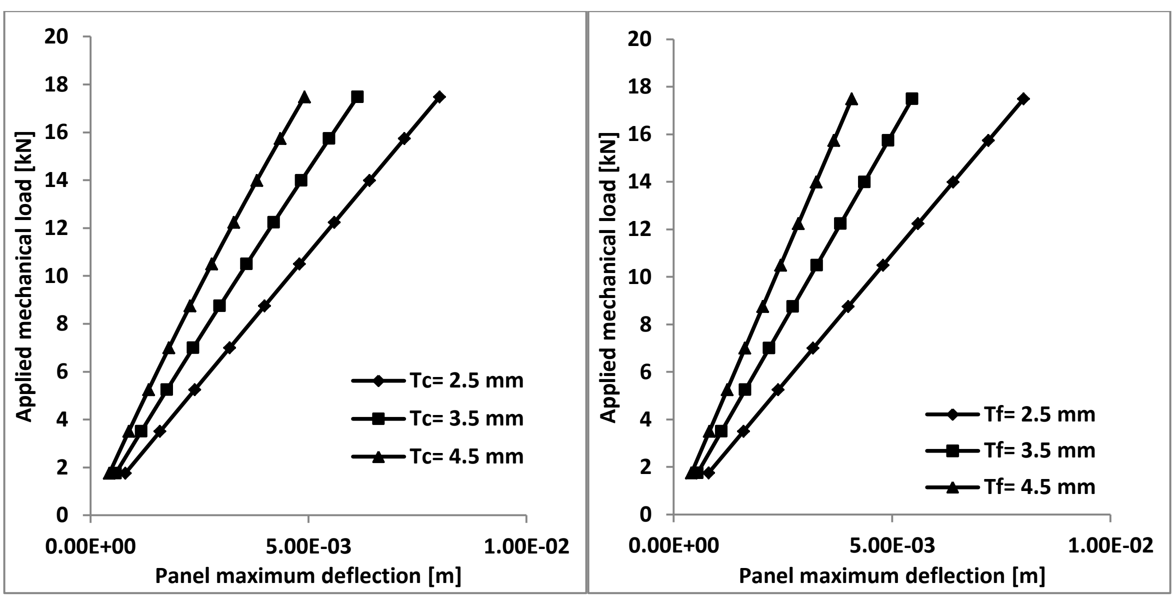

Figure 3-17 Core and face sheet thicknesses effect on panel maximum deflection

3.4. Failure Analysis

In the failure analysis, the failure scenarios through which the sandwich panel may experience a collapse should be recognized. Once the failure study is performed, the panel's hot spots in which the failure starts to propagate throughout the panel can be identified. There is no doubt that the proposed panel should be safe under the defined service load. However, in the case of excessive applied loading on the bridge deck beyond the assumed load safety factors, it is highly important to be familiar with the potential failures. The failure analysis can provide designers and manufacturers with useful information about the hot spot locations on the panel and how they can be addressed to postpone the damage.

One of the highly potential failures in the proposed steel corrugated sandwich panel is the spot weld collapse. As it was mentioned earlier, due to the limited shear load capacity of spot welds they have a high potential to fail in the case of extra unexpected loading. Therefore, the shear stress distribution at spot welds should be monitored precisely. In this regard, the overloading scenario is performed by gradually increasing the applied mechanical loading on the top face sheet above the working load limit. As the shear load magnitude in spot welds passes the defined load capacity, the welding detachment starts to occur. Therefore, depending on the amount of extra loading, a number of spot welds will be detached. Moreover, as the weld detachment continues, the rate of failed welds in terms of applied extra loading increases significantly.

3.4.1 Spot weld failure analysis algorithm

In order to simulate the failure mechanism of spot welds in the existing panel modeling, the concept of Birth and Death of elements is used in ANSYS. Based on the finite element feature, elements can be activated or deactivated during the solution process. Deactivated elements cannot contribute to the mechanical response of the sandwich panel since the dead elements corresponding indices in the global stiffness matrix are replaced with very small values close to zero. In order to obtain the advantage of the feature, the total applied loading should be divided to a number of load steps. The feature enables users to control the elements' contribution over the solution phase at each load step. The assumed spot weld shear force capacity is assumed 800 lbs. (3,570 N) (CMW, 2014). The obtained weld shear load capacity criterion is applied to a generic logical test added to the ANSYS simulation. According to the code, the tire load on the top face sheet is applied gradually through 10 equal load steps. Once the first load step is applied and the ANSYS solution is obtained, the program stores the shear force vector values of all spot welds in an output text file. As it is mentioned, the shear force vector at each spot weld consists of two components of F_x and F_z in x and z- directions in ANSYS global coordinate system, respectively. In order to be able to justify whether the shear force value in a spot weld exceeds the shear capacity limit of 800 lbs., the stored shear vector should be converted to a net value before the comparison. Thus, the code calculates the shear force magnitude at each weld based on the sum of the shear force vectors of F_x and F_z shown in Equation 3.4. Then, it compares the net shear force value with 3600 N to check whether the shear value is greater than the maximum allowable limit at each spot weld or not.

$$Total\ Shear\ force = \sqrt{{F_x}^2 + {F_z}^2} \tag{3.4}$$

While the code checks the condition for the entire panel, it provides a list of Beam188 element numbers in which the criterion is rejected. Finally, the provided list of the element numbers along with their corresponding coordinates will be stored as the collapsed spot weld connections at the end of the first load step. Consequently, before proceeding to the next load step, the code deactivates all the failed elements recorded in the output text file in order to eliminate their contribution to the stiffness matrix. In the next step, as the global stiffness matrix is updated, the entire FEM model is reconstructed and the applied load increases. Since the load should be applied gradually, the number of assigned load steps is 10. In other words, load step increment is selected to be 10% of the total applied load. Once the second load step solution is obtained, the code repeats the shear force criterion checking procedure and updates the existing output text file created in the first load step solution. Finally, after applying next eight load steps and completing the criterion checking, the last load step is applied and the list of failed elements is updated. It is noted that the list of failed elements also includes the coordinates of the associated elements which can be used to locate the position of these elements. As a result of the provided failed elements' coordinates, the pattern in which the detachment propagates can be plotted. The program flowchart which shows the introduced algorithm is presented in Figure 3-18.

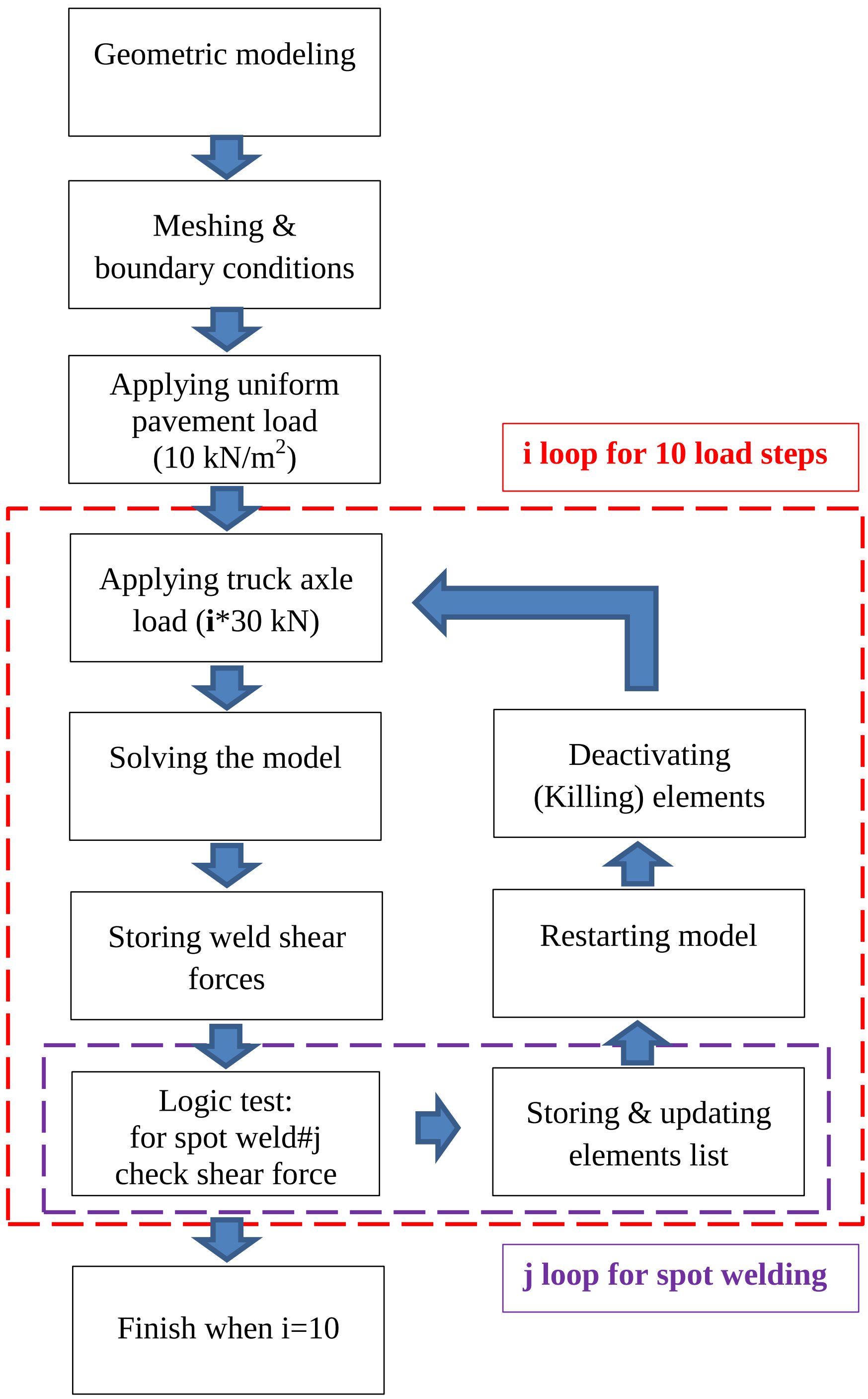

Figure 3-18 Spot weld failure analysis algorithm

As mentioned in the graph, the code includes two major loops; i-loop and j-loop. The i-loop represents the number of load steps which changes from 1 to 10 and the j-loop indicates the number of spot welds. As it is seen, in terms of the loop orders, the j-loop is located inside the i-loop which means that for any i-values, j-value changes from 1 to a maximum number of welds in order to check the failure condition.

In order to design a sandwich panel without a failure in spot welds under the defined working load limit, the last updated list of deactivated elements at the end of the last load step should not include any element numbers. In other words, the net shear force applied to all Beam188 elements should be less than 3600 N and none of the spot weld elements should fail under full loading. It is noted that the assumed boundary condition in this section is the same as explained in section 4.1.3. However, it is considered that another girder is located between the two end girders in a parallel direction underneath the panel. Therefore, the complete panel span is reduced to a half-length. The main reason of adding a girder is to accommodate the new added load of vehicle. Figure 3-19 shows the shear force values at spot welds along all welding paths over the entire top and bottom face sheets.

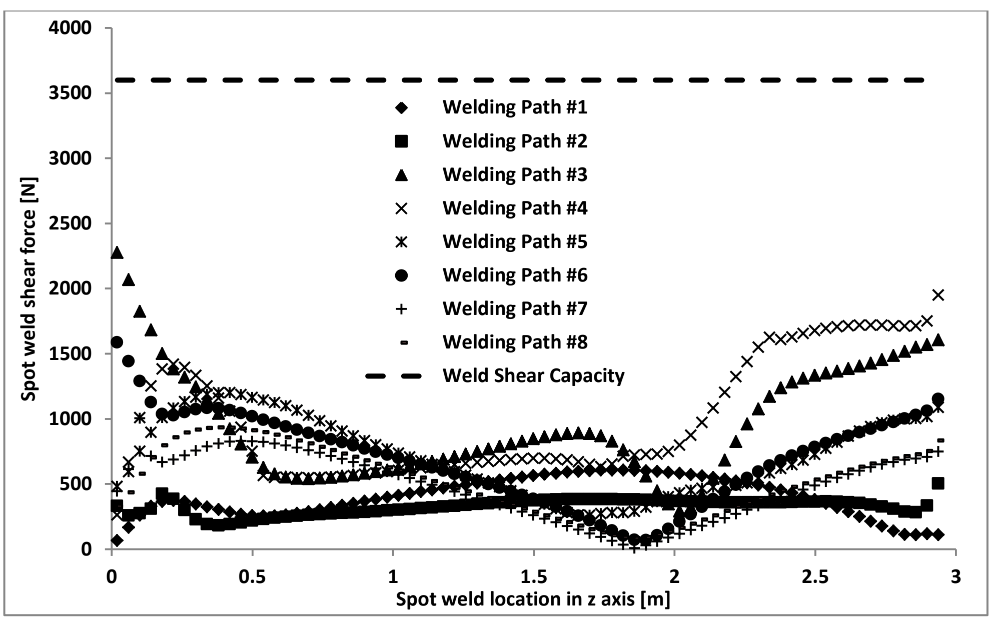

Figure 3-19 shear force values at spot welds along all welding paths over the entire top and bottom face sheets

Figure 3-19 reveals two main conclusions. First, the shear force values at all spot welds are remarkably below the breaking limit; therefore, the proposed panel with the assigned spot weld schedule would be sufficient for the 5000 kg vehicle. Second, the shear force distributions along eight welding paths indicate a non-uniform profiles in z direction. In general, the graph shows higher values at z = 0 m and z = 2.98 m. It is noted that z = 0 m and z = 2.98 m denote the mid location and end of the complete panel, respectively. Since all degrees of freedom are set to zero at z = 2.98 m, therefore, there is no displacement for the nodes located at z = 2.98 m. Indeed, the spot welds located near this edge experience a higher amount of shear force. Furthermore, the spot welds located close to z = 0 m also experience higher shear force values. As the third girder is assumed to be located at z = 0 m, mid-span of complete panel, the bottom face sheet sits on top of the girder flange at z = 0 m. Therefore, the displacement of all nodes located on top of the flange is assumed zero. The application of this boundary condition causes an increase in shear force at adjacent spot welds.

3.4.2 Spot weld failure analysis in sandwich panel under applied overloading

Regarding the excessive applied load failure scenario, the panel is subjected to a 300% overloading. The code applies the additional loading through 20 load steps of 10%. In other words, the vehicle weight is assumed 15,000 kg; therefore, the tire load would be three times more than the service load limit. Figures 3-20 (a) to 3-20 (h) show the shear force values at spot welds along eight welding paths at 100%, 200%, and 300% loading which are corresponding to 5,000 kg, 10,000 kg, and 15,000 kg vehicle weight, respectively. It is noted that the presented horizontal dashed line in all graphs indicates the 3,600 N shear strength capacity of spot welds. The graphs reveal that, in general, as the applied load increases the shear force values increase and the 200% and 300% extra loading curves are shifted upward. Regarding the spot weld failure, as mentioned earlier, shear force values for the 100% loading case at all welding paths are under 3,600 N, and as a result, there is no detached spot welds. However, for the case of 200% extra loading, presented graphs for welding paths 3, 4, 5, and 6 show that the number of failed spot welds are 6, 7, 1, and 4, respectively. Furthermore, in the case of 300% extra loading, plotted results reveal that for welding paths 2, 3, 4, 5, and 6 the number of detached welds are 1, 15, 21, 17, and 4, respectively.

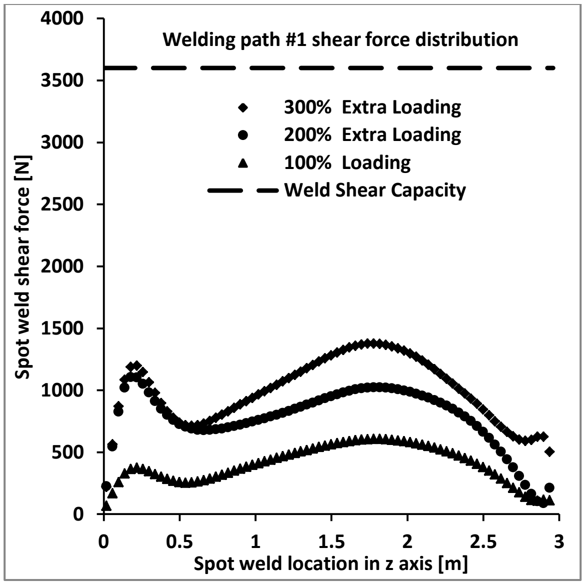
Welding path #1 shear force distribution
300% Extra Loading
200% Extra Loading
100% Loading
Weld Shear Capacity
Spot weld shear force [N]
Spot weld location in z axis [m]

(a)

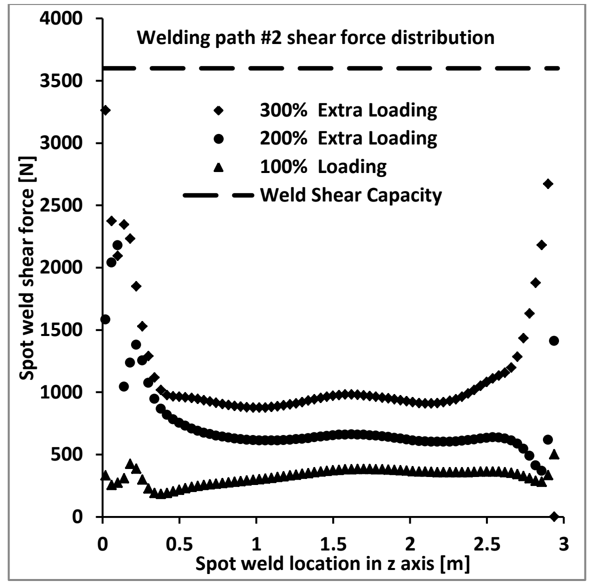
Welding path #2 shear force distribution
300% Extra Loading
200% Extra Loading
100% Loading
Weld Shear Capacity
Spot weld shear force [N]
Spot weld location in z axis [m]

(b)

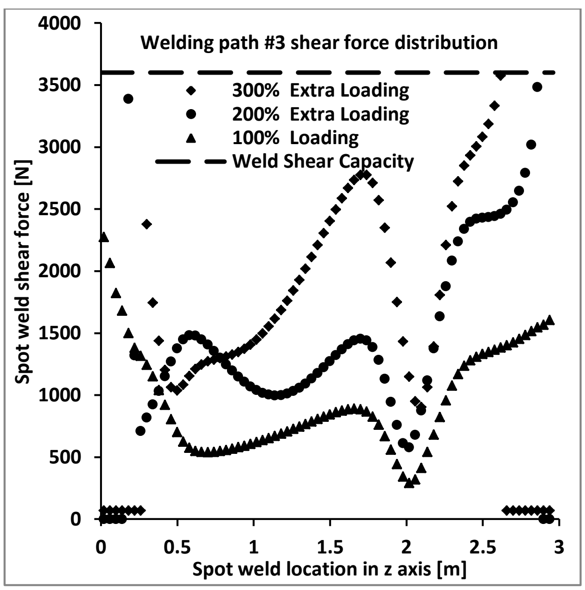
Welding path #3 shear force distribution
300% Extra Loading
200% Extra Loading
100% Loading
Weld Shear Capacity
Spot weld shear force [N]
Spot weld location in z axis [m]

(c)

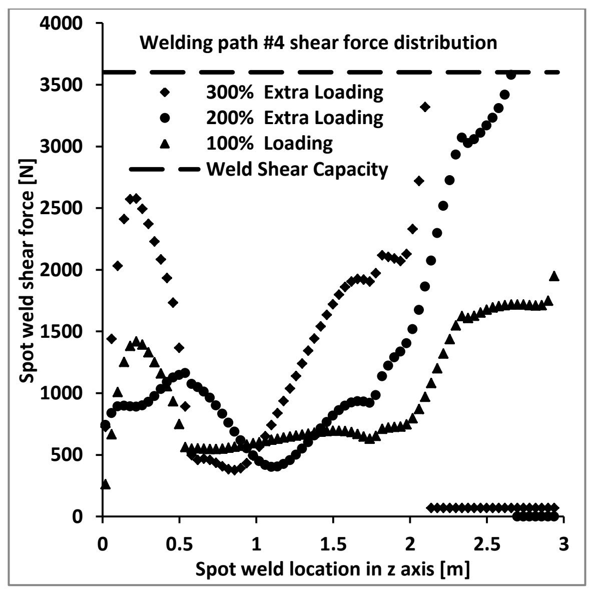
Welding path #4 shear force distribution
300% Extra Loading
200% Extra Loading
100% Loading
Weld Shear Capacity
Spot weld shear force [N]
Spot weld location in z axis [m]

(d)

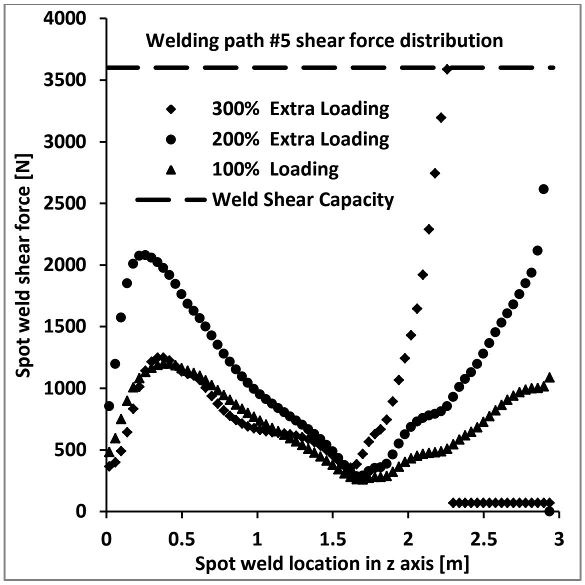

(e)

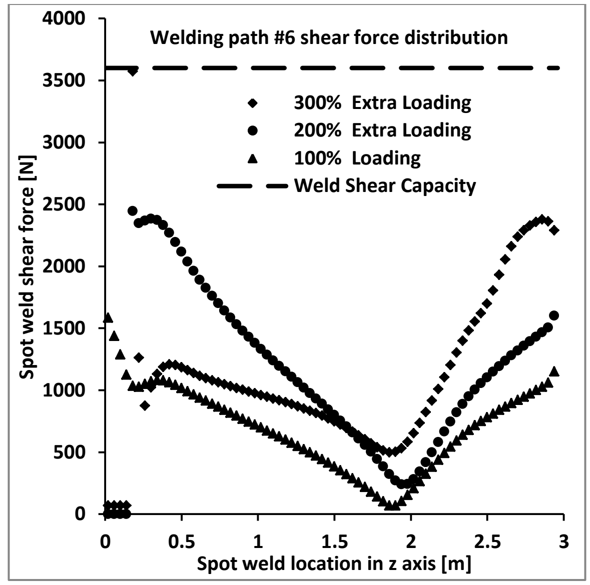

(f)

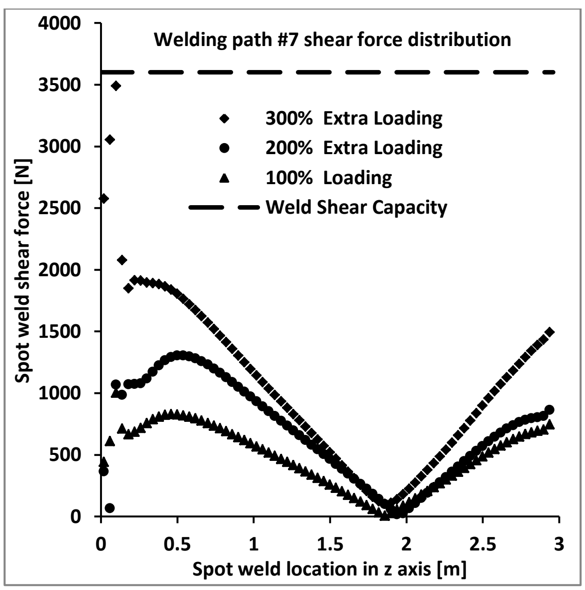

(g)

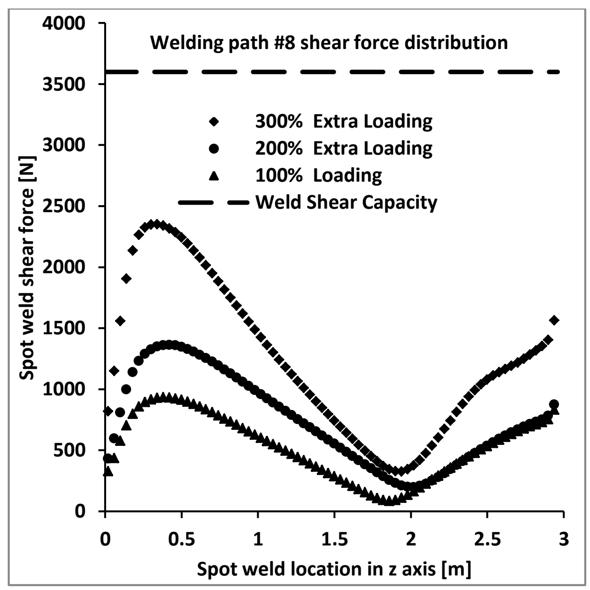

(h)

Figure 3-20 Shear force values at spot welds at loading 100%, 200%, and 300% of service load along a) welding path #1, b) welding path #2, c) welding path #3, d) welding path #4, e) welding path #5, f) welding path #6, g) welding path #7, h) welding path #8

It should be mentioned that once the shear force value at any spot weld passes the 3,600 N limit, the spot weld fails and its corresponding point in the graphs shows zero shear force. It is noted that in order to demonstrate the weld failure in graphs distinguishable, the corresponding failed spot weld points with zero shear force are presented in two separate lines in Figures 3-20 (a) to 3-20 (h) for 200% and 300% overlaodings. It is highly important to mention that in welding paths with failure, the weld detachment starts from both ends of the paths.

3.4.3 Spot weld failure propagation analysis

Undoubtedly, panels with different configurations may not experience similar failure patterns. As discussed earlier in the parametric study section, the mechanical response of sandwich panel is very sensitive to the geometrical parameters. Similarly, the failure behaviour could be noticeably affected by changing the panel geometry. Furthermore, beside the number of failed welds as a consequence of applying excessive loading, the pattern in which the spot weld failure occurs and propagates through the face sheets is also important. Locating the position of the failed welds could provide a failure pattern to demonstrate the propagation of the failure. Therefore, the number of collapsed welds and the failure path are two key indications of the panel response to excessive loading which should be monitored for different geometric configurations. In order to investigate the effect of geometric parameters on the failure response, sandwich panels with three core and face sheet thickness values of 2.38 mm, 3.17 mm, and 3.96 mm are selected to be compared. Figures 3-21 to 3-26 show the locations of failed spot welds at top and bottom face sheets in the plan view of sandwich panel for the three sheet thicknesses. It is noted that welding path numbers 1, 4, 5, and 8 refer to top face sheet spot welds, while path numbers 2, 3, 6, and 7 denote the bottom face sheet spot welds. In order to distinguish the top face sheet from the bottom one, the failed spot welds for each sheet thickness are shown in separate graphs. Figures 3-21, 3-23, and 3-25 denote the welds detachment at top face sheet and Figures 3-22, 3-24, and 3-26 denote the welds detachment at bottom face sheet.

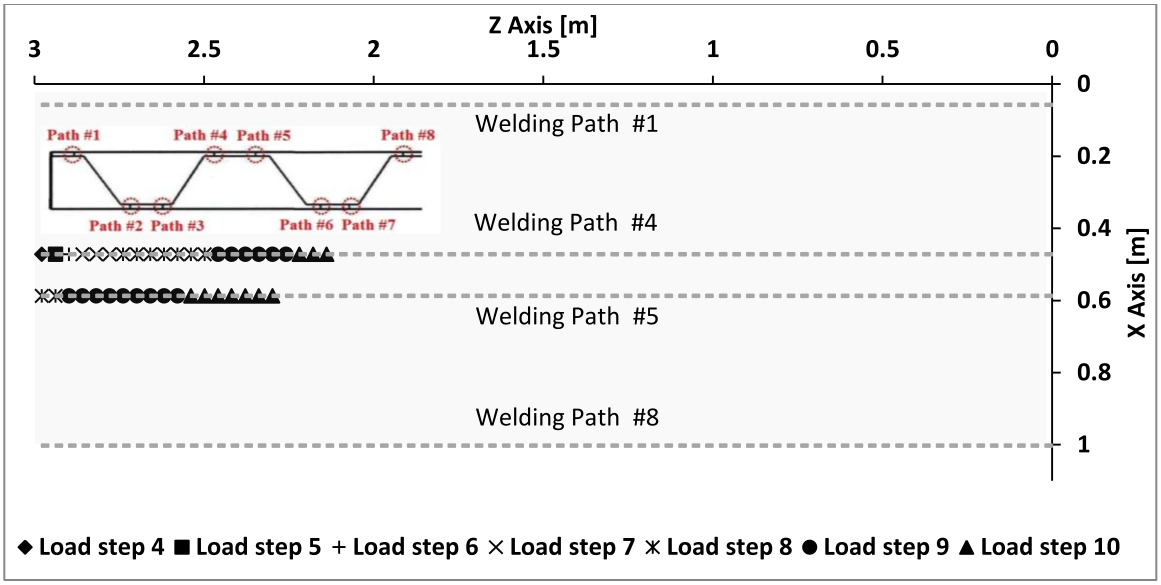

Figure 3-21 Location of failed spot welds on top face sheet for the panel with sheet thickness of 3.17 mm

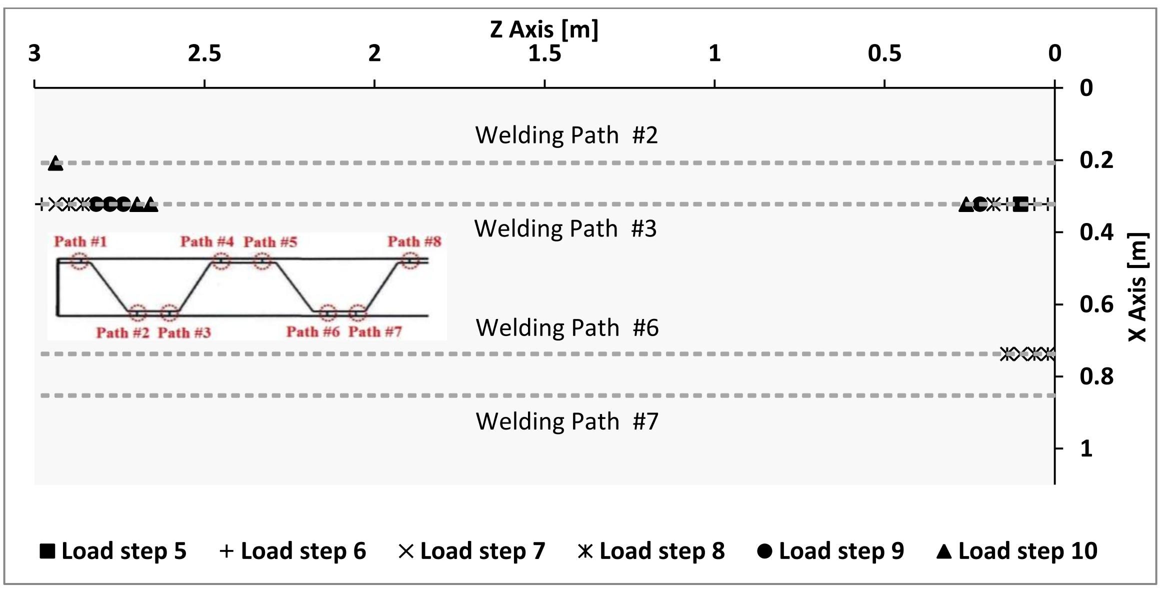

Figure 3-22 Location of failed spot welds on bottom face sheet for the panel with sheet thickness of 3.17 mm

Figures 3-21 and 3-22 indicate that for the panel with 3.17 mm sheet thickness spot weld failure occurs on top face sheet at welding paths 4 and 5 and on bottom face sheet at welding paths 3 and 6. The most important observation is that the failure starts from the complete panel end edges and center where the underneath girders are located. In other words, spot welds located close to underneath girders transfer higher amount of shear force to the core and they are highly potential to failure.

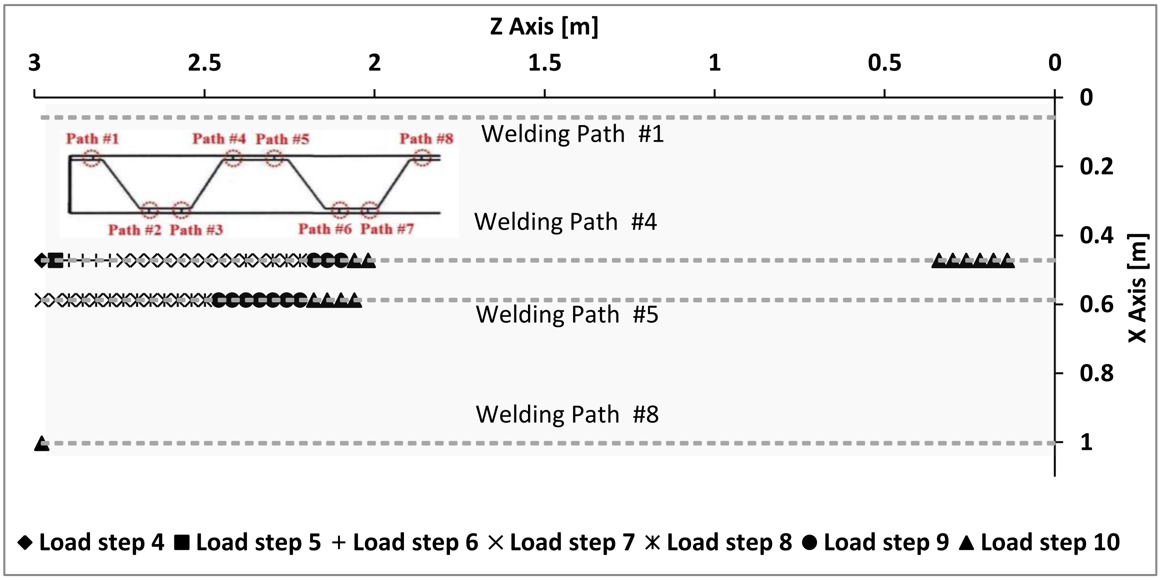

Figure 3-23 Location of failed spot welds on top face sheet for the panel with sheet thickness of 2.38 mm

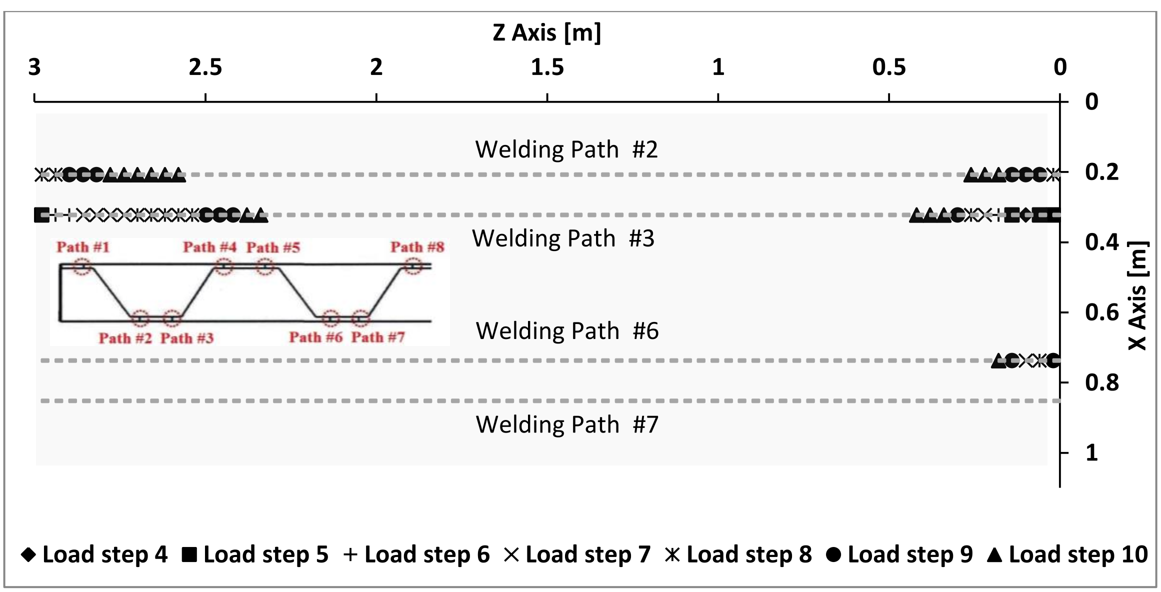

Figure 3-24 Location of failed spot welds on bottom face sheet for the panel with sheet thickness of 2.38 mm

Figures 3-23 and 3-24 show the spot weld failure propagation as the applied load increases above working load limit for the sandwich panel with core and face sheet thickness of 2.38 mm. The comparison between the failure propagation for the sheet thicknesses 3.17 mm and 2.38 mm reveals that the 2.38 mm sheet has the lower number of failed spot welds while the sheet with the thickness of 3.17 mm has higher number of failed spot welds.

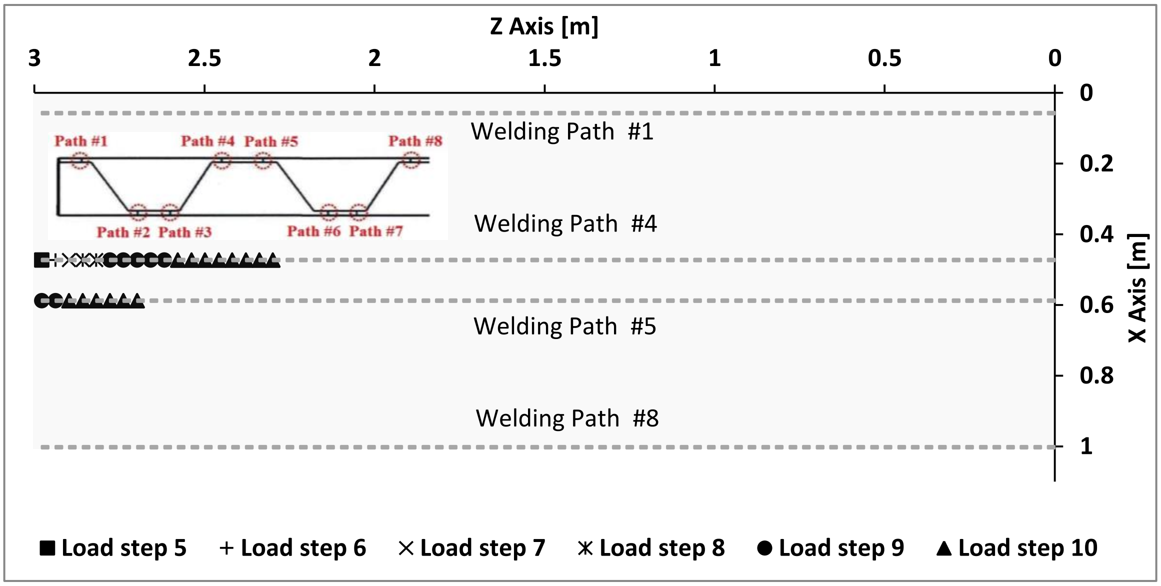

Figure 3-25 Location of failed spot welds on top face sheet for the panel with sheet thickness of 3.96 mm

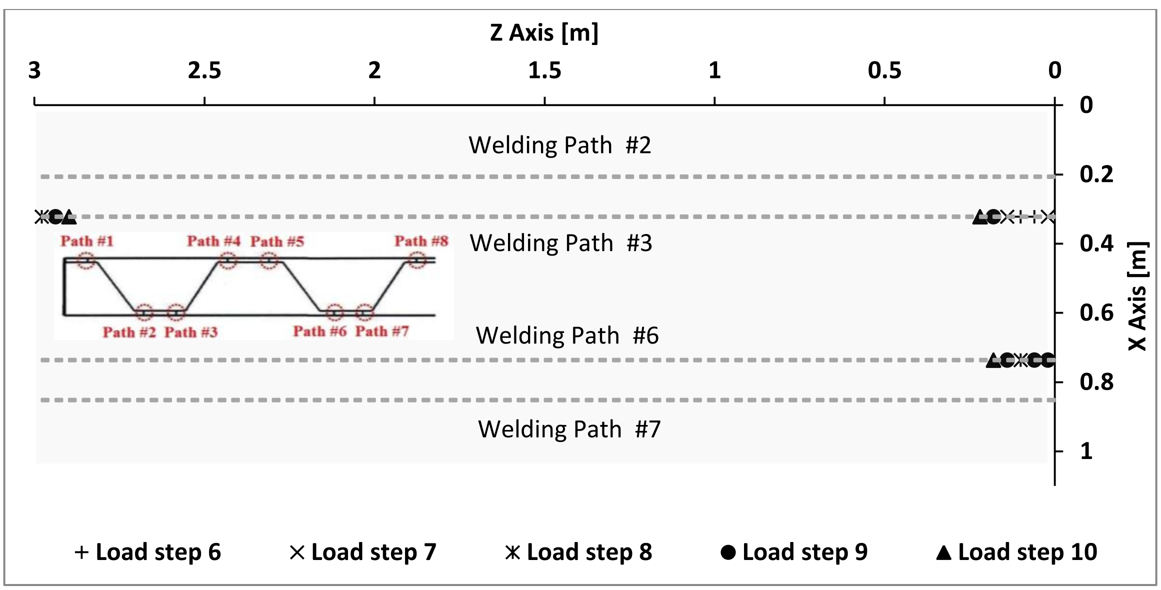

Figure 3-26 Location of failed spot welds on bottom face sheet for the panel with sheet thickness of 3.96 mm

Figures 3-25 and 3-26 present the spot weld failure propagation in sandwich panel with the sheet thickness of 3.96 mm. The comparison between the obtained results from sandwich panel with sheet thickness 3.17 mm and 3.96 mm shows that increasing the sheet thickness reduces the number of failed spot welds from 61 to 40. The decrease in the number of failed spot welds denotes the significant importance of the sheet thickness as one of the main geometric parameters.

As expected, due to the uniform distribution of the pavement dead load on the top face sheet as well as the symmetrical uniform concentrated truck load, the welds located closer to the two sides of panel near the support edges may experience a higher amount of shear force. Therefore, the failure probability on these two areas is higher than the interior and the centre of the panel. Figures 3-27 (a) to 3-27 (h) present the shear force distribution along all welding paths for sandwich panels with the three sheet thickness values at 300% applied overloading.

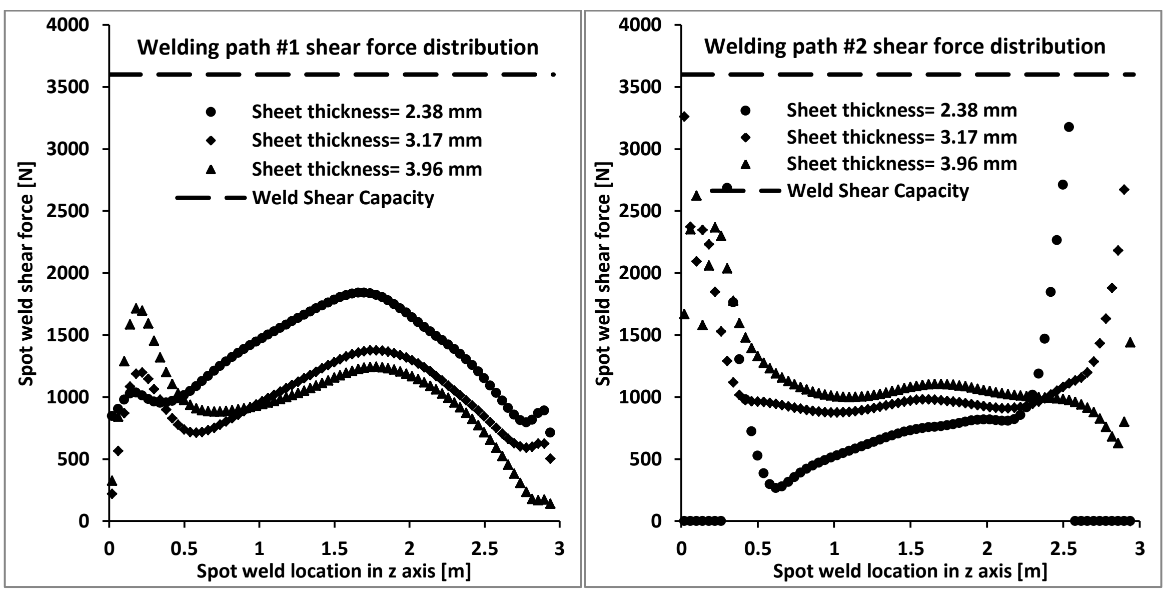

(a) (b)

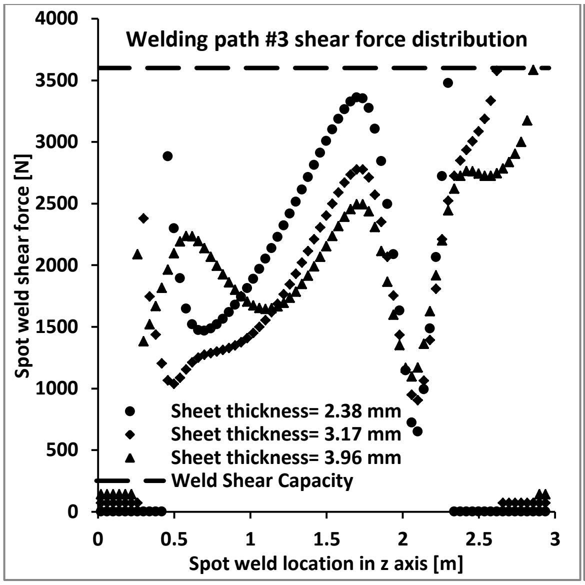
Welding path #3 shear force distribution
Spot weld shear force [N]
Spot weld location in z axis [m]
Sheet thickness= 2.38 mm
Sheet thickness= 3.17 mm
Sheet thickness= 3.96 mm
Weld Shear Capacity
0
500
1000
1500
2000
2500
3000
3500
4000
0
0.5
1
1.5
2
2.5
3

(c)

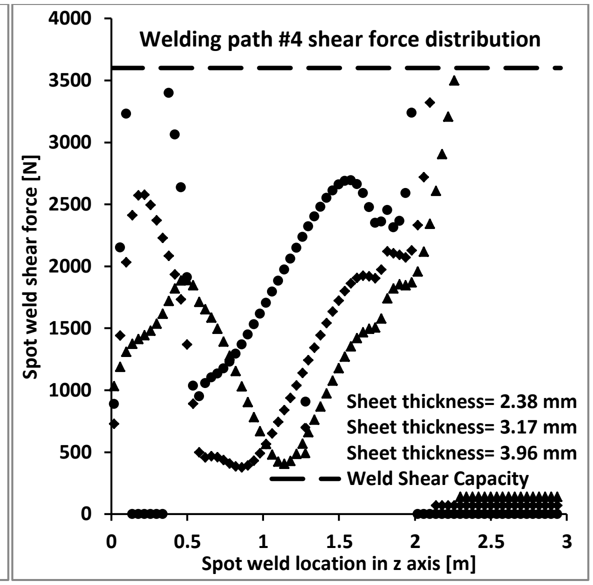
Welding path #4 shear force distribution
Spot weld shear force [N]
Spot weld location in z axis [m]
Sheet thickness= 2.38 mm
Sheet thickness= 3.17 mm
Sheet thickness= 3.96 mm
Weld Shear Capacity
0
500
1000
1500
2000
2500
3000
3500
4000
0
0.5
1
1.5
2
2.5
3

(d)

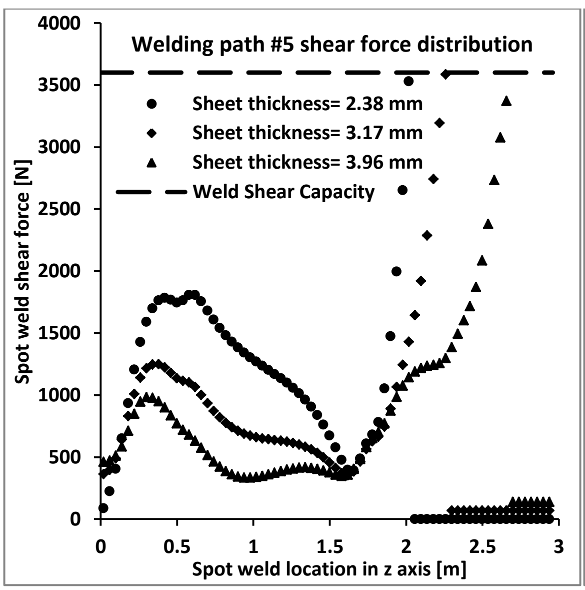
Welding path #5 shear force distribution
Spot weld shear force [N]
Spot weld location in z axis [m]
Sheet thickness= 2.38 mm
Sheet thickness= 3.17 mm
Sheet thickness= 3.96 mm
Weld Shear Capacity
0
500
1000
1500
2000
2500
3000
3500
4000
0
0.5
1
1.5
2
2.5
3

(e)

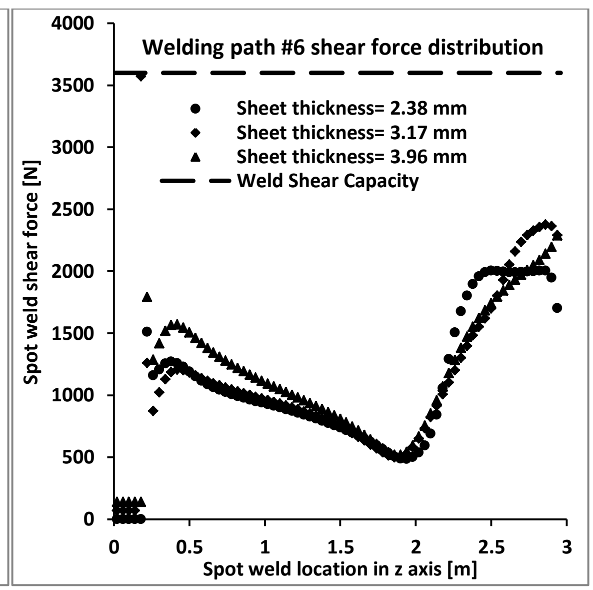
Welding path #6 shear force distribution
Spot weld shear force [N]
Spot weld location in z axis [m]
Sheet thickness= 2.38 mm
Sheet thickness= 3.17 mm
Sheet thickness= 3.96 mm
Weld Shear Capacity
0
500
1000
1500
2000
2500
3000
3500
4000
0
0.5
1
1.5
2
2.5
3

(f)

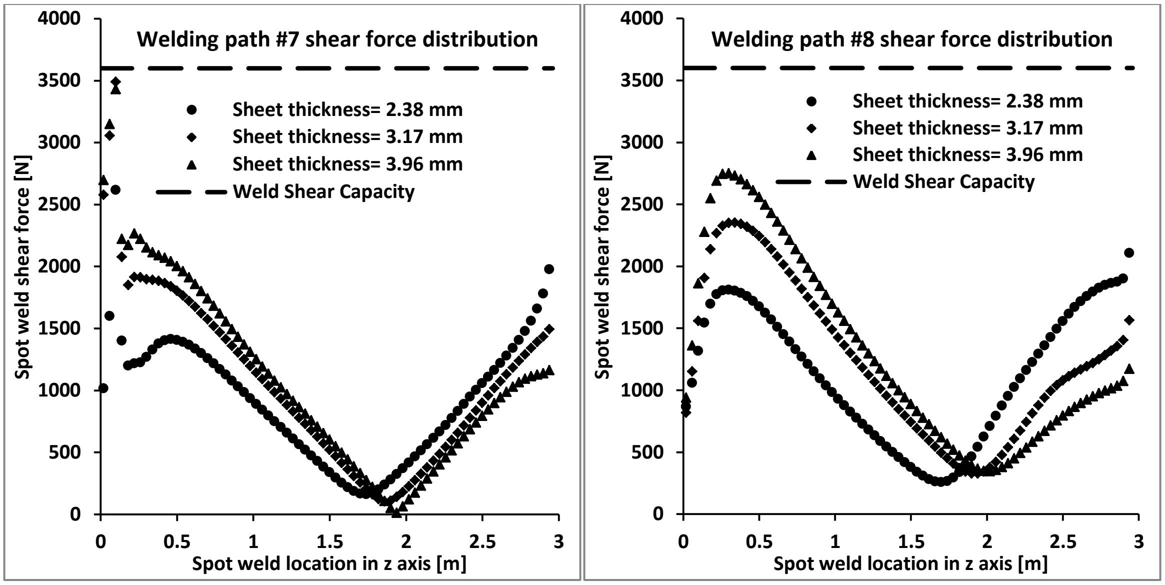

(g) **(h)**

Figure 3-27 Shear force values at spot welds at loading 300% of service load for sandwich panels with three sheet thickness values of 2.38 mm, 3.17 mm, and 3.96 mm along a) welding path #1, b) welding path #2, c) welding path #3, d) welding path #4, e) welding path #5, f) welding path #6, g) welding path #7, h) welding path #8

A sensitivity analysis can demonstrate the dependency of the number of failed welds on the added extra loading. Figures 3-27 (a) to 3-27 (h) show the number of failed spot welds at each load step for three sandwich panels with core and face sheet thickness values of 2.38 mm, 3.17 mm, and 3.96 mm. These graphs indicate that as the applied load increases above the allowable working load limit the number of failed welds nonlinearly increases. In other words, when the load increases above the limit at the first load step, the number of available spot welds which transfer the shear force flow from the face sheets to the corrugated core decreases significantly. Consequently, in the next load step, the remained attached welds should compensate for the share of failed welds in the shear transfer. Thus, as the number of detached welds increases, the remained spot welds would be more vulnerable to the additional loading. Therefore, the failure rate drastically increases in the following load steps. Figure 3-28 also denotes that as the sheet thickness increases the number of failed spot welds decreases.

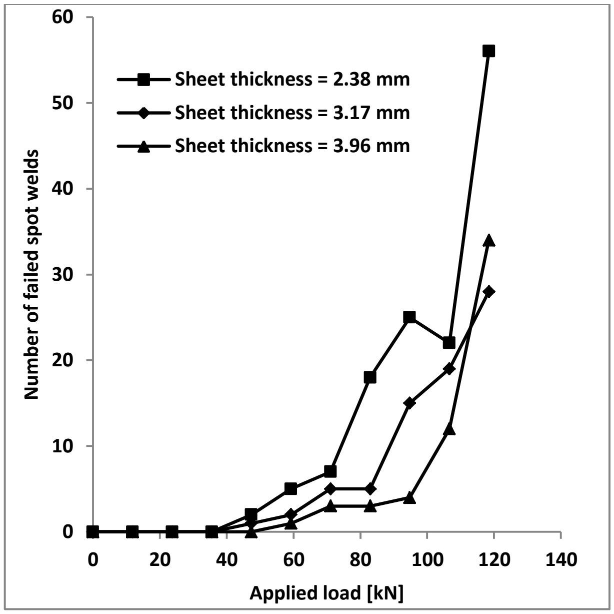

Figure 3-28 Number of failed spot welds at each load step for three sandwich panels with core and face sheet thickness values of 2.38 mm, 3.17 mm, and 3.96 mm

In addition to the described shear force distribution response to the excessive loading for the sandwich panels with different sheet thicknesses, the panel maximum deflection response is also of interest. As spot weld failure propagates through welding paths, it is expected that the load carrying capacity of the sandwich panel decreases and, consequently, the panel maximum deflection increases significantly. Figure 3-29 shows the load capacity curves for the sandwich panels with three sheet thickness values of 2.38 mm, 3.17 mm, and 3.96 mm.

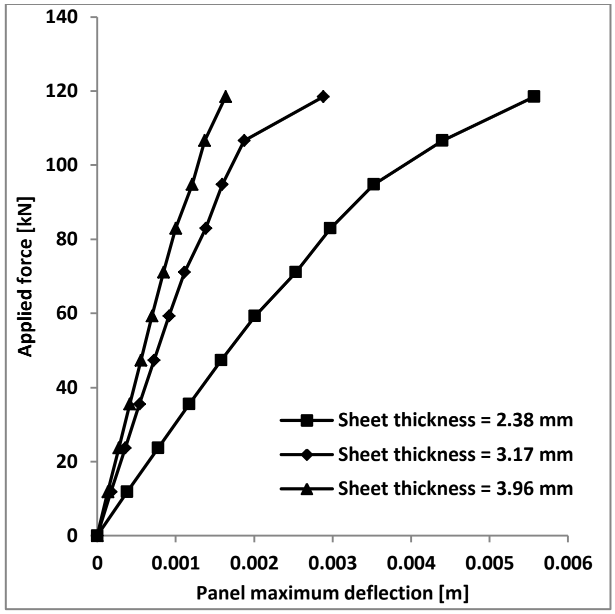

Figure 3-29 load capacity curves for the sandwich panels with three sheet thickness values of 2.38 mm, 3.17 mm, and 3.96 mm

As observed in Figure 3-29, panels with 2.38 mm and 3.17 mm sheet thicknesses experience a noticeable decrease in load carrying capacity at last two load steps while the panel with 3.96 mm sheet thickness shows a marginal decrease. The change in the curve slope shows the way in which the sandwich panel structural integrity starts to degrade by the spot weld failure propagation. Figure 3-29 also shows as the sheet thickness increases from 2.38 mm to 3.17 mm, the curve slope increase is considerably higher than the curve slope increase for thickness change from 3.17 mm to 3.96 mm. This implies that even with the same increment different sheet thicknesses changes the load deflection response in different ways.

Chapter 4: Summary and Conclusion

4.1. Summary

The presented study investigated the effect of geometric parameters on the mechanical behavior of corrugated-core steel sandwich panel by analyzing the panel maximum deflection and shear force profile through all welding paths. The effect of five geometric factors including spot weld spacing [S], spot weld radius [R], core sheet thickness [T_c], face sheet thickness [T_f], and welding path transverse distance [P] on the mentioned responses were discussed. Based on the obtained effect values for the five factors, regression equations were developed for the panel maximum deflection and maximum shear force at spot welds responses. Due to the limited shear force capacity of spot weld, the failure scenarios in which spot welds may experience a shear failure in the case of sandwich panel overloading were also investigated. Regarding the spot weld failure propagation patterns, the location of failed welds were plotted for each load step along all welding paths.

4.2. Conclusion

The obtained results from full factorial analysis of the five geometric parameters revealed that core and face sheet thicknesses are the two most important input factors which contribute to the panel maximum deflection response. Each of [T_c] and [T_f] factors showed a normalized effect of 41% among all five factors. Moreover, it was shown that [T_cT_f] and [T_fP] interactions are the two significant first-order interactions that contribute to panel maximum deflection response. Furthermore, it was concluded that the spot weld spacing and the core sheet thickness are the two input factors with the highest contribution in spot weld maximum shear force response with the normalized effects of 49% and 22% among all five factors, respectively. The most noticeable interactions are [SR] and [T_cT_f] among all ten first-order interactions for the maximum shear force response.

Based on the obtained geometric parameters contributions, two linear regression equations were developed to mathematically represent the mechanical behavior of the sandwich panel. A comparison between ANSYS FEM results and regression equation outputs for the two random sandwich panel models showed a difference of 12% and 20% for the panel maximum deflection response. It is concluded that due to highly nonlinear mechanical response of the sandwich panel, the presented regression equations predict the maximum deflection and maximum shear force responses within a bandwidth of actual results obtained from FEM analysis.

Moreover, the sandwich panel response for three input factors including panel height and core and face sheet thicknesses in a wider range of input variation to illustrate how nonlinearly the panel mechanical response changes. The obtained results indicated that as the panel height increases, the panel flexural strength increases and, as a result, the panel maximum deflection decreases. Furthermore, the shear force profile graphs in all welding paths except for the path #1 depicted that the shear force values at spot welds decreases when the panel height increases. Increasing the thickness of core and face sheets decreases the panel maximum deflection and shear force values at spot welds. It has been also observed that increasing the face sheet thickness lowers the maximum deflection more compared to that of increased core sheet thickness.

Regarding the spot weld failure analysis under applied overloading, based on the element birth and death feature in ANSYS, an algorithm was developed to monitor the shear force value at each spot weld while the applied truck loading was being increased. The embedded code in ANSYS checks whether the shear force at any spot weld exceeds the shear strength limit. If at any load step, the shear force value at any spot weld passes the limit, ANSYS deactivates the spot weld connection and reconstructed the sandwich panel model without considering these killed spot welds. Since the deactivated elements cannot contribute to the panel stiffness, obtained list of killed elements showed an increase in the rate of number of deactivated elements in the next load steps. The provided weld failure patterns indicated that the spot welds located near girders experience higher amount of shear forces and are more likely to detach. It has been observed that once the failure starts to propagate along a welding path, it starts from the quarter panel edges and continues towards the panel center.

4.3. Future study recommendation

The presented results and discussions in this study can be applied to further investigations in order to make such steel sandwich panels more efficient and economic. The future recommendations are as follows.

- Regarding the fabrication of the corrugated-core sandwich panel, laser welding is also one available option to attach the face sheets to the core. As in this study the spot welding connection was applied, it is also recommended to investigate the model with laser welding.

- Regarding the failure analysis, the buckling of inclined portion of the core is also another reason to experience failure in the sandwich panel. Therefore, it is important to check the buckling capacity of the panel as well.

- One of the input factors which may also play a role in the sandwich panel mechanical response is the number of unit cells in the corrugated core. As the number of corrugations increases the panel stiffness increases. Thus, it is recommended that the number of unit cells to be considered in the full factorial analysis.

- As mentioned in the introduction, the corrugated sandwich panels are fabricated with different core geometries. In this study, the modified V-core geometry was considered. Therefore, other geometries, for instance, O-core, Z-core, etc. could be also investigated.

- The effect of uncertainties in the mechanical properties and geometries should be considered in future studies.

References

AASHTO LRFD Bridge Design Specifications. 2005. Interim Revisions, American Association of State Highway and Transportation Officials, Washington, D.C.

Abbott, S.P., Caccese, V., Thompson, L., Blomquist, P.A., Hansen, E.E. 2008. Automated Laser Welded High Performance Steel Sandwich Bridge Deck Development.

Allen, H.G. 1969. Analysis and design of structural sandwich panels. Oxford: Pergamon Press.

ANSYS Release 14.0. 2012, Ansys Inc. Southpointe 275 Technology Drive Canonsburg PA.

Bezazi, A., Scarpa, F., Remillat, C. 2005. A novel centre symmetric honeycomb composite structure. Composite Structures 71, 356–364.

Canadian Highway Bride Design Code. 2005.

Chiras, S., Mumm, D.R., Evans, A.G., Wicks, N., Hutchinson, J.W., Dharmasena, K., Wadley, H.N.G., Fichter, S. 2002. The structural performance of near-optimized truss core panels. International Journal of Solids and Structures 39 (15), 4093–4115.

Chung, J., Waas, A. M. 2000. The inplane elastic properties of circular cell and elliptical cell honeycombs. Acta Mechanica 144, 29–42.

CMW spot welding catalog by Spot Welding Consultants Company. 2014.

Deshpande, V.S., Fleck, N.A., Ashby, M.F. 2001. Effective properties of an octet truss lattice material. J Mech Phys Solids, 49:1747–69.

Evans, A.G., Hutchinson, J.W., Fleck, N.A., Ashby, M.F., Wadley, H.N.G. 2001. The topological design of multifunctional cellular metals. Progress in Materials Science 46, 309–327.

Fung, T.C., Tan, K.H., Lok, T.S. 1996. Shear Stiffness DQy for C-Core Sandwich Panels, Journal of Structural Engineer in., ASCE., Vol. 128, N5, pp.683-689.

Gibson, L. J., Ashby, M. F. 1999. Cellular Solids. Structure and Properties, second edition. Cambridge University Press.

Goswami, S. 2006. On the prediction of effective material properties of cellular hexagonal honeycomb core. Journal of Reinforced Plastics and Composites 25, 393–405.

Intelligent Engineering Canada Limited. 2002. SPS Bridge Deck Panels For Austrian Military. Intelligent Engineering Canada Limited, Ottawa, ON.

Kennedy, D.J.L., Dorton, R. A., Alexander, S.D.B. 2002 .The Sandwich Plate System For Bridge Decks. Proceedings of the 19th Annual International Bridge Conference.

Kennedy, S.J., Murray, T.M. 2004. Ultimate Strength of an SPS Bridge-The Shenley Bridge, Quebec, Canada. 2004 Annual Conference of the Transportation Association of Canada Quebec City, Quebec, September 19-20 Session, pp. 1-13.

Klanac, A., Kujala, P. 2004. Optimal design of steel sandwich panel applications in ships. In: Proceedings of the ninth symposium of ships and other floating structures. Luebeck-Travemuende, Germany, p. 907–14.

Kujala, P., Klanac, A. 2002. Plate analysis of all steel sandwich panels under uniform pressure load. In: Proceedings of the XVth symposium on theory and practice in shipbuilding. Sorta; 2002.

Libove, C., Batdorf, S. B. 1948. A general small-deflection theory for flat sandwich plates, NACA TN 1526.

Libove, C., Hubka, R.E. 1951. Elastic constants for corrugated-core sandwich plates. NACA TN 2289, Langley Aeronautical Laboratory, Langley Field, Va.; 1951.

Lloyd, S. R. 2000. A new concept for a new age - the Sandwich Plate System (SPS) for shipbuilding. Marine Bulletin, Issue 3, No 24.

Lok, T.S., Cheng, Q.H. 2000. Elastic stiffness properties and behavior of truss core sandwich panel, ASCE Journal of Structural Engineering, Vol.126, pp.552-559.

Paik, J.K. 2003. Innovative structural designs of tankers against ship collisions and grounding: a recent state-of-the-art review. Mar Technol; 40:25–33.

Plantema, F. 1966. Sandwich Construction. John Wiley and Sons, Inc., New York, USA.

Qiu, X., Deshpande, V.S., Fleck, N.A. 2003. Finite element analysis of the dynamic response of clamped sandwich beams subject to shock loading. European Journal of Mechanics (A) Solids 22 (6), 801–814.

Rathbun, H.J., Wei, Z., He, M.Y., Zok, F.W., Evans, A.G., Sypeck, D.J., Wadley, H.N.G. 2004. Measurement and simulation of the performance of a lightweight metallic sandwich structure with a tetrahedral truss core. Journal of Applied Mechanics 71 (5), 368–374.

Rathbun, H.J., Zok, F.W., Evans, A.G. 2005. Strength optimization of metallic sandwich panels subject to bending. International Journal of Solids and Structures.

Sypeck, D. J., Wadley, H. N. G. 2001. Multifunctional micro-truss laminates: Textile synthesis and properties. Journal of Materials Research 16 (3), 890–897.

Tan, K. H., Montague, P., Norris, C. 1989. Steel sandwich panels: Finite Element, Closed Solution, and Experimental Comparisons, on a 6 m • 2.1 m Panel. Structural Engineering, Vol. 67, pp.159 -166.

Tsakopoulos, P. A., Fisher, J.W. 2003. Full-Scale Fatigue Test of Steel Orthotropic Decks for the Williamsburg Bridge. Journal of Bridge Engineering, American Society of Civil Engineers, Vol. 8, No. 5, 323-333.

Vaughn, D., Canning, M., Hutchinson, J.W. 2005. Coupled plastic wave propagation and column buckling. Journal of Applied Mechanics, ASME 72 (1), 139–146.

Wadley, H.N.G., Fleck, N.A., Evans, A.G. 2003. Fabrication and structural performance of periodic cellular metal sandwich structures. Composites Science and Technology 63 (16), 2331-2343.

Wallach, J. C., Gibson, L. J. 2001. Mechanical behavior of a three-dimensional truss material. International Journal of Solids and Structures 38, 7181–7196.

Wicks, N., Hutchinson, J.W. 2001. Optimal truss plates. Int J Solids Struct; 38:5165–83.

Xue, Z.Y., Hutchinson, J.W. 2003. Preliminary assessment of sandwich plates subject to blast loads. International Journal of Mechanical Sciences 45 (4), 687–705.

Xue, Z.Y., Hutchinson, J.W. 2004. A comparative study of impulse-resistant metal sandwich plates. International Journal of Impact Engineering 30 (10), 1283–1305.

Zenkert, D. 1995. An Introduction to Sandwich Construction. Engineering Materials Advisory Services, London.

Zok, F.W., Rathbun, H., He, M., Ferri, E., Mercer, C., McMeeking, R.M. 2005. Structural performance of metallic sandwich panels with square honeycomb cores. Philos Mag; 85:3207–34.